Thermal Properties of Selected Channel Compounds

by
R. Shane Harnish

Submitted in partial fulfillment of the requirements
for the degree of Master of Science
at
Dalhousie University
Halifax, Nova Scotia
July 1997

Dedicated to my parents

TABLE OF CONTENTS

FIGURE CAPTIONS

LIST OF TABLES

ABSTRACT

The melting behavior of binary compounds can be related to the fundamental thermodynamic property, Gibbs energy. The binary compounds investigated are inclusion compounds. An inclusion compound consists of a host lattice that contains cavities (cages, channels, layers, *etc.*) in which guest molecules reside. Urea and perhydrotriphenylene (PHTP) are the host lattices studied here. These molecules form lattices containing long channel cavities where the guest molecules reside. The guest chosen was the *n*-alkane, hexadecane ($C_{16}H_{34}$).

The melting behavior of binary compounds can be either congruent or incongruent. Congruent melting of a binary compound leads directly to the liquid phase. Incongruent melting of a binary compound leads to decomposition to give liquid and one of the pure (solid) components over a temperature range until melting is complete.

The melting behavior was determined here using differential scanning calorimetry and hot-stage microscopy. The heat capacity and derived Gibbs energy were determined using adiabatic calorimetric methods.

By understanding the relative stability, *i.e.* Gibbs energy, of the host-guest inclusion compound compared to the pure components, some generalizations can be made concerning general melting behavior in binary compounds. Lower Gibbs energy for the inclusion compound than the pure components tends to favor congruent melting, whereas a lower Gibbs energy for one of the pure components than the inclusion compound, tends to favor incongruent melting.

LIST OF SYMBOLS AND ABBREVIATIONS

E_s	Potential of d.t.a. heater
T_s	Sample temperature
T_r	Reference temperature
ΔT	Difference between T_r and T_s (T_r-T_s)
T_{sm}	Monitored sample temperature
T_{rm}	Monitored reference temperature
R_s'	Thermal resistance between sample and instrumentation
R_r'	Thermal resistance between reference and instrumentation
R_s	Thermal resistance between sample and heater
R_r	Thermal resistance between reference and heater
R	Thermal resistance
dq_s/dt	Heat flow into a system (for sample)
T_h	Temperature of heater
dq_r/dt	Heat flow into a system (for reference)
dT_s/dt	Scanning temperature rate for sample
C_s	Heat capacity of sample and container
C_r	Heat capacity of reference and container
dT_r/dt	Scanning temperature rate for reference
dT/dt	Scanning temperature rate at dynamic equilibrium (or operators scanning rate)
T_g	Temperature of glass transition

ΔH_{trans}	Enthalpy of transition
T_{hs}	Temperature of heater on sample side
T_{hr}	Temperature of heater on reference side
T_{phase}	Temperature of phase transition (solid-solid)
T_{melt}	Temperature of melting (solid-liquid)
C_p	Heat capacity under constant pressure
C_v	Heat capacity under constant volume
Q	Energy (heat) input
T_1	Temperature of sample before energy input
T_2	Temperature of sample after energy input
T_{avg}	The average of T_1 and T_2; The temperature at which C_p is measured
V_h	Heater voltage
t	Length of time energy input is applied
R_h	Heater resistance
$T_1^{(1)}$	Temperature before heating #1
$T_2^{(1)}$	Temperature after heating #1
ΔH	Change in enthalpy
ΔS	Change in entropy
ΔG	Change in Gibbs energy
$G_{inclusion\ compound}$	Gibbs energy of the inclusion compound.
G_{guest}	Gibbs energy of the guest molecule
G_{host}	Gibbs energy of the host molecule

H	Change in enthalpy
S	Change in entropy
G	Change in Gibbs energy
X_B	Mole fraction of component B
L_B	Melting enthalpy of component B
L_C	Melting enthalpy of component C
L_A	Melting enthalpy of component A
T_A	Melting temperature of component A
T_B	Melting temperature of component B
T_C	Melting temperature of component C
W	Interaction term to account for non-ideality
$G(AB)$	Relative Gibbs energy of compound AB
$G(B)$	Relative Gibbs energy of component B
$G(A_xB_y)$	Relative Gibbs energy of the binary compound A_xB_y
$S(A_xB_y)$	Entropy of the binary compound A_xB_y
$S(A)$	Entropy of the component A
$S(B)$	Entropy of the component B
$T_{fus}(A_xB_y)$	Melting temperature of the binary compound A_xB_y
$T_{fus}(A \text{ or } B)$	Melting temperature of either component A or B

ACKNOWLEDGEMENTS

I would like to take this opportunity to thank Prof. Mary Anne White for her assistance and expertise for without whom this work would not have been possible.

I would like to acknowledge the Faculty of Graduate Studies, Dalhousie University and the Department of Chemistry for their provision of funding during my graduate work.

I would like thank Prof. T. Fyles, University of Victoria for chemical synthesis and separation of perhydrotriphenylene and Prof. S. Grossert for his assistance and expertise in stereoisomer chemistry.

I would like to acknowledge Defence Research Establishment Atlantic (DREA), Department of National Defence for use of their facility. I would like to thank I. Keough for his assistance while at DREA.

I would like to thank D. Jackson for the use of the hot-stage microscope and his expertise in video microscopy.

Finally I would like to thank my friends and family for their support and encouragement throughout the many stages of this work.

CHAPTER 1

INTRODUCTION

1.1 Introduction

Inclusion compounds consist of two (or more) components where one component forms a host lattice for the other component(s) to reside as guests. Such compounds offer a unique opportunity to study structure-property relations. By examining these relations we can add to our general understanding of thermal properties of molecular solids, such as thermal conductivity[1.1,1.2,1.3,1.4,1.5] and heat capacity and related lattice dynamic properties.[1.6,1.7,1.8,1.9,1.10,1.11,1.12,1.13,1.14,1.15] Studies of the relative Gibbs energies of inclusion compounds and their pure components have shown that Gibbs energy is the driving force for melting congruency in binary compounds (for the ideal case).[1.16]

This work concerns the investigation of the melting behavior of inclusion compounds with the same guest in two different channel compounds : hexadecane inclusion compounds with urea (polar host lattice) and with perhydrotriphenylene (PHTP, a non-polar host lattice). Farina and co-workers have suggested[1.17] that the incongruent melting in urea-alkanes results from the immiscibility of the liquid components. Although immiscibility can influence melting behavior, it is believed that the relative Gibbs energies of the inclusion compound and components are the driving force of melting congruency. Through experimental determination of the relative Gibbs energies of the inclusion compound and their components, some conclusions can be made about how the guest-host interactions affect melting congruency. The low vapor pressure of hexadecane guest allows the assumption that only liquid-solid equilbra need be considered.

To study melting congruency, many techniques were implemented. To determine the melting points and enthalpies, differential scanning calorimetry (or d.s.c.) results were used to determine the phase diagram (by the method proposed by Farina *et al*[4,17]). Hot-stage microscopy was used to observe the physical properties of melting. Adiabatic calorimetry was used to obtain heat capacities which were used to determine the relative Gibbs energies for the inclusion compounds and their pure components.

1.2 Melting Behavior

The melting behavior of an inclusion compound (or binary compound) is either congruent or incongruent. For congruent melting, the binary compound leads directly to liquid region, with sold-liquid coexisting at a single temperature (the melting point) with the liquid having the same composition as the solid (see Figure 1.1). For incongruent melting, the binary compound decomposes at a temperature that is lower than its melting point to a solid component and a liquid. At the end of the melting temperature range the solid component melts leaving one the liquid phase (see Figure 1.1).

The matter of the melting behavior can be of considerable importance in preparation of the binary compound. Solidification of a solution with the appropriate composition will form a congruent melting compound; one of the components solidifies first and hampers compound formation in the case on incongruent melting compounds. From the view of material preparation and/or use of these material around their melting point, it is important to understand the driving forces responsible for congruency / inconcruency of melting.

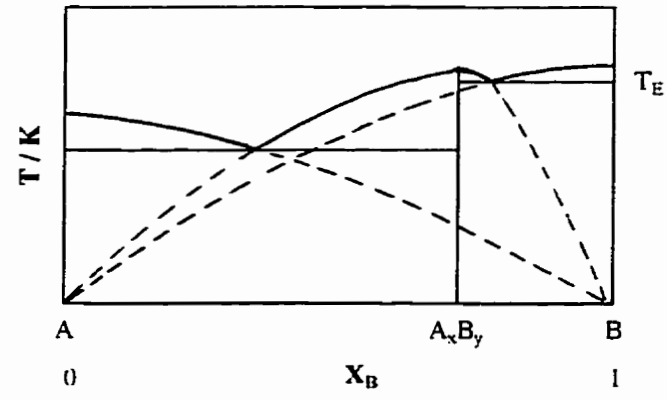

(a)

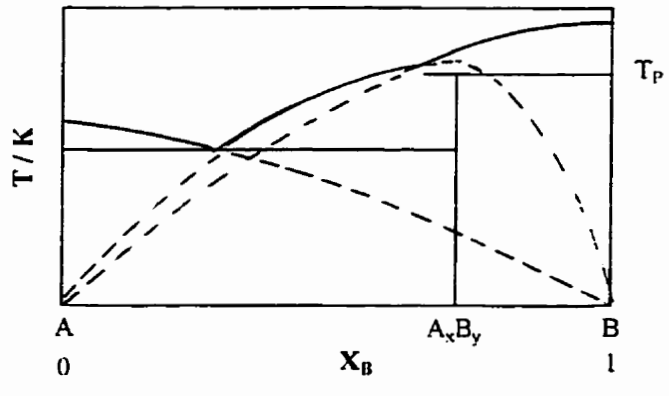

(b)

Figure 1.1 **Example of an A_xB_y compound melting (a) congruently and (b) incongruently.**

CHAPTER 2

METHODS FOR STUDYING THERMAL BEHAVIOR

2.1 Introduction

To study the melting behavior of binary systems such as inclusion compounds, many techniques are available. This chapter deals with such techniques as differential thermal analysis, differential scanning calorimetry, and adiabatic calorimetry with the latter two being used to investigate urea and perhydrotriphenylene inclusion compounds.

Differential scanning calorimetry has been used to study the thermal effects above room temperature (> 300K) which include the melting of the inclusion compounds. This melting of inclusion compounds is dealt in greater detail in later sections pertaining to the individual inclusion compounds (Chapter 3 and 4).

Adiabatic calorimetry allows for accurate heat capacity data below room temperature (30 K- 400K). The data obtained allows for in-depth studies into the relative stability of host-guest interactions by relating the heat capacity to Gibbs energy. A detailed treatment is again given in Chapters 3 and 4.

The following deals with the instruments and techniques used throughout this thesis. A detailed handling of differential scanning calorimetry and adiabatic calorimetry is now offered.

2.2 Thermal analysis

Differential scanning calorimetry (d.s.c.) is a vital thermal analytical tool which measures the difference in heat flow to a substance and a reference as a function of temperature as the two are subjected to a controlled temperature program. The difference between differential thermal analysis (d.t.a.) and differential scanning calorimetry is that d.s.c. is a calorimetric method (i.e. measures differences in energy) where as d.t.a. measures the difference in temperature. Differential scanning calorimetry has become the leading thermal analytical method since it first appearance in 1964.[2.1]

There are four main methods of obtaining differential thermal data; classical d.t.a., power-compensated d.s.c., Boersma d.t.a. (or heat flux d.s.c.) and modulated (or oscillating) d.s.c.[2.2]

2.2.1 Classical d.t.a.

In order to fully understand the basis of d.s.c., differential thermal analysis or 'classical d.t.a'[2,3] must be investigated. There is only one heater (Figure 2.1) with d.t.a. compared with the two heaters in d.s.c. (see Section 2.2.2). This heater is maintained by the potential E_s from the sample thermocouple to provide a linear sample temperature increase (or decrease) at a set temperature rate. The signal from the sample and reference thermocouples are also converted to temperatures (T_s and T_r respectively) and the difference (ΔT) is plotted as a function of temperature on a d.t.a. plot.

The thermocouples are directly embedded within the sample and reference materials, therefore, the monitored temperature of the sample, T_{sm}, is equal to the actual temperature of the sample T_s ($T_{sm} = T_s$). The same applies to the reference material, $T_{rm} = T_r$. The result is no thermal resistance R_s' (and R_r') to the heat flow between the sample (and reference) and the thermocouple. The controlling thermal resistance associated with the heat flow between the thermocouple and the heater is R_s (and R_r). For simplicity these values are taken to been equal ($R_s = R_r = R$). The difference between T_r and T_s gives rise to the analytical signal,[2,3]

$$signal = T_r - T_s = T_{rm} - T_{sm}. \qquad (2.1)$$

Now considering that the heat flow into a system, according to Newton, is proportional to the temperature difference and thermal resistance between the sample (and reference) and surroundings, assuming that the temperature of the sample (and reference) is uniform and equal to that of the container and the thermal resistance is constant over the temperature range of interest[2,3]

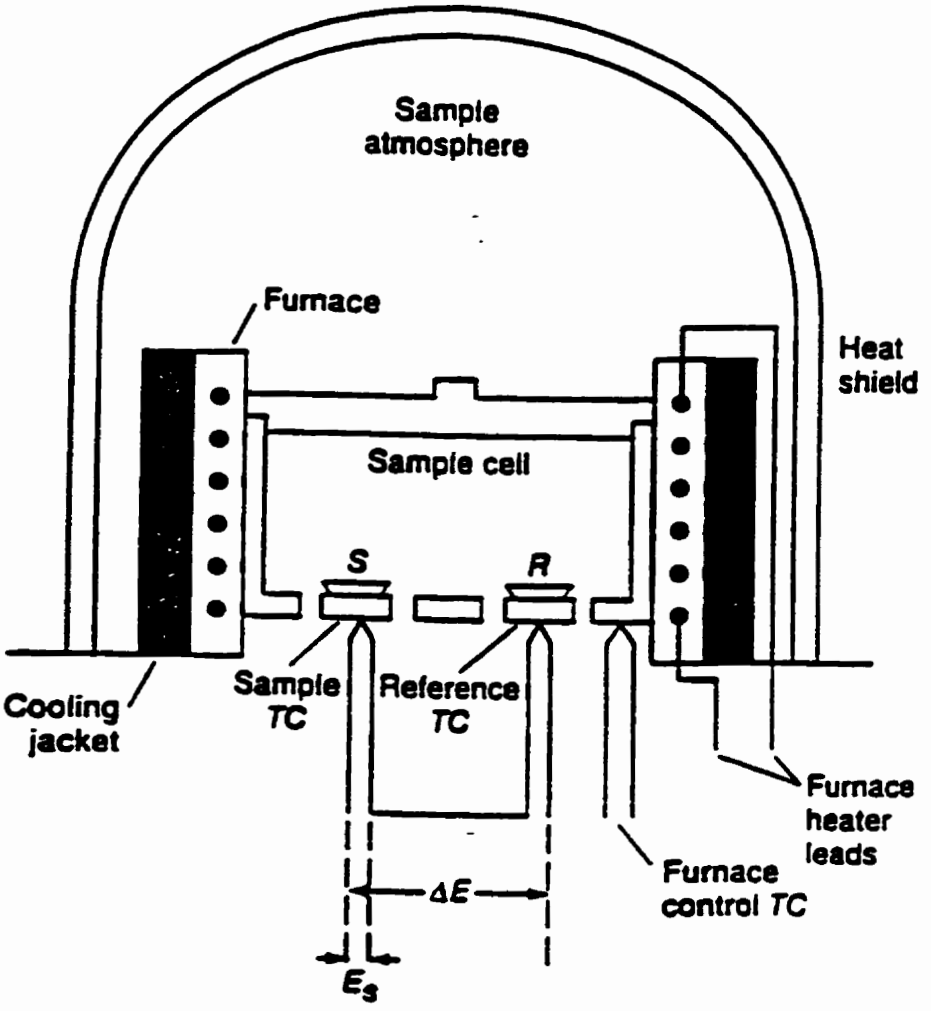

Figure 2.1 Schematic of a typical instrument for differential thermal analysis (TC = thermocouple). [2,3]

$$\frac{dq_s}{dt} = \frac{1}{R_s}(T_h - T_{sm}) = \frac{1}{R_s'}(T_{sm} - T_s) \tag{2.2}$$

and

$$\frac{dq_r}{dt} = \frac{1}{R_r}(T_h - T_{rm}) = \frac{1}{R_r'}(T_{rm} - T_r) \tag{2.3}$$

where dq_s and dq_r are the changes in heat (or energy) to the sample and reference over a small change in time, dt, and therefore dq/dt is the heat flow over two different temperatures. Subtracting Eq. (2.3) from Eq. (2.2) gives the signal in terms of the heat flow[2.3]

$$R_s \frac{dq_s}{dt} - R_r \frac{dq_r}{dt} = T_{rm} - T_{sm} = T_r - T_s. \tag{2.4}$$

Assuming that the heat capacities of the sample and container remain constant over the temperature range of interest, the heat capacity (C_s and C_r for sample and reference respectively) can be related to the heat flow if the sample is heated at a controlled scanning temperature rate (dT_s / dt)[2.3]

$$\frac{dq_s}{dt} = C_s \frac{dT_s}{dt}. \tag{2.5}$$

The same holds true for the reference

$$\frac{dq_r}{dt} = C_r \frac{dT_r}{dt}. \tag{2.6}$$

Substituting Eqs. (2.5) and (2.6) into (2.4) and using the assumption that R_s and R_r are equal (replaced by R)[2.3]

$$R\left(C_s \frac{dT_s}{dt} - C_r \frac{dT_r}{dt}\right) = T_r - T_s. \tag{2.7}$$

The scan rate for the sample and the reference are the same (at a dynamic equilibrium) and equal to the operator's scan rate (dT/dt). Eq (2.7) can then be re-written as[2.3]

$$signal = T_r - T_s = R\frac{dT}{dt}(C_s - C_r). \qquad \textbf{(2.8)}$$

There is now a relationship between the signal and the heat capacity. The temperature scan rate (dT/dt) is set by the operator so only the thermal resistance (R) is needed to obtain the heat capacity difference. This is not an easy task, since the thermal resistance is temperature dependent and a product of the sample and reference materials (as well as a product of the instrument itself). As a result, d.t.a. is semi-quantitative and the thermal resistance has to be calibrated for every temperature range and information about the sample configuration is needed (i.e. pellets vs. powders vs. liquids). The difficulty in obtaining thermal resistance is one of the major disadvantages of d.t.a., however, the temperature of the sample is monitored directly and there is no sample-thermometer temperature lag associated with d.t.a. A summary of the advantages and disadvantages of both d.t.a. and d.s.c. is tabulated in Section 2.2.5.

Figure 2.2 is a simplified d.t.a. thermograph of the linear heating of a polymer until its decomposition, which serves as an example of an experimental d.t.a. plot. At T_g, the polymer undergoes a glass transition which is typical of most polymers, as the polymer goes from a rigid glass state to a more flexible rubber-like state. Since this transition contains no absorption or evolution of heat, the enthalpy of the transition is zero ($\Delta H_{trans}=0$). The heat capacities of the two states are different, and therefore a change in baseline is observed. Peaks which are the result of an increase in ΔT ($= T_s-T_r$) are said to

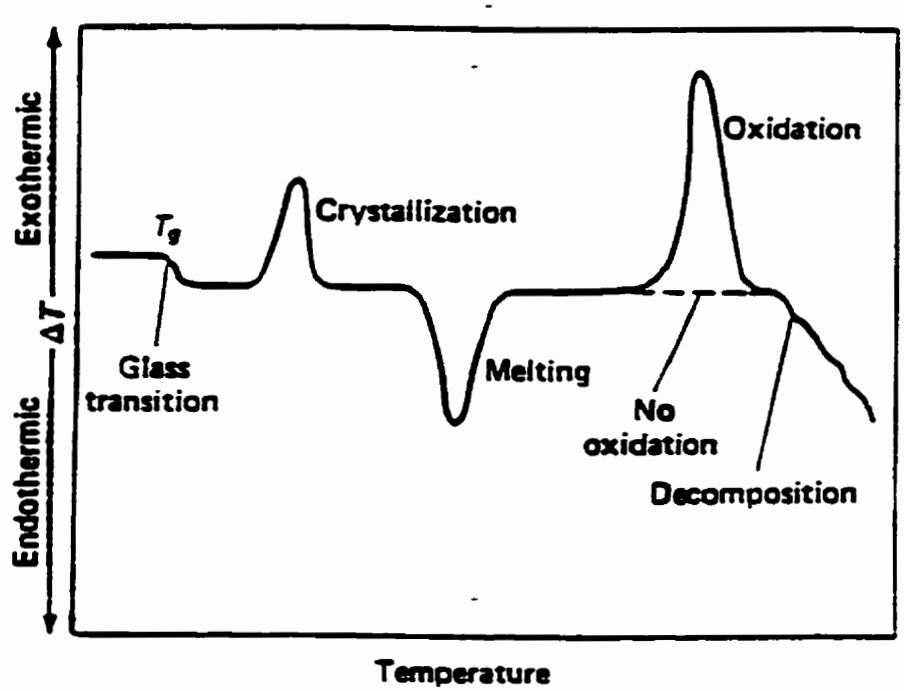

Figure 2.2 Schematic differential thermograph showing types of changes encountered with polymeric material. [2-4]

be exothermic (such as adsorption and crystallization) and those which are a result of a decrease in ΔT are said to be endothermic (such as melting, vaporization, and desorption). Figure 2.2, shows examples of both exothermic and endothermic peaks. The fall in ΔT after oxidation is the result of decomposition of the polymer to a variety of products.[2-4]

2.2.2 Power-compensated d.s.c.

A power-compensated d.s.c. can be divided into two loops, an average temperature control loop and a differential temperature control loop (Figure 2.3). The average temperature control loop supplies the power to both the sample and reference as dictated by the programmer, to maintain the sample and reference temperatures equal at an average temperature. The temperatures of both sample and reference are relayed from platinum thermocouples embedded in the sample and reference heater pans (Figure 2.4), to an average temperature computer. The whole loop determines the average temperature which is charted as temperature markings on a d.s.c. plot.

The differential temperature loop controls the differential power which is sent to either the sample or reference in order to maintain an average temperature. The temperatures of the sample and reference are relayed from the platinum thermometers to a differential temperature amplifier via a comparator circuit. The amplifier supplies power to the sample and reference heaters in the direction and magnitude necessary to maintain an average temperature. This loop provides the differential power which is plotted as a function of the average temperature to give a full d.s.c. plot (Figure 2.5).

Unlike d.t.a., the thermometers are located outside the sample and reference pans, therefore R_s' and R_r' are no longer zero. Since the individual heaters are located directly beneath the sample and reference pan, one can assume no thermal resistance ($R_s = 0$ and $R_r = 0$) and the temperature of the heater on the sample side are equal ($T_{hs}=T_{sm}$) and the same for the reference side ($T_{hr} = T_{rm}$). Since the programmer controls the temperature of the sample and reference heaters, T_{sm} and T_{rm} are the same temperature, $T_{sm} = T_{rm}$. With

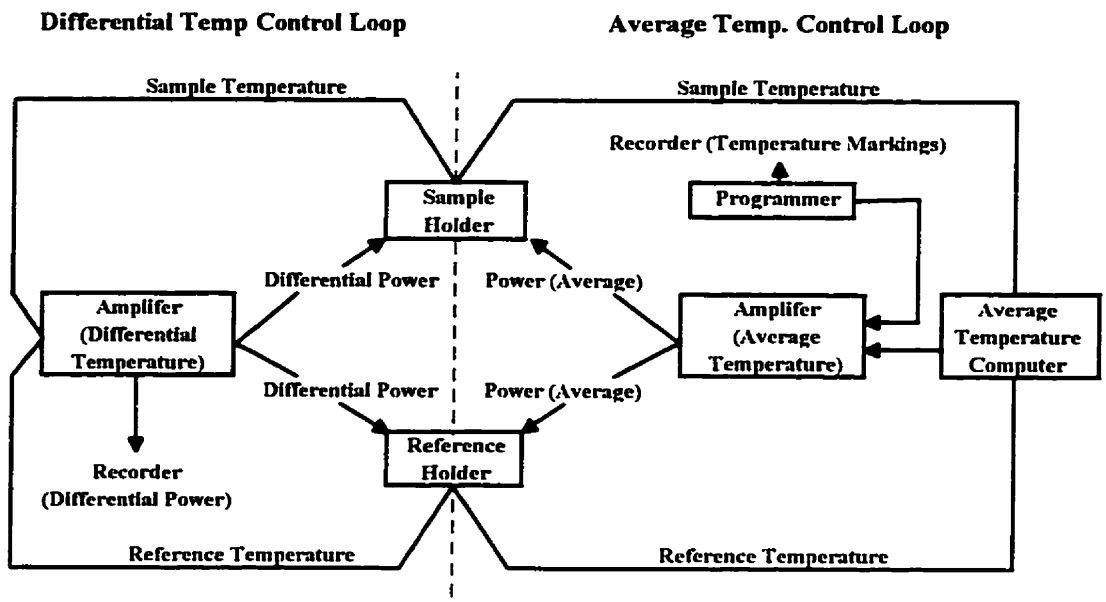

Figure 2.3 Block diagram, Perkin-Elmer differential scanning calorimeter.[2.1]

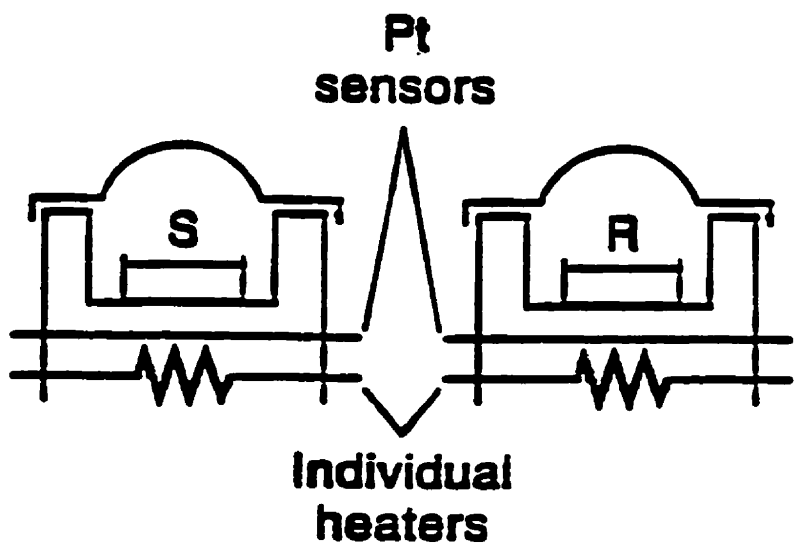

Figure 2.4 Schematic of differential scanning calorimeter sample holder and furnaces. [2.5]

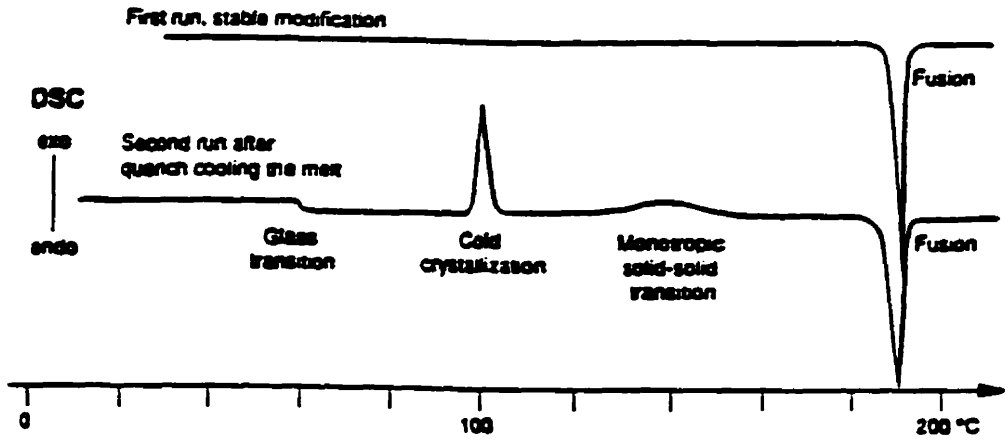

Figure 2.5 D.s.c. curve of sulfapyridine heated at a rate of 5 K min^{-1}.[2.6]

d.s.c. one is measuring the differential power need to maintain the sample and reference pans at an equal temperature. Therefore, the signal is directly related to the differential power[2.3]

$$signal = \frac{dq_s}{dt} - \frac{dq_r}{dt} = C_s \frac{dT_s}{dt} - C_r \frac{dT_r}{dt} \tag{2.9}$$

and at dynamic equilibrium the scan rate is equal to the programmer's scan rate dT/dt

$$signal = \frac{dq_s}{dt} - \frac{dq_r}{dt} = \frac{dT}{dt}(C_s - C_r). \tag{2.10}$$

There is now a direct relationship between the heat capacity and the signal modified by the programmer's temperature scan rate with no contribution from thermal resistance. Since the monitoring temperature is not in direct contact with the sample, T_{sm} is not equal to T_s and the difference is a product of the instrument's thermal resistance (R_s'), the scan rate (dT/dt), and the sample's heat capacity. Using Eq. (2.2) and (2.5)[2.3]

$$\frac{1}{R_s'}(T_{sm} - T_s) = \frac{dq_s}{dt} = C_s \frac{dT_s}{dt} \tag{2.11}$$

$$(T_{sm} - T_s) = R_s' C_s \frac{dT_s}{dt} \tag{2.12}$$

one can obtain an equation which represents the sample temperature lag with respect to the sample temperature. The signal is not dependent on thermal resistance, although the temperature lag is. Typically the temperature lag gives rise to variations in the temperature within a few tenths of a Kelvin. Most times the temperature lag can be adjusted with the use of standards that have transitions within the range of interest. Standards typically used include cyclopentane (T_{phase} = 122.38 K, solid-solid), indium (T_{melt} = 429.7485 K, solid-liquid), lead (T_{melt} = 600.61 K, solid-liquid), as well as others[2.7].

2.2.3 Boersma d.t.a (or Heat-Flux d.s.c.)

The Boersma d.t.a. (or more commonly heat-flux d.s.c.) is very similar to the power-compensated d.s.c. except for a slight variation in its design. Figure 2.6 is a schematic of a typical heat-flux d.s.c.. In this device, the sample and reference pan are heated by constantan (nickel-copper alloy) thermoelectric pans. The sample and reference pans sit on a raised platform which sits on the constantan pans. Heat is transferred up through the constantan pans to the sample and the temperature (T_{sm}) is measured at the contact between the constantan pans and the platform.

Due to the location of the heaters, there is a resulting thermal resistance (R) associated with the heaters. As a result, the signal from a heat flux instrument would have the form[2.3]

$$signal = T_{rm} - T_{sm} = R\frac{dT}{dt}(C_s - C_r). \qquad \textbf{(2.13)}$$

This is similar to the signal for classical d.t.a. (Eq (2.8)) except that R is a function of the instrument's design and can be corrected for. The thermal resistance is still a function of temperature, but most heat flux instruments automatically correct the signal for the thermal resistance at any temperature. The relationship between T_{sm} and T_s (or the temperature lag) can be addressed in the same manner as the power-compensated d.s.c.

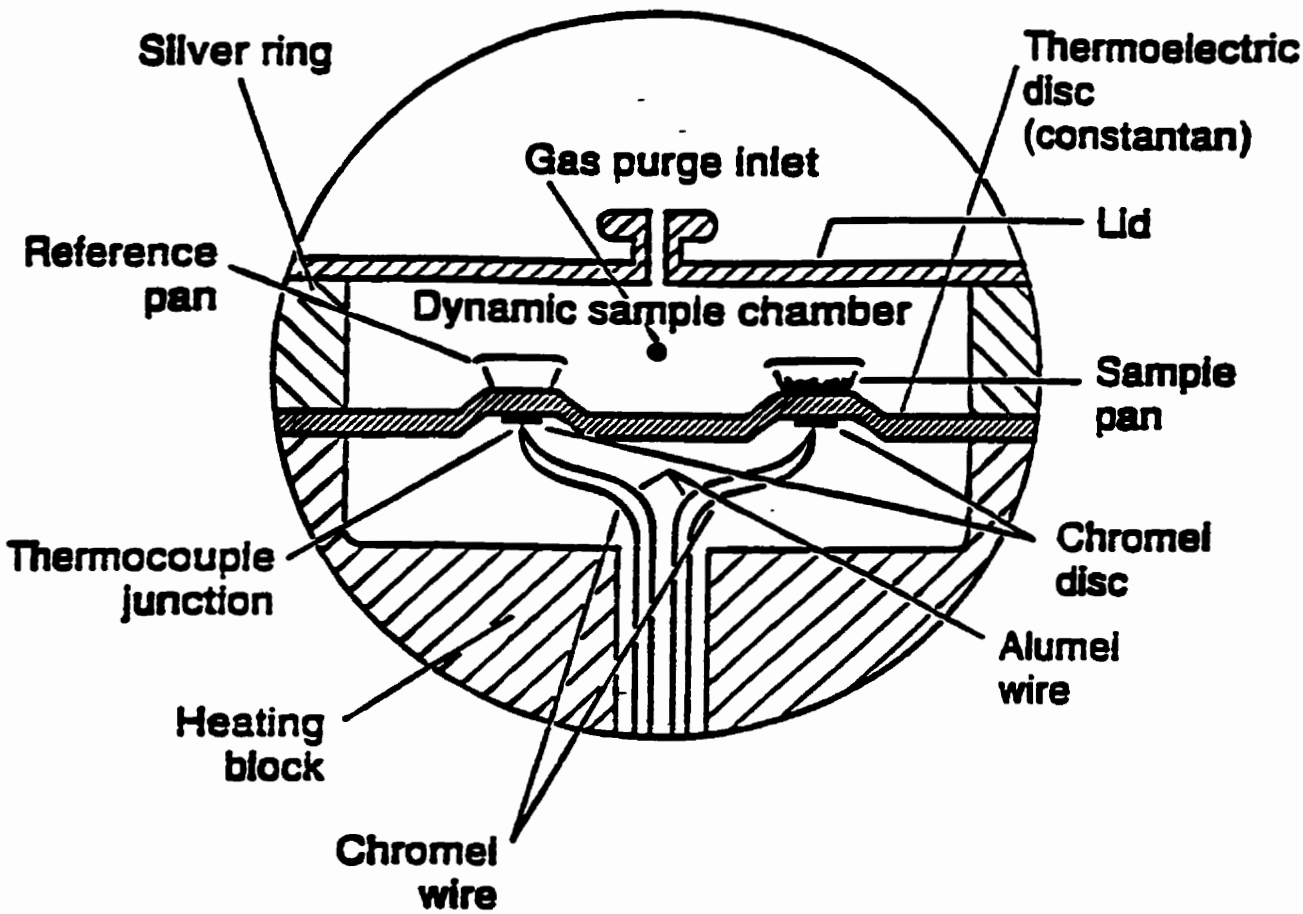

Figure 2.6 Schematic of heat flux d.s.c. cell. [2.4]

2.2.4 Modulated d.s.c. (or Oscillating d.s.c.)

Modulated (or oscillating) d.s.c. is really no more than an extension of power-compensated or heat-flux d.s.c.. With modulated d.s.c., a small perturbation (such as a sine wave) is applied to the linear temperature and the resulting data is mathematically deconvoluted so that the reversible and irreversible nature of thermal effects can be examined [2.2]. In this treatment of data, signals with overlapping peaks can be resolved, there is an improvement in resolution and sensitivity, and metastable melting can now be detected more readily. This new technique definitely improves the viability of d.s.c. as a tool for thermal analysis.

2.2.5 Summary of the similarities and differences of d.t.a. and d.s.c. instruments

In 'classical d.t.a.' the thermocouples are in direct contact with the sample and there is no sample temperature lag. The thermal resistance (R) is a product of the instrument, sample geometry, and temperature which are difficult to measure. This thermal resistance can be corrected with the use of standards, making the technique semi-quantitative.

In power-compensated d.s.c., the thermocouples are located below the sample, therefore, T_s does not equal T_{sm} and a temperature lag as described with Eq (2.12) is observed. With separate heating pans located in direct contact with the sample pan there is no thermal resistance as a product of the instrumentation. The temperature difference associated with the sample temperature lag can be corrected quite easily with use of standards. Since the instrument must be calibrated for each sample (as well with any new scan rates), it is only semi-quantitative.

Heat-flux d.s.c. has the same properties as power-compensated d.s.c. except for the thermal resistance (R) associated with the heater assembly, which must be corrected at each temperature.

A summary of the advantages and disadvantages of both d.t.a. and d.s.c. is given in tabular form (Table 2.1, 2.2 and 2.3)[2.8].

Table 2.1 Advantages and disadvantages of classical d.t.a[2.8].

Advantages	Disadvantages
Simple to set up experiments	Only semiquantitative for ΔH experiments
Commercial instruments available	Not an equilibrium method
Small samples (few mg)	Not an absolute measurement (requires calibration)
Rapid experiments	Thermal events may appear to overlap due scanning
Heating and cooling	nature
Ease of investigation of thermal	May not be accurate for C_p near transitions
history effects	T > 100 K for commercial instruments
No temperature lag	
Good for very high temperatures	

Table 2.2 Advantages and disadvantages of differential scanning calorimetry[2.8].

Advantages	Disadvantages
Commercial instruments available	Not an equilibrium method
Small samples (few mg)	Not an absolute measurement (requires calibration)
Rapid experiments	Thermal events overlap
Heating and cooling	May not be accurate for C_p near transitions
Determine ΔH	T > 100 K for commercial instruments
Ease of investigation of thermal	Inherent temperature lag
history effects	
High-pressure experiments possible	

Table 2.3 Advantages and disadvantages of Boersman d.t.a. (or heat-flux d.s.c)[2.8].

Advantages	Disadvantages
Commercial instruments available	Not an equilibrium method
Small samples (few mg)	Not an absolute measurement (requires calibration)
Rapid experiments	Thermal events may appear to overlap due to
Heating and cooling	scanning nature
Ease of investigation of thermal	May not be accurate for C_p near transitions
history effects	T > 100 K for commercial instruments
High-pressure experiments possible	Temperature lag
Quantitative ΔH determinations	
Good for very high temperatures	

2.2.6 Heat capacity measurements using d.s.c.

In all d.s.c. experiments the signal for each instrument is a function of the heat capacity of the sample. D.s.c. can (and has) been used for the measurement of heat capacities. D.s.c. offers many advantages for the measurement of heat capacities over more traditional methods (such as adiabatic calorimetry). The most important advantage is the relative ease in obtaining the heat capacity over a wide temperature range fairly quickly. Also, smaller sample sizes are required (milligrams compared to grams). This allows for expensive and hard to purify samples to be easily examined. Another advantage is the ease in which a sample is loaded. A sample can be loaded within a matter of minutes compared to hours with an adiabatic calorimeter. Finally, with most commercial instruments the heat capacity can be measured during cooling, and this cannot readily be performed with more classical methods.

It may seem that with these advantages there should be less of a need for such classical techniques as adiabatic calorimetry, however, the disadvantages tend to hamper d.s.c. as a replacement of classical techniques in the measurement of heat capacities. The biggest disadvantage arises from the largest advantage, that being the relative ease of d.s.c.. Since d.s.c. is so easy to use, it is also very easy to abuse. Unless extreme care is taken, many systematic errors can be introduced leading to poor heat capacities. Another disadvantage is that many d.s.c. instruments today are not equipped to handle low temperatures (below 100K). For most solid-state chemists, this is unacceptable since many of the transitions and phenomena associated with solid-state chemistry occur at low temperatures. Finally, d.s.c. can obtain fairly accurate heat capacities (within a few

percentages) but is still not as accurate as traditional adiabatic calorimeters (within a few tenths of a percentages or lower).

2.3 Adiabatic calorimetry

As the name suggests, adiabatic calorimetry is a calorimetric method (measures changes in energy) under adiabatic conditions (thermal isolation with the surroundings). Adiabatic calorimetry is an excellent technique for obtaining very accurate heat capacities, through measurements are extremely long and data intensive (compared to d.s.c.). New computers and data acquisition software allows for more efficient handling of the large amounts of data generated. The program AC4AUTO.BAS has been developed here for use with PC-DOS based computers and has improved data collection and manipulation tremendously. To make matters more difficult, adiabatic calorimeters are not commercially available. Despite these disadvantages, adiabatic calorimeters provide high-quality heat capacity determinations over a wide range of temperatures (near 0 K to above room temperature).

2.3.1 Instrumentation

Heat capacity is typically measured under constant pressure conditions (C_p), however, measurements have been performed with constant volume conditions (C_v).

In adiabatic calorimetry, the heat capacity is defined as the energy input, Q, divided by the change in temperature (temperature before (T_1) and after (T_2) heating)

$$C_p = \frac{Q}{(T_2 - T_1)} \tag{2.14}$$

at an average temperature, T_{avg} :

$$T_{avg} = \frac{(T_1 + T_2)}{2}. \tag{2.15}$$

The energy input into the system is a function of the heater voltage and resistance as well as the length of time the energy (heat) pulse is applied

$$Q = \frac{V_h^2 t}{R_h} \tag{2.16}$$

where V_h is the heater voltage, t is the length of time the voltage is applied and R_h is the heater's resistance.

To measure temperature a highly accurate and reproducible thermometer is needed. Typical thermometers for adiabatic calorimetry are the platinum resistance thermometer (temperature range from 20 K to above room temperature) and semiconductor resistance thermometers (from millikelvin (mK) temperatures to 30 K). These thermometers must be calibrated to within a few millikelvins using the 1990 International Temperature Scale[2.9] in order to meet the requirements for adiabatic calorimeters. Since temperature is so important and must be accurate to within a few

millikelvins, the effects of electromotive forces (EMFs) at the junctions in the thermometry circuit must be accounted for. This is usually done using an a.c. bridge or by applying a d.c. current both in the forward then reverse directions and averaging the two (see Figure 2.7). This averaging is performed automatically by the software.

In order to obtain the necessary adiabatic conditions, a number of conditions must be met in the construction. Figure 2.8 is a schematic diagram of the adiabatic calorimeter[2.10,2.11] used to study the heat capacities of urea, perhydrotriphenlyene and their inclusion compounds with *n*-alkanes. All wires used in the apparatus must be very fine and soldered with thermal-free solder in order to minimize heat leaks. The whole apparatus is hung from nylon filaments (poor conductors of heat) and suspended in an evacuated chamber. The vacuum is maintained using a two-pump system, a rotary pump (roughing pump) and a diffusion pump, to give necessary pressures below 10^{-5} mbar. To achieve constant temperatures the sample is surrounded by an adiabatic shield. This shield maintains adiabatic conditions between energy pulses and gives rise to a zero temperature drift rate (in practice, $\pm$ 0.003 K min^{-1} drift rates can be tolerated).

The sample being measured was located in a sample vessel (Figure 2.9). The size of the sample was usually around one gram and sample geometry is not a problem as with d.s.c. because the sample is in a helium atmosphere and thermal equilibrium is achieved. The sample vessel was sealed tightly with brass screws as well as a fine (0.1mm diameter) indium o-ring. The sample vessel sat within the heater thermometer assembly and Apiezon T grease (Fisher, low-vapor pressure (5×10^{-9} Torr) sealing agent and lubricant) was used to make good thermal contact between the sample vessel and heater. The

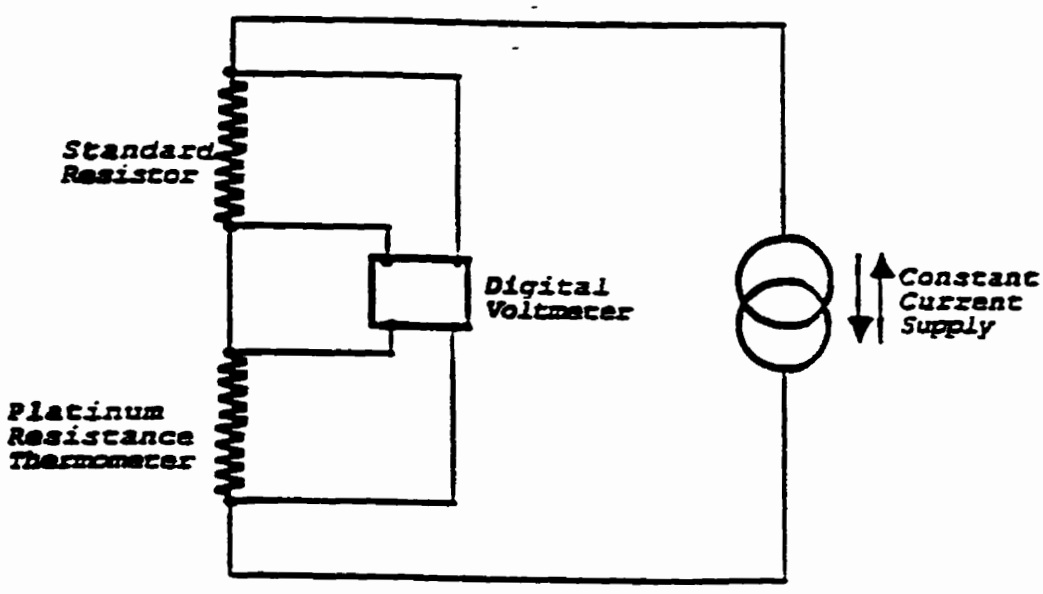

Figure 2.7 Schematic circuit for the d.c. determination of the resistance of a thermometer. [2.10]

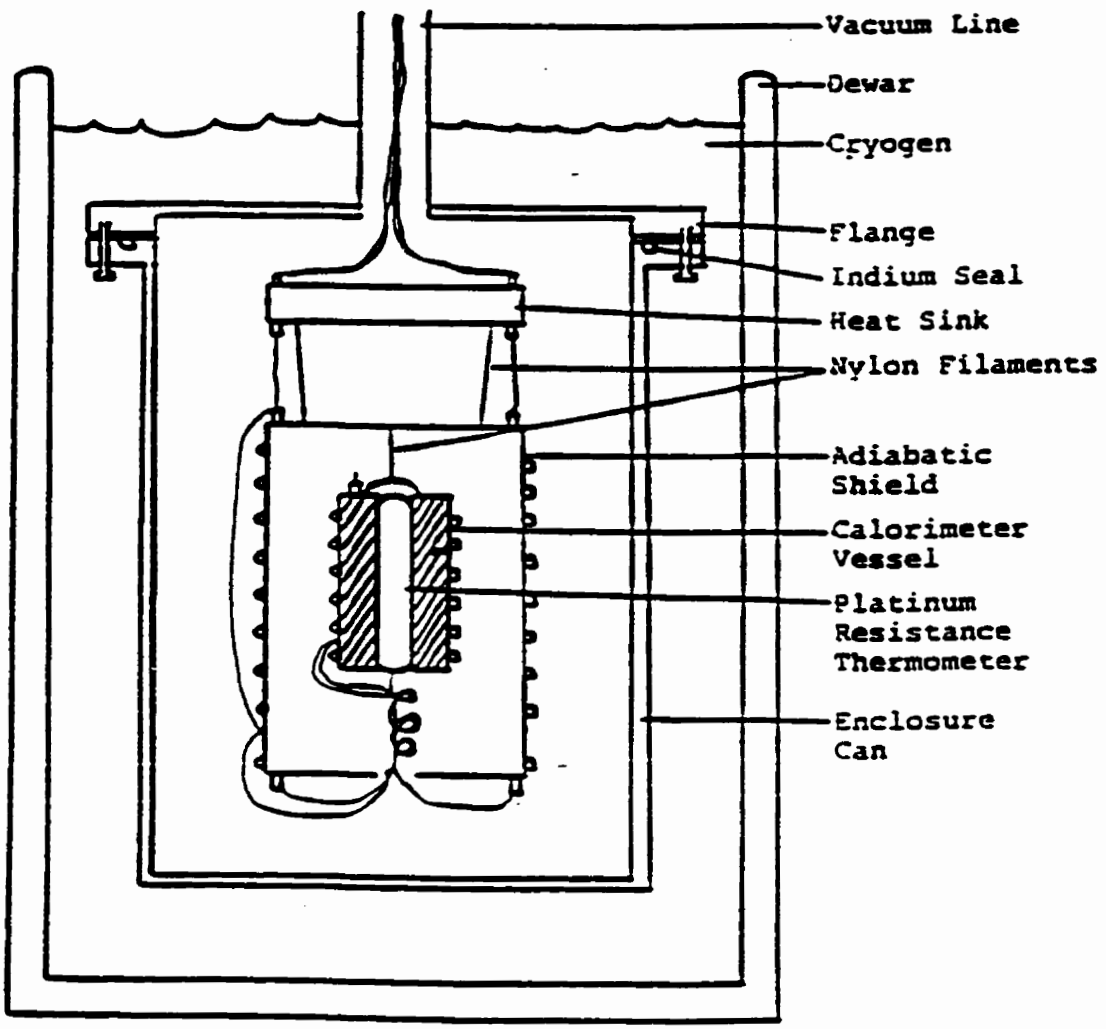

Figure 2.8 Schematic diagram of the adiabatic calorimeter.[2.10]

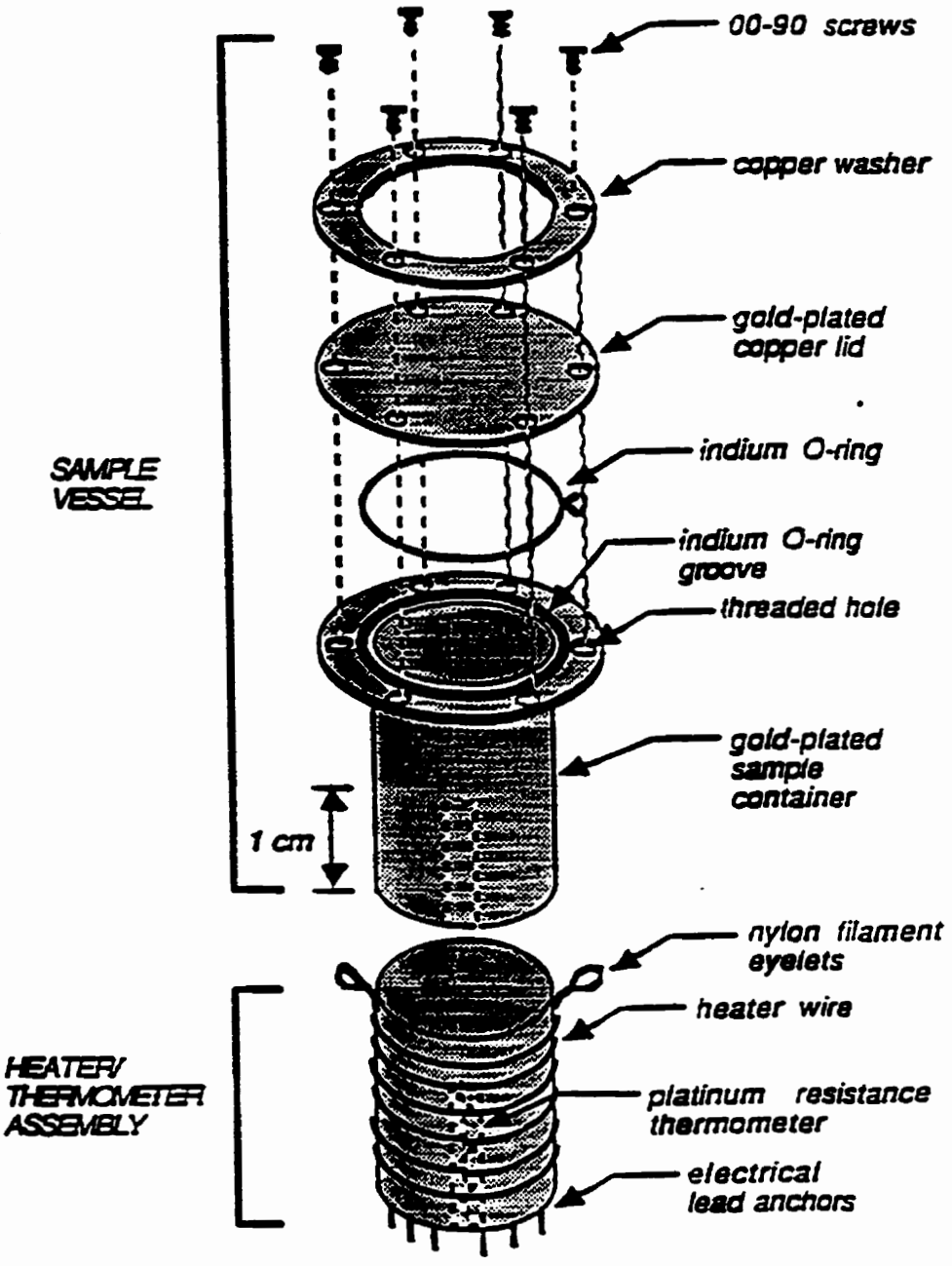

Figure 2.9 Sample vessel and heater/thermometer assembly (adiabatic calorimeters II, III, IV and V).[2.11]

thermometer was located on the heater sleeve such that when the sample vessel and the heater were assembled, the thermometer was located in the center of the sample.

The temperature of the system was influenced by the surroundings. For temperatures below room temperature, a cryogenic fluid was needed. The calorimeter was enclosed in a vacuum jacket (sealed with 1 mm diameter indium wire) and this can was immersed within the cryogenic fluid. Large double-walled glass Dewars were used to hold the cryogenic fluid. For temperatures from 77 K to above room temperature, liquid nitrogen was used as the cryogenic fluid. For temperatures below 77 K, liquid helium was used. For liquid helium, a second Dewar was needed and was immersed in a Dewer containing liquid nitrogen. The calorimeter was cooled using cold helium exchange gas before the transferring of the liquid helium. More information regarding this adiabatic calorimeter is given elsewhere[2.10,2.11].

Since adiabatic calorimetry is an absolute measurement technique, standards are not used for calibration of heat capacities. Standards are only used to test the instrument's performance or new calorimeters. Typical standards include benzoic acid (for low temperature to room temperatures) and commercial sapphire (for high temperatures). The heat capacity obtained is comprised of that of the sample, indium, vessel and Apiezon T grease heat capacities. To obtain just the heat capacity for the sample the heat capacities for indium[2.12,2.13], Apiezon T grease[2.14], and empty vessel must be known over the entire temperature range of interest.

2.3.2 Theory

The determination of heat capacity in an adiabatic calorimeter can be summed in Figure 2.10 which shows the determination of heat capacities at two temperatures. In the figure, $T_1^{(1)}$ is the forward projected temperature at the midpoint of the energy pulse. $T_2^{(1)}$ is the reverse projected temperature at the midpoint of the energy pulse. The heat capacity is then the energy pulse divided by the difference of $T_2^{(1)}$ and $T_1^{(1)}$ as in Eq (2.14) and the temperature is the average temperature of $T_1^{(1)}$ and $T_2^{(1)}$ as given by Eq (2.15).

One of the major advantages of obtaining accurate heat capacities is their use it the determination of the chemical thermodynamic parameters such as enthalpy change (ΔH), entropy change (ΔS) and Gibbs energy change (ΔG) :

$$\Delta H = \int_{T_1}^{T_2} C_p dT \qquad \textbf{(2.17)}$$

$$\Delta S = \int_{T_1}^{T_2} \frac{C_p}{T} dT \qquad \textbf{(2.18)}$$

$$\Delta G = \Delta H - T\Delta S . \qquad \textbf{(2.19)}$$

Gibbs energy is one of the major parameters in this thesis as it relates to the relative stability of materials. This becomes important when studying the melting of supramolecular compounds (such as inclusion compounds) as it shows that such compounds will melt congruently if the stability of the host lattice is less then the host-guest inclusion compound and incongruently if the inclusion compound is less stable compared to the host lattice[2.15]. This relationship will be describe in great detail in later sections.

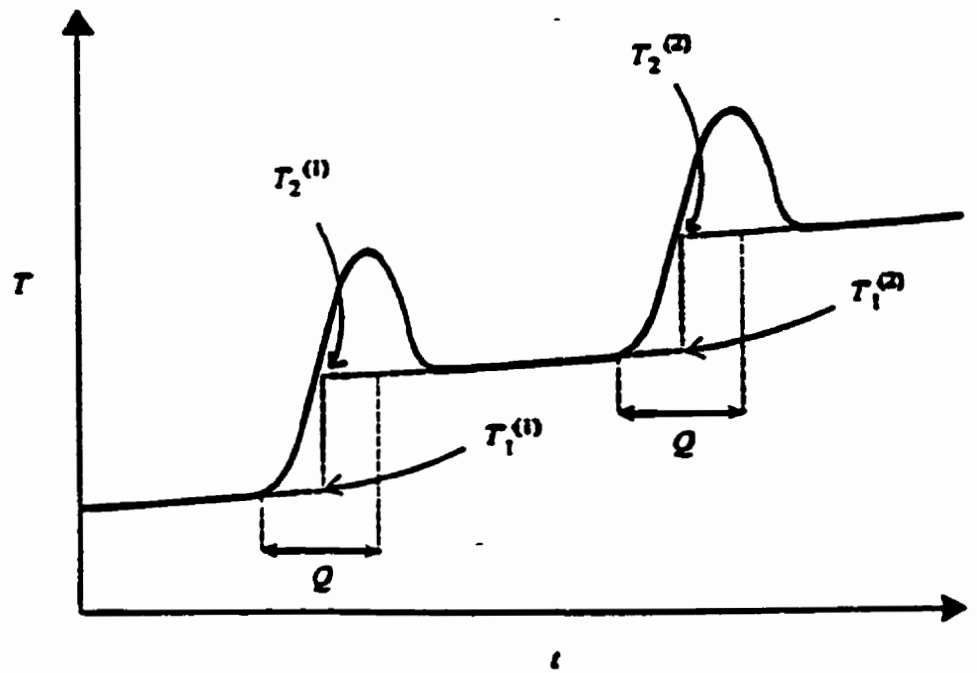

Figure 2.10 Schematic of temperature as a function of time during two heat capacity measurements by adiabatic heat-pulse calorimetry.[2.8]

2.3.3 Advantages and disadvantages of adiabatic calorimetry

As presented, adiabatic calorimeters can give very accurate heat capacities which are essential in the determination of such thermodynamic parameters such as entropy, enthalpy, and Gibbs energy. The major disadvantages are that these instruments are they not commercially available and data acquisition is tedious and intensive. Other advantages and disadvantages are summarized in Table 2.4[2.8].

Table 2.4 Advantages and disadvantages of adiabatic calorimetry[2,8].

Advantages	Disadvantages
Equilibrium measurements	Not available commercially
Absolute method	Slow method
Accurate heat capacity determinations	Generally only in heating direction
Can observe gradual contributions to heat capacity	May require large sample (ca. 1 g or more)
Sample morphology and geometry relatively unimportant	Requires adiabatic conditions

CHAPTER 3

UREA INCLUSION COMPOUNDS

3.1 Introduction

Urea inclusion compounds have been known since the 1940's when Bengen[3.1] accidentally discovered the formation of the needle-like crystals in a mixture of urea ($(NH_2)_2CO$, Figure 3.1) and milk. He was able to show that 1-octanol was included in the crystalline adduct. It was not understood until 1952 when Smith[3.2] presented the X-ray data which showed that urea formed a host framework in which guest molecules could reside. His paper is considered the birth of urea inclusion chemistry. Since then the field of urea inclusion chemistry has grown immensely, branching also into thiourea and selenourea inclusion compounds.

The structure of pure urea crystals is tetragonal (Figure 3.2) and they are held together by hydrogen bonds. In urea inclusion compounds the urea makes a hexagonal structure[3.2]. The urea molecules are held together by hydrogen bonds in helical ribbons (Figure 3.3) and woven together to form hexagonal channels (Figure 3.4). Each urea inclusion crystal grows either as a right-handed ($P6_122$) or left-handed ($P6_522$) enantiomorph. The channels are parallel to the c-axis and there are no connections between channels as in some channel-type materials (e.g. zeolites).

The chemistry of the urea inclusion compounds is related to the hydrogen bonding within the urea framework. The potential of the urea to hydrogen bond to the guest is limited because the hydrogen bonds in the urea framework point away from the channel

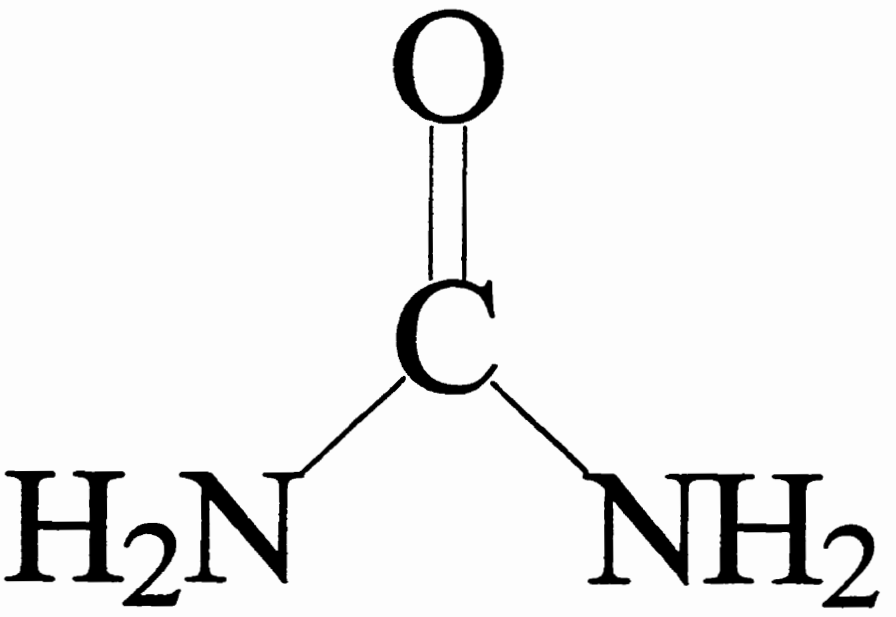

Figure 3.1 Chemical formula and structure of urea.

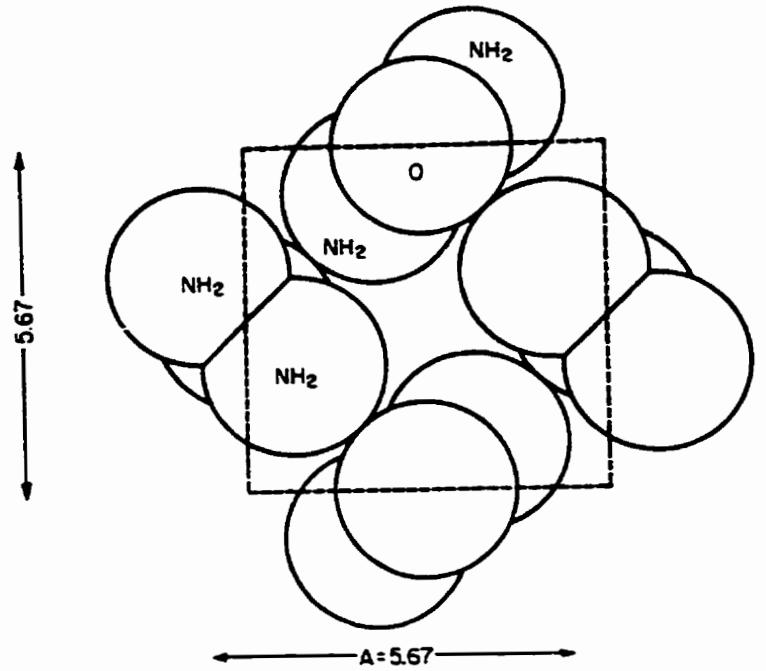

Figure 3.2 Pure urea packs with a tetragonal structure.[3.2]

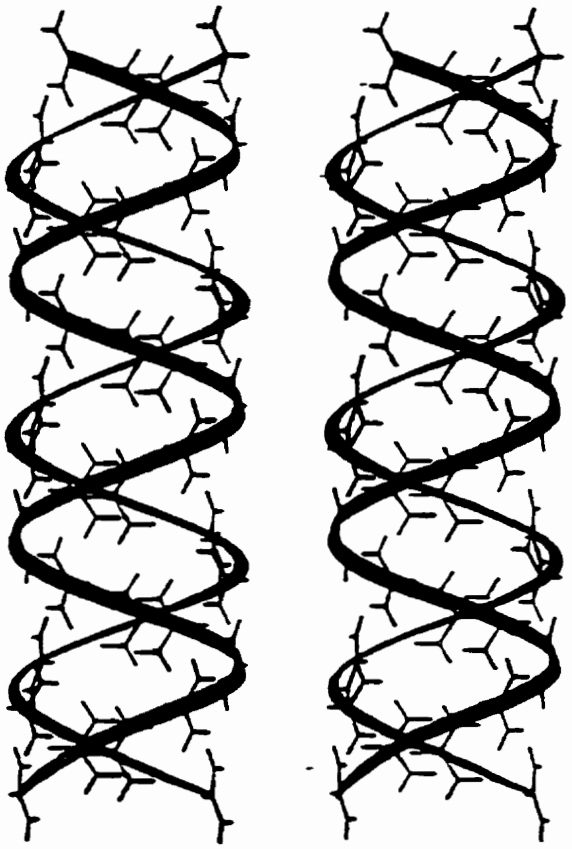

Figure 3.3 **Urea molecules in the inclusion compound are held together by hydrogen bonds in a helical ribbons. Both enantiomers are shown here.**[3.3]

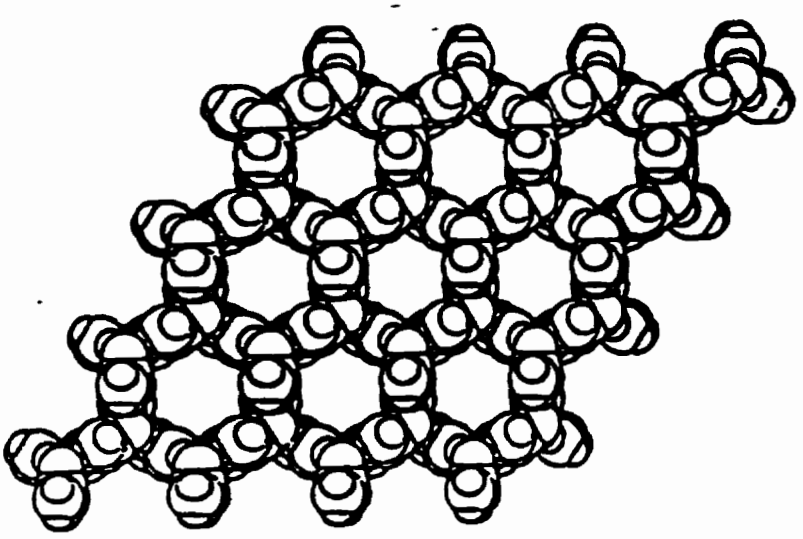

Figure 3.4 Hexagonal channels in urea inclusion compounds accommodate guest molecules.[3-4]

and only the faces of the urea molecule (the nitrogen atoms) are turned towards the guest. This leaves "smooth" channel walls and as a result the guest molecules are held only loosely (mainly van der Waals forces), thus for the purposes of our studies the inclusion compound can be considered to be a binary compound. This loose bonding allows for greater freedom such as torsion, libration, translation and reorientation within the channels. This freedom within the channel makes urea inclusion compounds nonstoichiometric. To determine the mole-ratio for the urea-*n*-alkanes one needs to know the length of the hydrocarbon included. Knowing the C-C bond distance is 1.54 Å, the C-C-C bond angle is 109°28′ and the van der Waals radius of a CH_3 group is 2.0 Å, the length of the hydrocarbon can be approximated by[3.2] :

$$l = 1.256\ (n - 1) + 4.0\ \text{Å} \qquad \textbf{(3.1)}$$

where l is the length of the hydrocarbon and n is the number of carbons in the hydrocarbon (assuming all trans configuration).

From the X-ray data the urea c-repeat distance is 11.01 Å and the number of ureas per unit cell is six. Knowing this in conjunction with the hydrocarbon length, the mole-ratio can be determined as follows[3.2] :

$$m = 0.6848\ (n - 1) + 2.181 \qquad \textbf{(3.2)}$$

where m is the mole-ratio and n is the number of carbons in the hydrocarbon.

The mole-ratio can also be determined using d.s.c. peak areas[3.5] From this treatment an equation for the mole-ratio is obtained :

$$m = 0.69\ n\ + 1.5 \qquad \textbf{(3.3)}$$

where m is the mole-ratio and n is the number of carbons in the hydrocarbon.

The urea inclusion compounds are selective as to the guest molecules that can be included since the repeat distance is 11.01 Å and the channel width is 5.50-5.80 Å[3.6]. Long-chain hydrocarbons, *n*-alkanes and *n*-alkenes, will all form inclusion compounds so long as the main carbon chain length is greater than six carbons. A carbon chain length of six is the lower limit for stable urea-paraffins[3.7]. Some substitution is allowed such as halogen substitution on the first carbon (e.g. 1-bromooctane), and for the smaller halogens (such as fluorine) substitution can occur on other carbons besides the first. For the oxygen derivatives of the *n*-alkanes and *n*-alkenes the hydroxyl and carbonyl group still allow inclusion compound formation.

Apart from inclusion with the *n*-alkanes and *n*-alkenes and their derivatives, urea will also form inclusion compounds with aldehydes, ketones, carboxylic acids, dicarboxylic acids, amines, nitriles, thioalcohols and thioethers provided their main carbon chain is sufficiently long (usually greater than or equal to six carbons). Some aromatics can form inclusion compounds as long as they contain a long chain substituent (e.g. octadecylbenzene).

The urea inclusion compound is not a static compound and the dynamics of both the motion of guests within the channel[3.3,3.8] and the host urea in the hexagonal lattice structure[3.9,3.10] have been studied.

3.2 Preparation of urea-hexadecane

Urea forms channel inclusion compounds with most long chain aliphatic hydrocarbons. As previously stated, the structure of pure urea is tetragonal, however in the presence of the long chain hydrocarbons the structure becomes hexagonal allowing for long channels in which the hydrocarbons are located[3.2]. This channel structure only allows a selected number of hydrocarbons to form inclusion compounds.

The formation of urea inclusion compounds is a simple matter[3.11]. Urea-hexadecane was prepared by the addition of hexadecane (Aldrich, 99%) (~5 mL) to powdered urea (Fisher, 98%) (saturated) in hot methanol (~30 mL). These crystals were filtered and washed with methanol and allowed to air dry. The urea-hexadecane was examined using d.s.c. and adiabatic calorimetry and compared to the literature values[3.12,3.13,3.14,3.15].

3.3 D.s.c. thermograms of urea and urea-hexadecane

A Pyris-1 Perkin-Elmer d.s.c. was used to examine the urea-hexadecane. The sample was lightly ground with a mortar and pestle to give finer crystals (which allows for better sample to pan contact). Aluminum pans and lids were used to contain the samples. The mass of the empty pan and lid was determined, the sample added and then the mass was determined again. The pan was then sealed with a press that crimped the lid tightly to the pan. To calibrate the instrument, a sample of high grade (Aldrich, 99.999 + %, m.p. 155 °C) indium was used. The indium melts at 428 K which falls close to the temperature region where urea-hexadecane melts.

Urea-hexadecane was heated at a scan rate of 10 K / min from 343 K to 433 K, then held isothermally for 1 minute, cooled down to 343 K at a scan rate of 10 K / min., then held isothermally for 60 minutes and then re-heated to 433 at 10 K / min. The sample showed two endothermic peaks on the first heating. On cooling and re-heating only one endothermic peak was observed (solidification and melting of urea). A sample of pure urea was run under the same conditions (except that it was held isothermally for 1 minute after cooling) and one endothermic peak was observed at 406 K (literature value: 406 K)[3.16] on the first heating. On cooling and re-heating, only one endothermic peak was observed (solidification and melting of urea). Plots of the thermographs (with the corrected onset temperatures) are given in Figure 3.5 and Figure 3.6.

The onset temperature is the temperature where the upside slope of the peak intersects the baseline. This is the point at which the compound begins to melt and is known as the onset temperature (Figure 3.7).

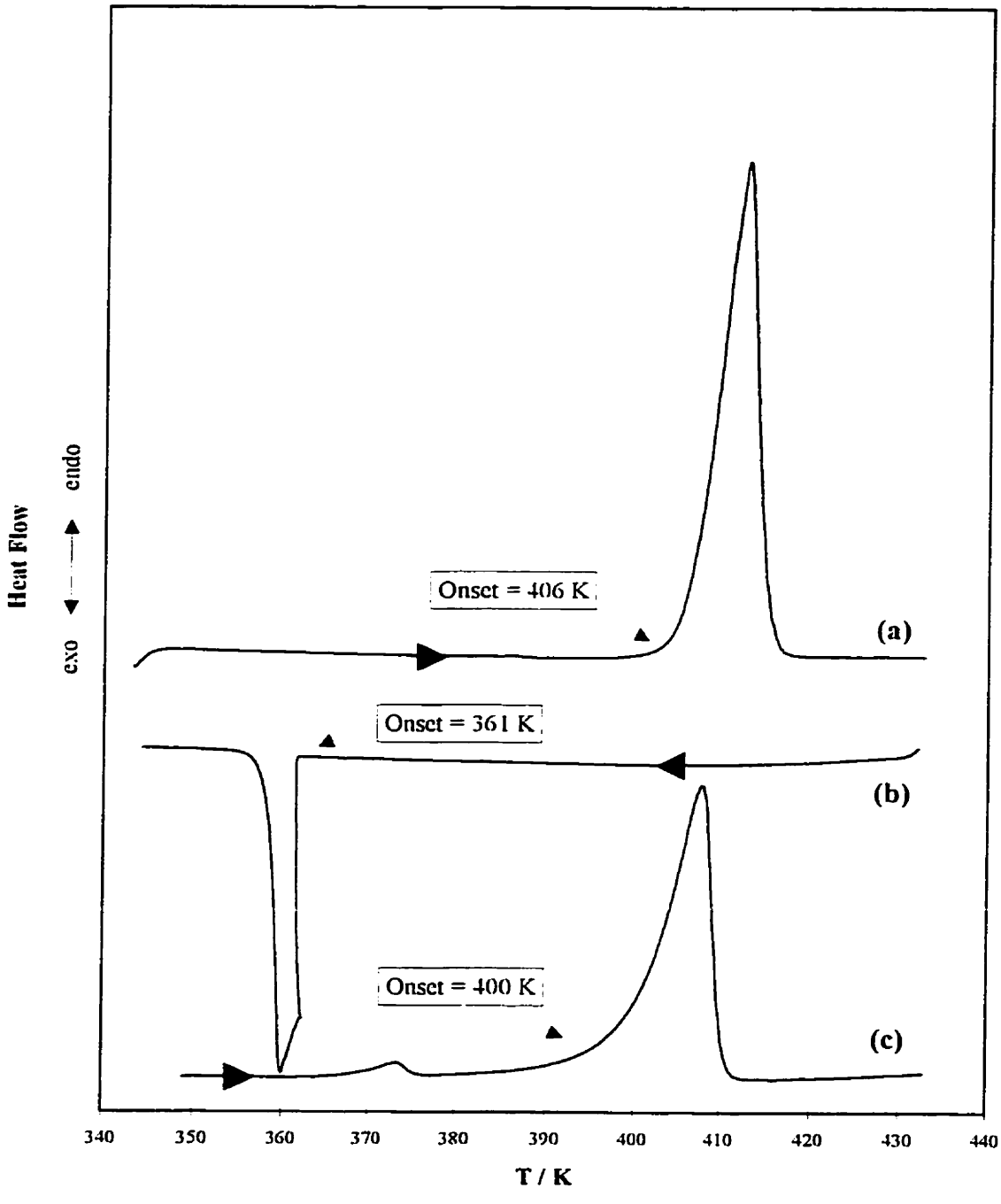

Figure 3.5 Heating and cooling d.s.c. thermograms of urea. (a) Heated from 343 - 433 K at 10 K / min. (b) Held at 433 K for 1 min, then cooled to 343 K at 10 K / min. (c) Held at 343 K for 1 min., then heated to 433 K at 10 K / min.

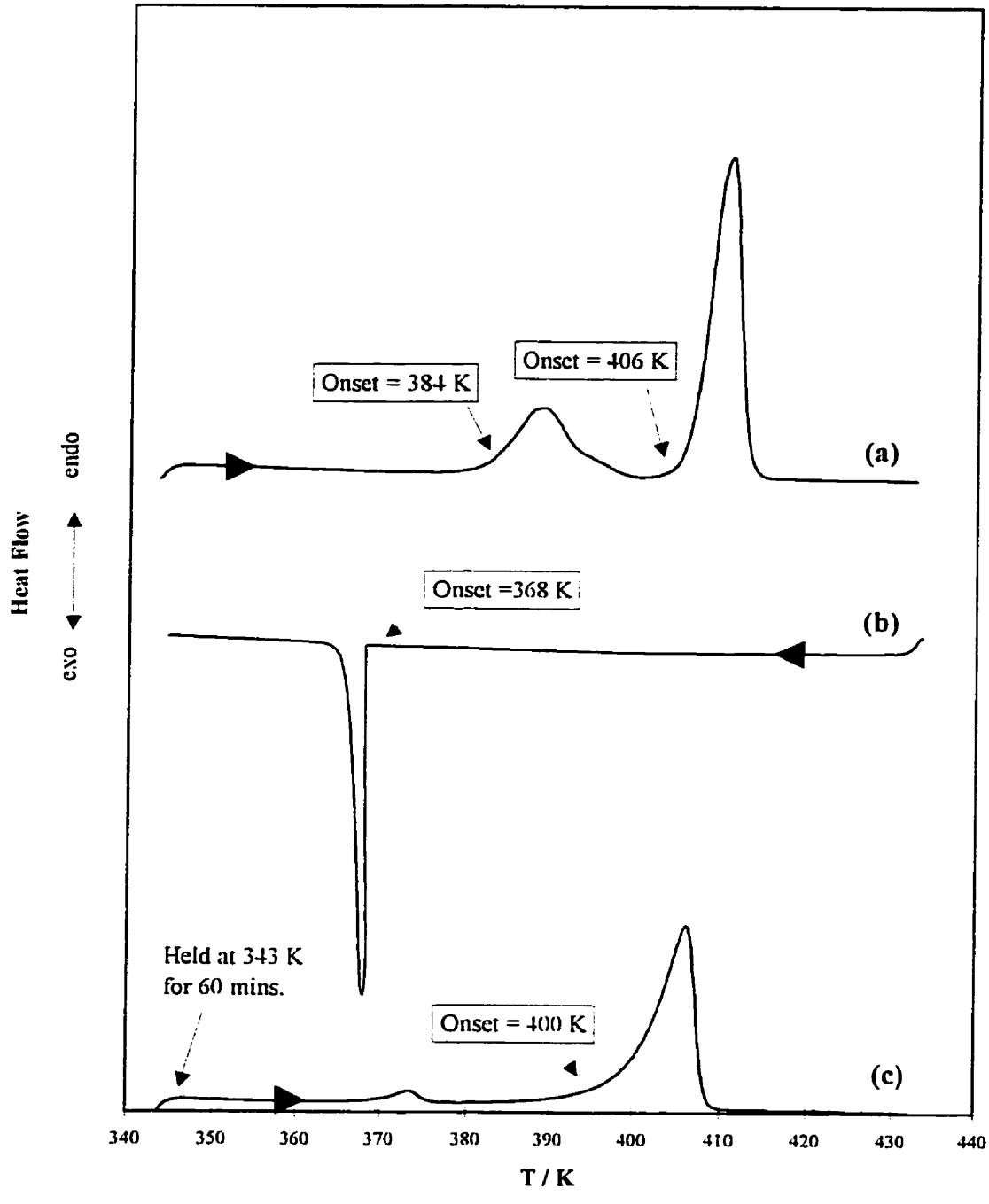

Figure 3.6 **Heating and cooling d.s.c. thermograms of urea-hexadecane. (a) Heated from 343 - 433 K at 10 K / min. (b) Held at 433 K for 1 min., then cooled to 343 K at 10 K / min. (c) Held at 343 K for 60 mins., then heated to 433 K at 10 K / min.**

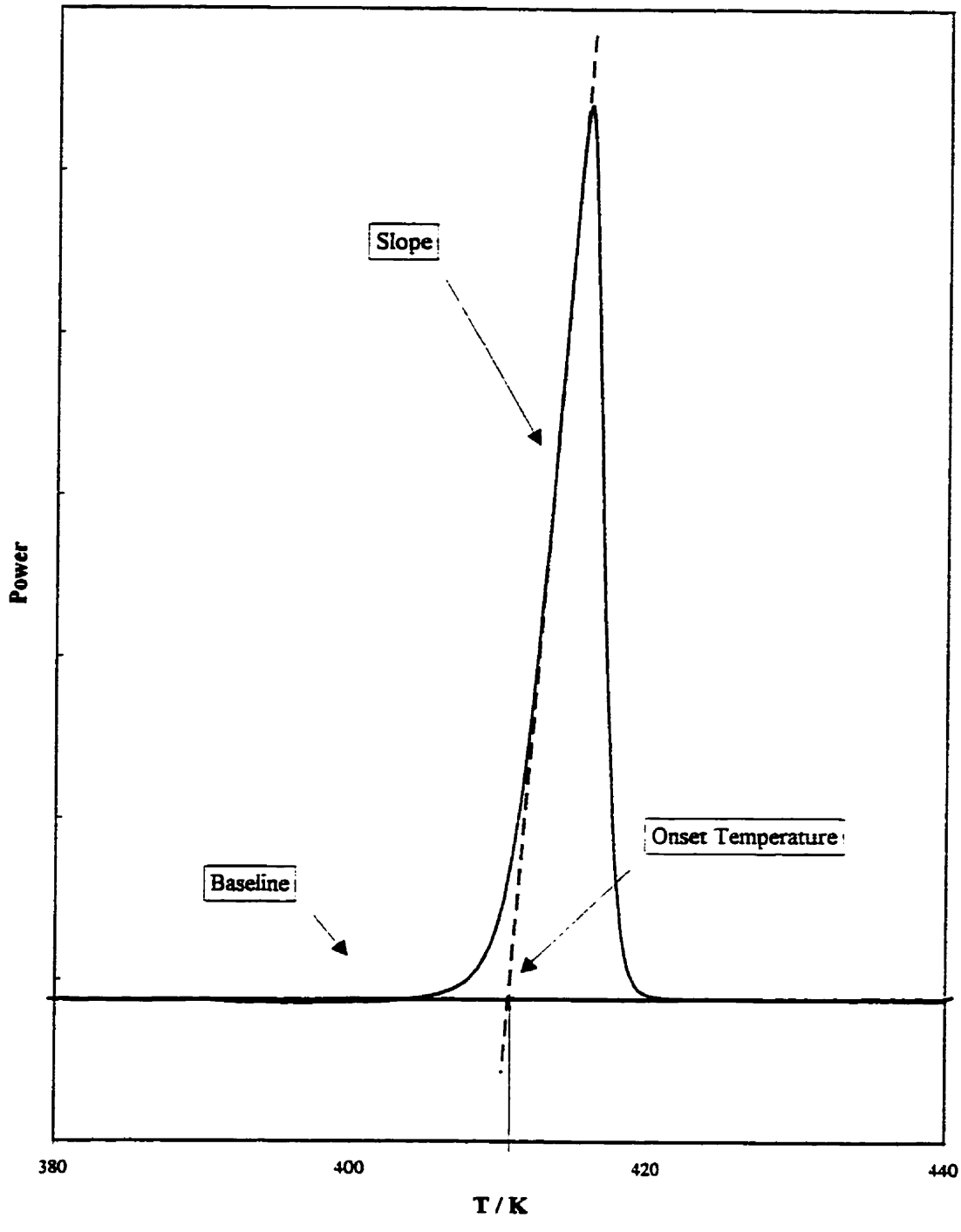

Figure 3.7 Simple diagram of an onset temperature.

As explained in Chapter 1, melting is either congruent or incongruent. By examining the thermographs one can conclude that the peak that occurs around 400 K in urea-hexadecane is due to the melting of solid urea. The low-temperature endotherm is attributed to the breakdown of the inclusion compound into urea (solid) and the hexadecane (liquid). The temperature of this endothermic peak does not correspond with the melting of the host or the guest and there is a peak at higher temperatures attributed to the melting of solid urea. This is incongruent melting. As temperature is increased, to the melting point, the polar urea and non-polar hexadecane would separate and form solid urea and liquid hexadecane (first endothermic peak). As the temperature is further increased, the solid urea melts and forms an immiscible solution of the two liquids.

Cooling of the urea-hexadecane results in only one peak. This peak is lower in temperature than the melting peak and is attributed to the solidification of urea. On re-heating, only one peak is observed. This peak is the melting peak of the urea (shifted slightly and lower in enthalpy due to some decomposition). This cooling and re-heating support the fact that urea-hexadecane melts incongruently and cannot be prepared directly from the melt.

From the areas of the endothermic peaks ($\Delta_{fus}H$), the mole-ratio of urea to hexadecane in the sample can be calculated. The $\Delta_{fus}H$ of the urea peak was determined to be 247 ± 2 J / g. The $\Delta_{fus}H$ of the urea-hexadecane peak was 189 ± 6 J / g. So in 1 gram of compound there is 0.772g urea or 0.0127 ± 0.0005 moles. The number of moles of hexadecane would therefore be $(1.0380 \pm 0.00013) \times 10^{-7}$. So the mole-ratio of urea to hexadecane is 12.25 ± 0.45.

3.4 Hot-stage microscopy

A single crystal of urea-hexadecane was melted on a hot-stage microscope and the melting behavior was observed. The hot-stage microscopy apparatus was supplied by D. Jackson of Biology, Dalhousie University. The apparatus consisted of a black and white video camera, a melting point apparatus and video recording instrument (S-VHS). Once the melting was recorded, still frames were captured on computer and arranged in order of increasing temperature followed by cooling (see Figure 3.8). The melting behavior observed is consistent with the d.s.c. results, *i.e.* incongruent melting :

$$\underset{}{\overset{T_1 = 384\ K}{\text{Urea-}C_{16}H_{34}(s) \rightarrow \text{Urea(s)} + C_{16}H_{34}(l)}} \overset{T_2 = 406\ K}{\rightarrow \text{Urea(l)} + C_{16}H_{34}(l)}$$

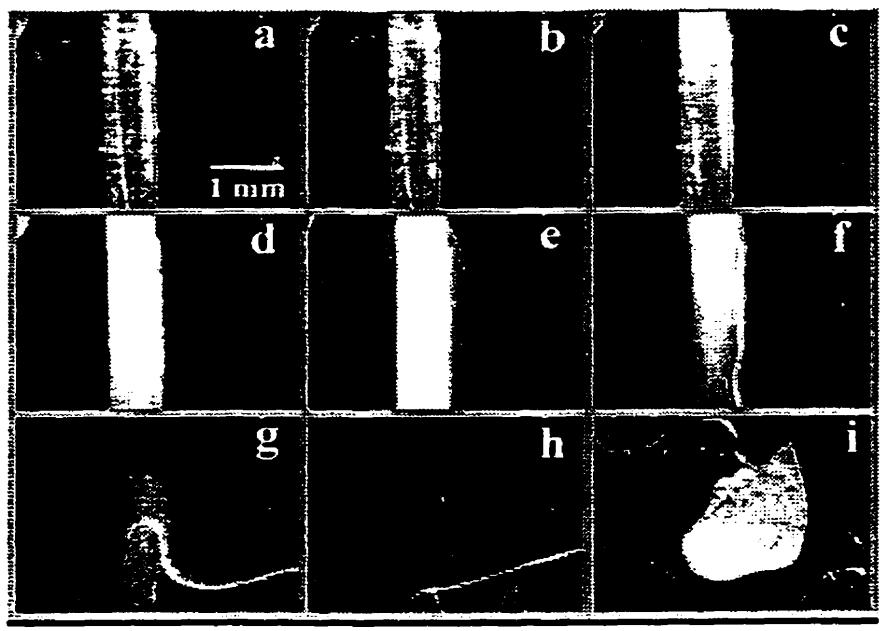

Figure 3.8 A needle of urea-hexadecane as it melts incongruently. a) Before heat is applied, b) the onset of melting of the inclusion compound, c),d), and e) various stages in the region of melting (urea(*s*) + hexadecane(*l*)), f) onset of the melting of the urea (*s*), g) and h) various stages after urea(*s*) has melted giving urea(*l*) + hexadecane(*l*). i) Solidification of urea upon cooling. The sample was heated on a melting point apparatus and filmed using a B&W video camera and recorded on S-VHS.

3.5 Heat capacity of urea and urea-hexadecane

In order to fully understand the thermal properties of a compound one must look at its properties at low temperature (below room temperature). The heat capacity data was used to calculate Gibbs energy.

The heat capacity for urea-hexadecane was obtained from 10 K to 300 K by Pemberton and Parsonage[3.13] and extrapolated to 380 K (no thermal anomalies were observed in the d.s.c.). The smooth fit data for urea-hexadecane is given in Table 3.1 and the graphs of heat capacity, H, S and G are given in Figures 3.9, 3.10, 3.11 and 3.12 respectively. The Gibbs energy (G) can be related directly to the heat capacity through the change in enthalpy (H) and the change in entropy (S) by the equation

$$G = H - TS\,. \tag{3.4}$$

The values for H and S are obtained from the heat capacity through the integrals

$$H(T) \equiv H(T) - H(T = 0K) = \int_{T=0K}^{T} C_p dT \tag{3.5}$$

and

$$S(T) \equiv S(T) - S(T = 0K) = \int_{T=0K}^{T} \frac{C_p}{T} dT\,. \tag{3.6}$$

These integrals were evaluated using Simpson's Rule and presented in Tables 3.1, 3.2 and 3.3.

The heat capacity for urea from 10 K to 310 K was obtained from Andersson, Matsuo, Suga and Ferloni[3.15] and presented in Table 3.2 and graphed as heat capacity, H, S and G in Figures 3.13, 3.14, 3.15 and 3.16 respectively. Finally the heat capacity, H, S

Table 3.1 Smooth heat capacity, H, S and G data for urea-hexadecane[3.13]

T	C_p	H	S	G
K	J K^{-1} (mol urea)$^{-1}$	J (mol urea)$^{-1}$	J K^{-1} (mol urea)$^{-1}$	J (mol urea)$^{-1}$
0	0	0	0	0
20	6.6	41	3.1	-20
40	21.8	320	12.1	-165
60	35.8	903	23.7	-522
80	46.4	1730	35.6	-1115
100	54.9	2747	46.9	-1941
120	62.5	3921	57.6	-2986
140	69.0	5238	67.7	-4240
160	75.7	6828	78.3	-5706
180	81.8	8404	87.6	-7366
200	89.1	10111	96.6	-9208
220	96.3	11966	105.4	-11229
240	103.7	13966	114.1	-13425
260	111.9	16120	122.7	-15794
280	120.4	18442	131.3	-18334
300	128.9	20933	139.9	-21047
(320)	(137.4)	(23596)	(148.5)	-(23932)
(340)	(145.9)	(26429)	(157.1)	-(26988)
(360)	(154.4)	(29431)	(165.7)	-(30216)
(380)	(162.8)	(32603)	(174.3)	-(33616)

Note : Data below 300 K is from reference 3.13.
Data above 300 K is by extrapolation.

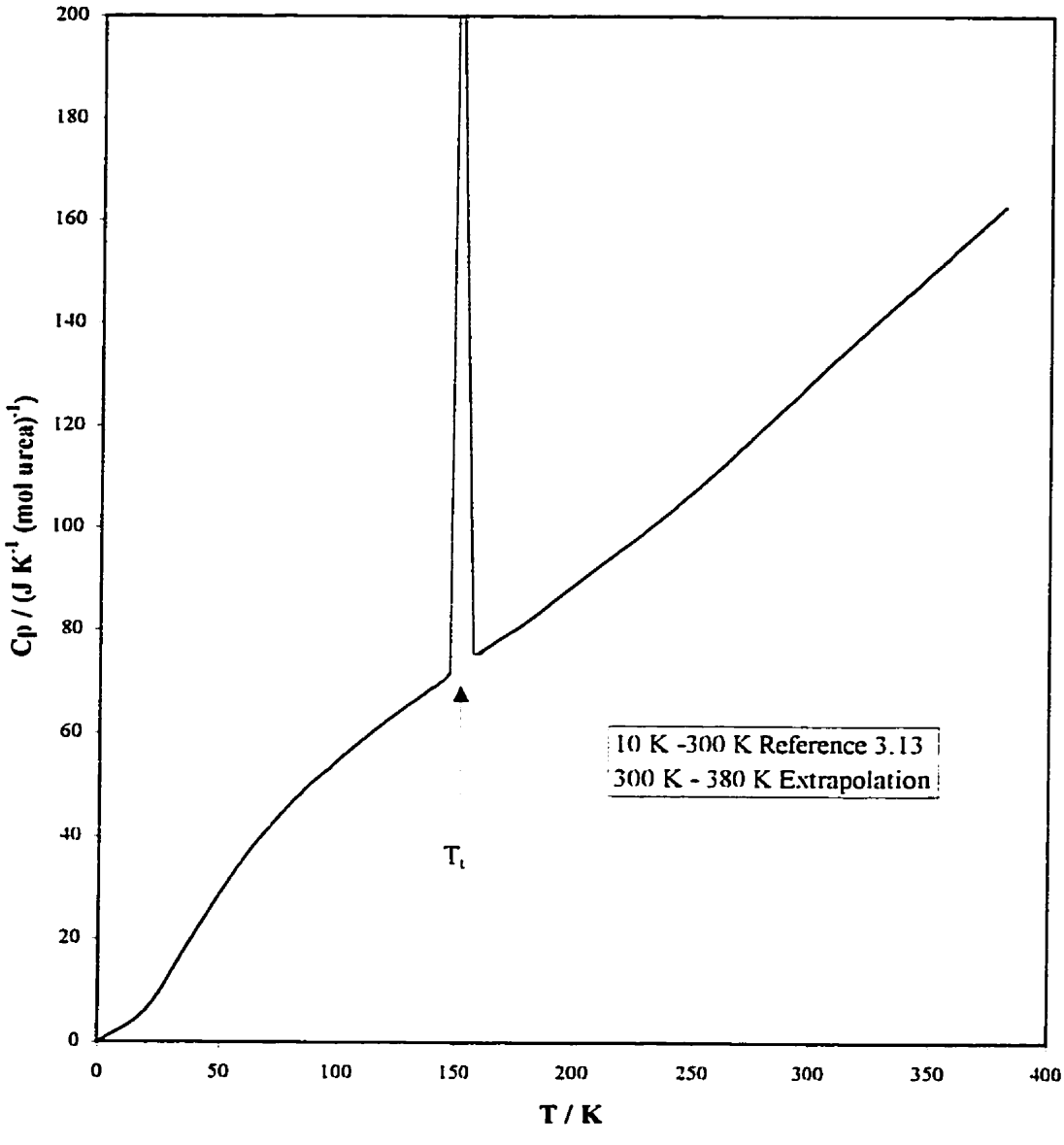

Figure 3.9 Heat capacity (C_p) of urea-hexadecane

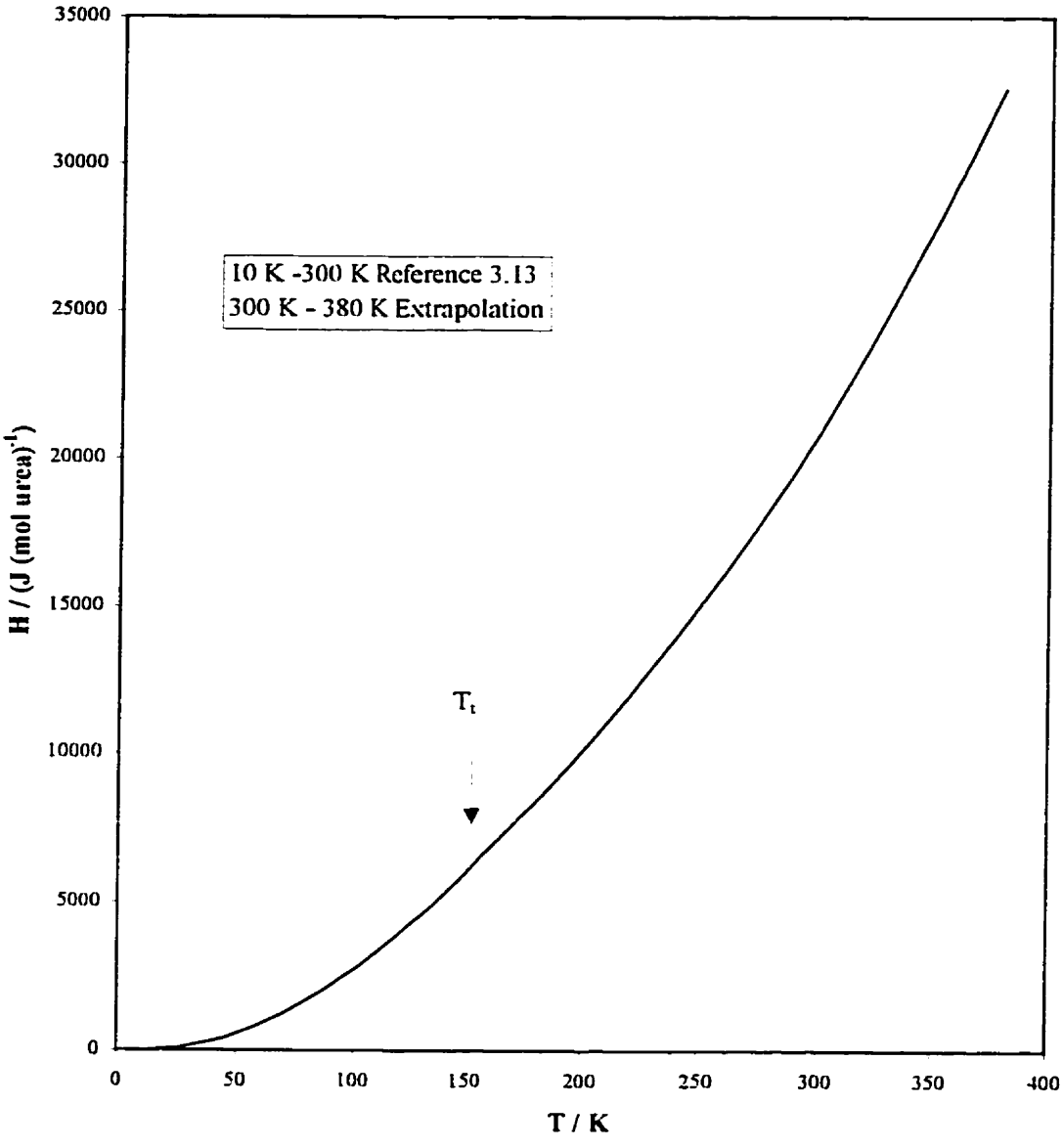

Figure 3.10 **Enthalpy (H) of urea-hexadecane**

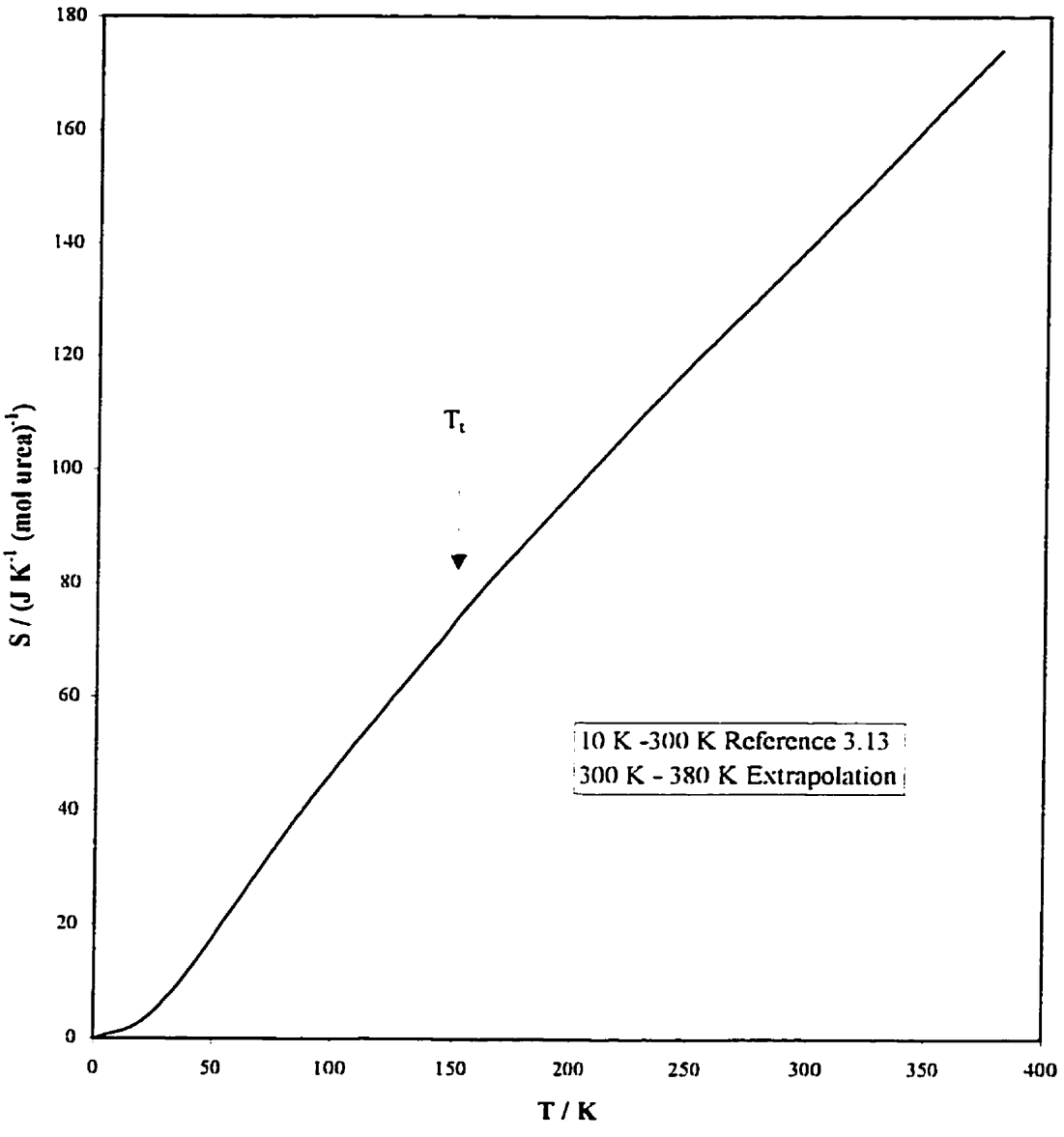

Figure 3.11 Entropy (S) of urea-hexadecane

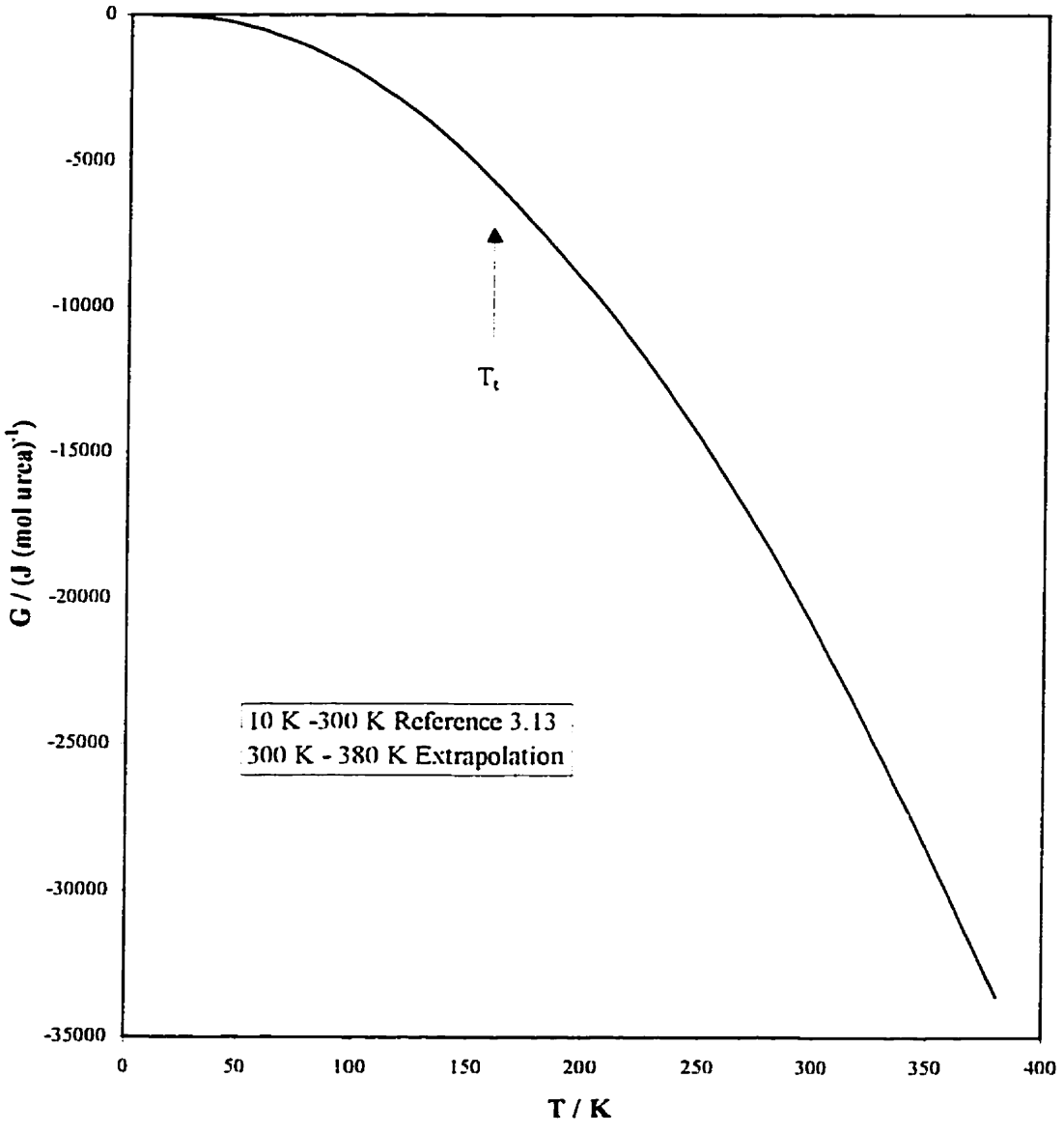

Figure 3.12 Gibbs energy (G) of urea-hexadecane

Table 3.2 **Smooth heat capacity, H, S and G data for urea[3.15]**

T	C_p	H	S	G
K	J K^{-1} mol^{-1}	J mol^{-1}	J K^{-1} mol^{-1}	J mol^{-1}
0	0	0	0	0
20	5.1	29	2.1	-13
40	18.0	259	9.5	-122
60	28.3	728	18.9	-406
80	35.6	1370	28.1	-877
100	41.3	2140	36.7	-1525
120	46.2	3015	44.6	-2339
140	51.2	3988	52.1	-3307
160	56.3	5063	59.3	-4421
180	61.5	6240	66.2	-5677
200	66.8	7522	73.0	-7068
220	72.1	8911	79.6	-8594
240	77.4	10405	86.1	-10250
260	82.7	12006	92.5	-12036
280	88.0	13712	98.8	-13948
300	93.3	15525	105.0	-15987
(320)	(98.4)	(17442)	(111.2)	-(18150)
(340)	(103.6)	(19462)	(117.3)	-(20435)
(360)	(108.9)	(21587)	(123.4)	-(22843)
(380)	(114.1)	(23817)	(129.4)	-(25372)
(400)	(119.3)	(26151)	(135.4)	-(28020)

Note : Data above 300 K is by extrapolation; otherwise data is from ref. 3.15

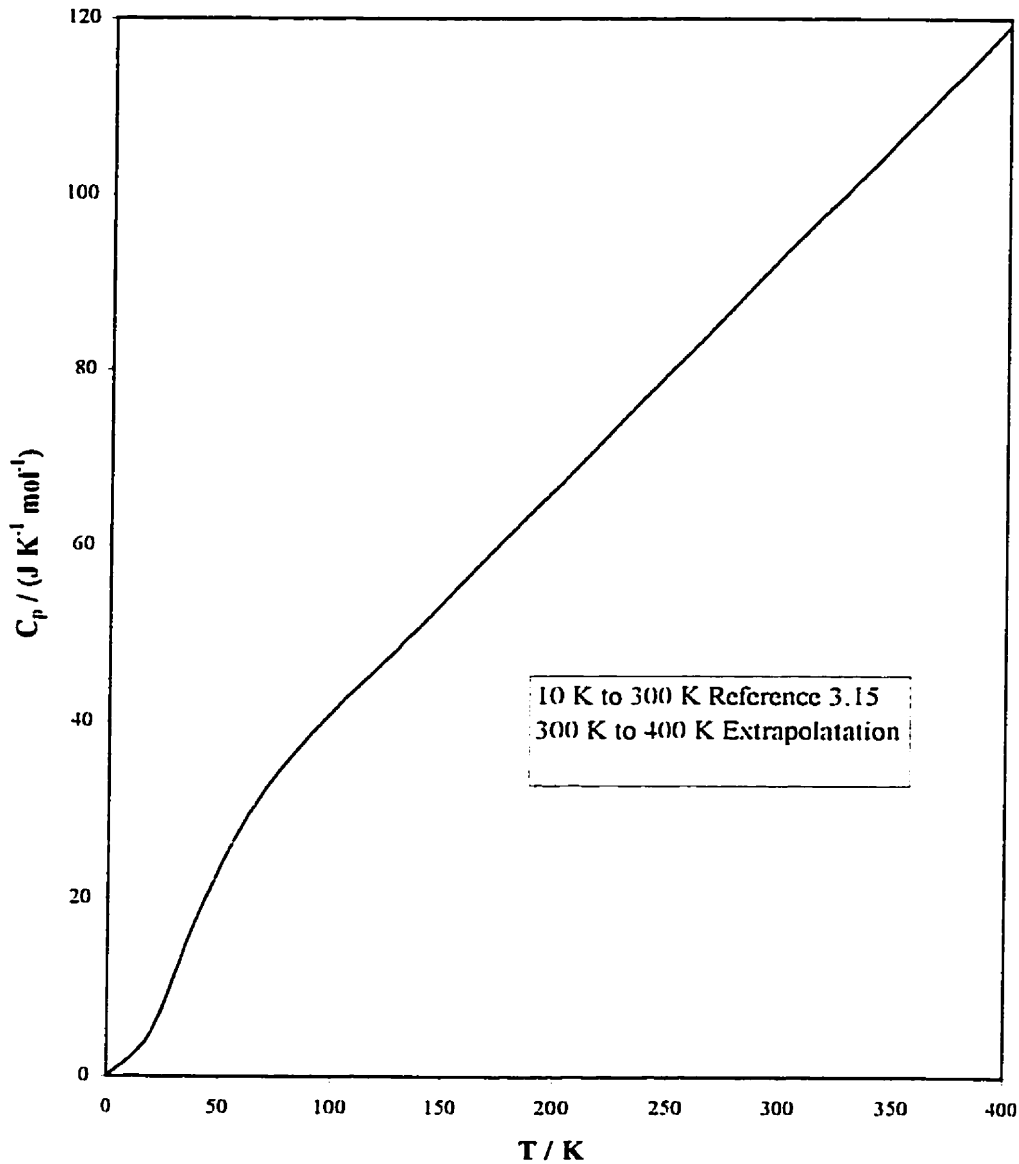

Figure 3.13 **Heat capacity (C_p) of urea**

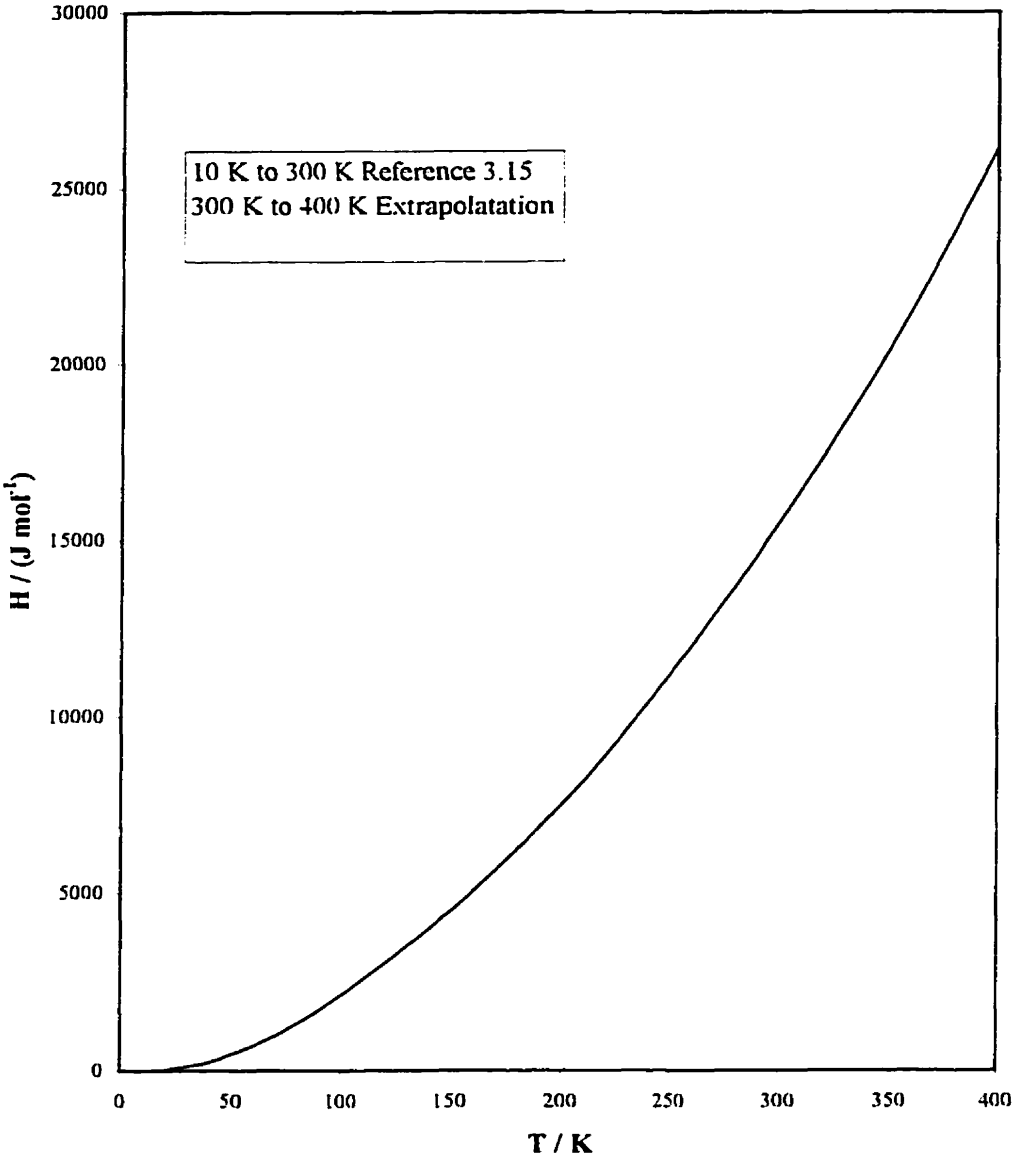

Figure 3.14 Enthalpy (H) of urea

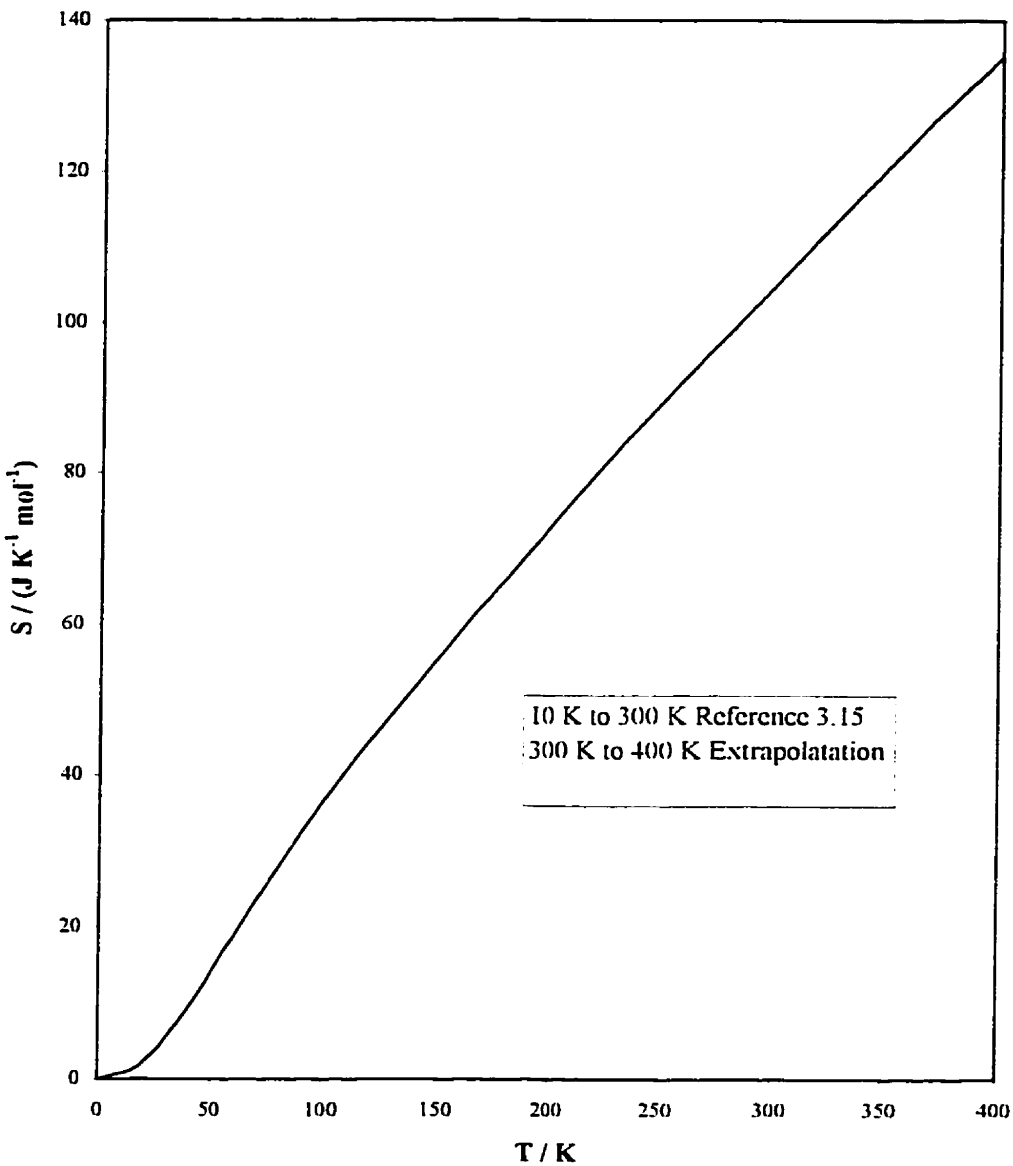

Figure 3.15 Entropy (S) of urea

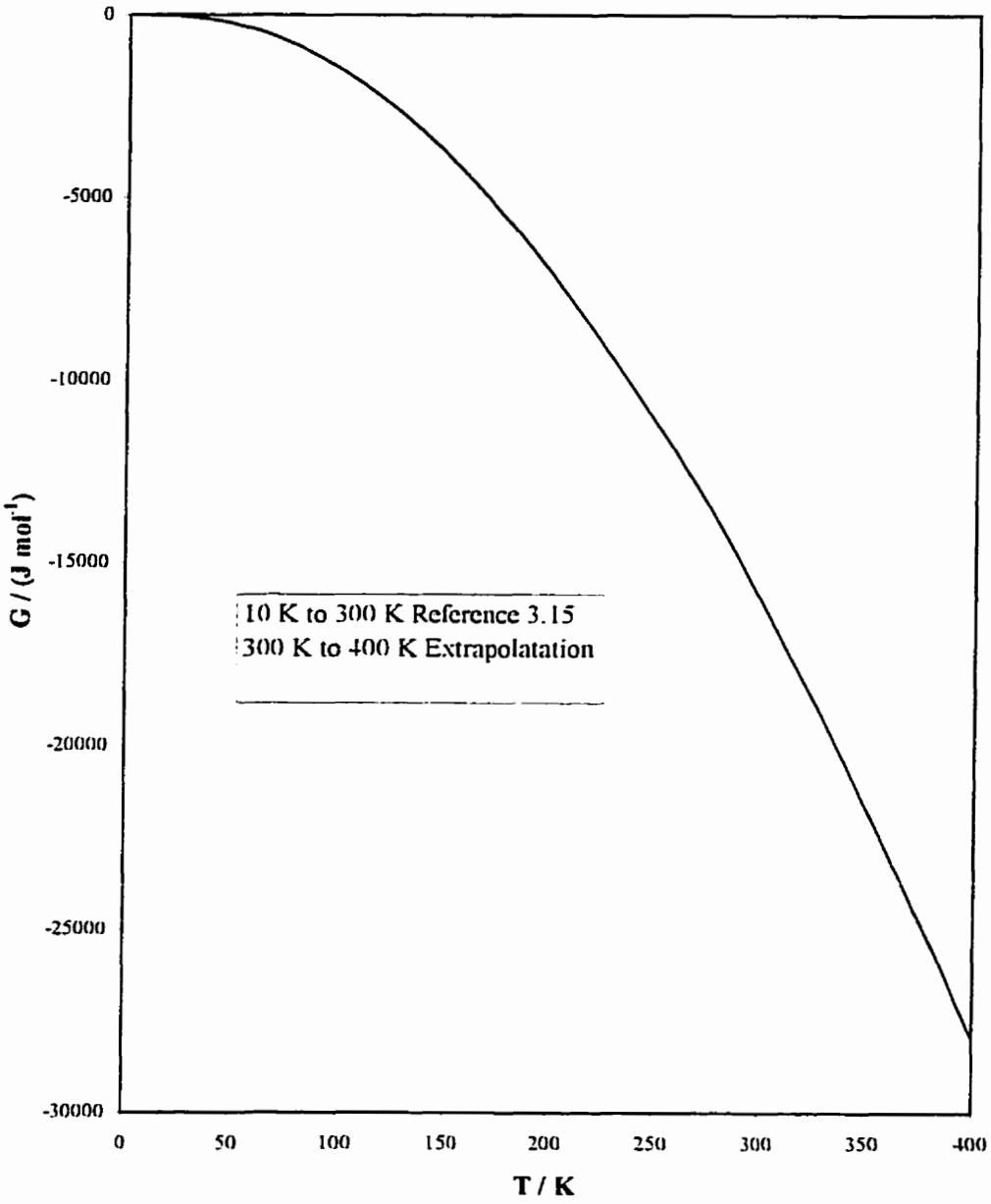

Figure 3.16 Gibbs energy (G) of urea

and G for hexadecane from 12 K to 320 K was obtained from Finke, Gross, Waddington, and Huffman[3.14] and presented in Table 3.3 and graphed in Figures 3.17, 3.18, 3.19 and 3.20. A greater treatment of the data is given in Section 3.6.

Table 3.3 **Heat capacity, H, S and G data for hexadecane[3.14]**

T	C_p	H	S	G
K	J K^{-1} mol^{-1}	J mol^{-1}	J K^{-1} mol^{-1}	J mol^{-1}
0	0	0	0	0
20	17.2	95	6.7	-40
40	64.5	905	32.9	-412
60	110.8	2669	68.0	-1413
80	147.8	5265	105.1	-3146
100	176.9	8517	141.3	-5613
120	200.9	12296	175.7	-8785
140	222.2	16534	208.3	-12628
160	242.2	21179	239.3	-17107
180	262.1	26218	268.9	-22191
200	283.2	31662	297.6	-27858
220	306.1	37547	325.6	-34091
240	331.5	43909	353.3	-40880
260	361.8	50842	381.0	-48223
280	400.3	58447	409.2	-56124
300	502.7	120612	622.7	-66185
320	515.1	130789	655.5	-78968
(340)	(527.7)	(141217)	(687.1)	-(92396)
(360)	(540.3)	(151896)	(717.6)	-(106445)
(380)	(552.9)	(162828)	(747.2)	-(121094)
(400)	(565.5)	(174012)	(775.8)	-(136326)
(420)	(578.1)	(185447)	(803.7)	-(152123)

Note : Data above 320 K is by extrapolation; otherwise data is from ref. 3.14

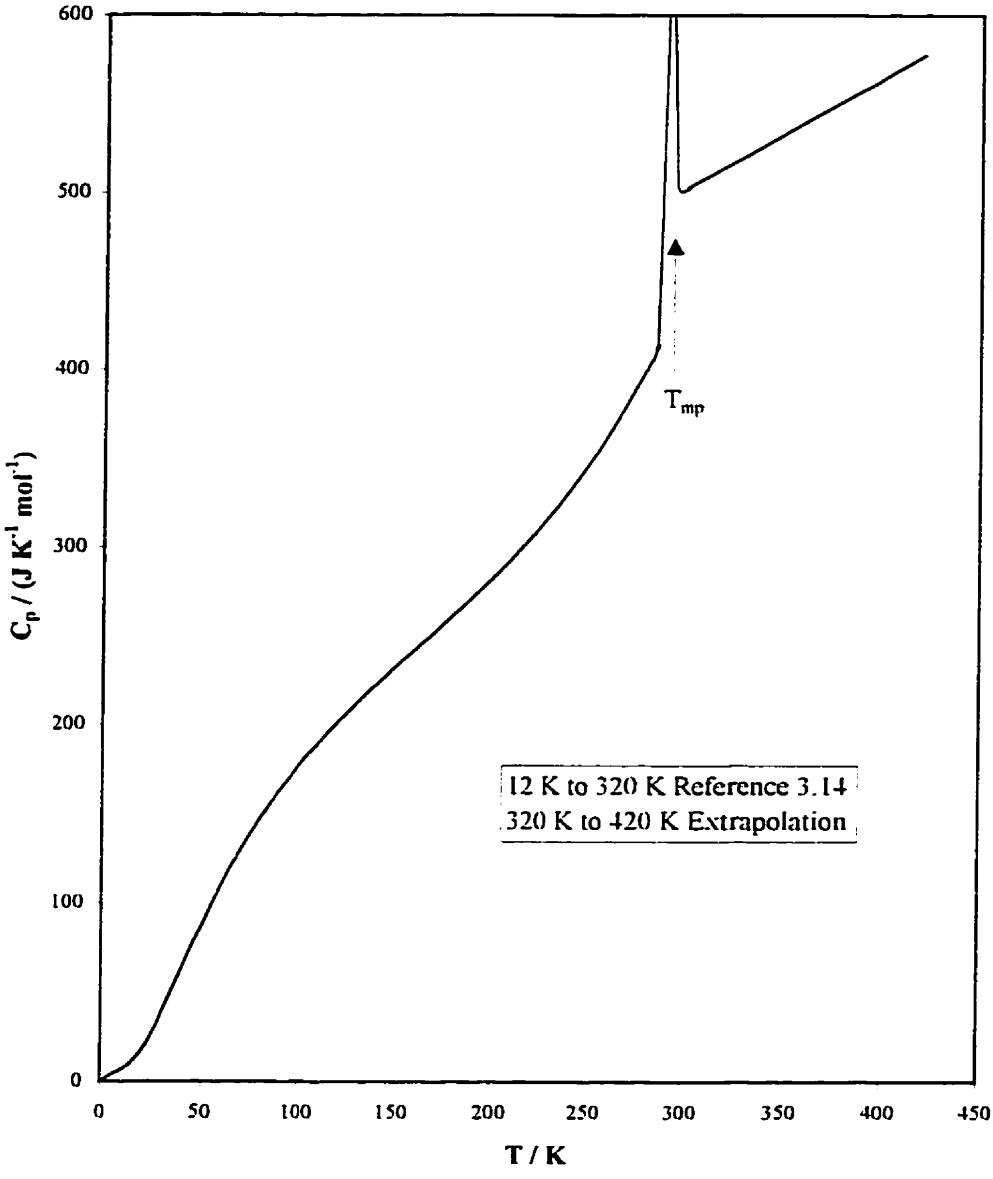

Figure 3.17 Heat capacity (C_p) of hexadecane

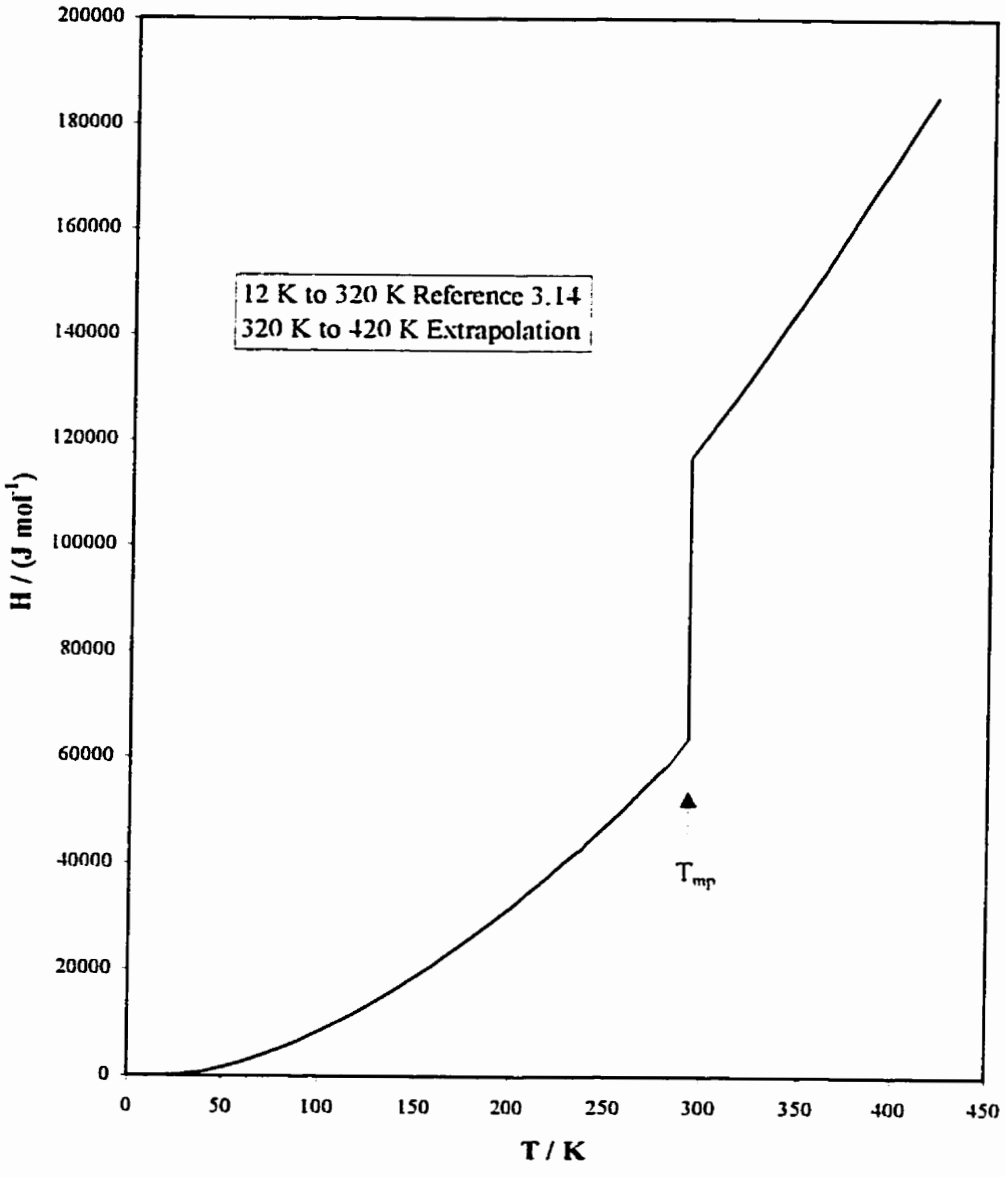

Figure 3.18 **Enthalpy (H) of hexadecane**

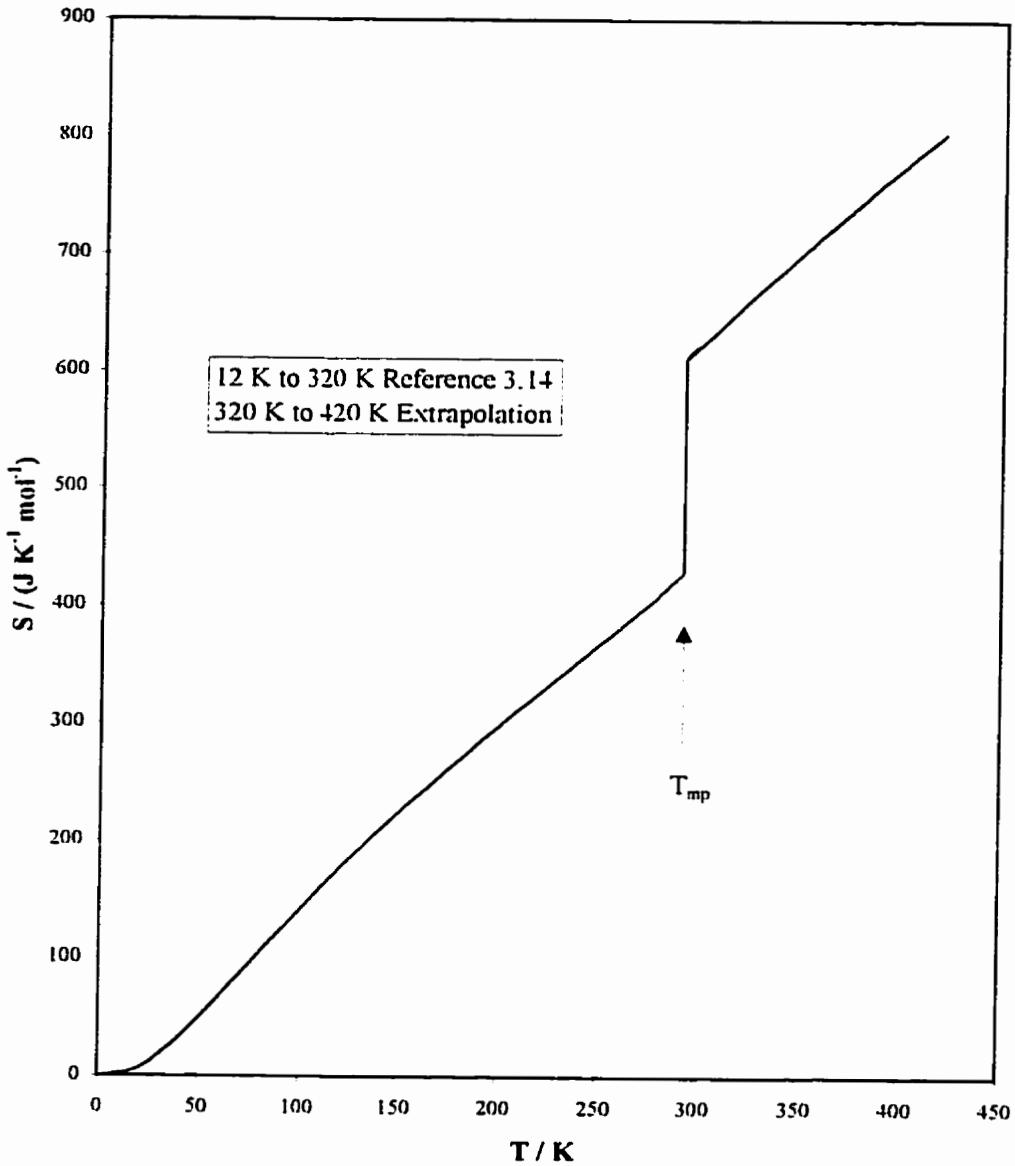

Figure 3.19 **Entropy (S) of hexadecane**

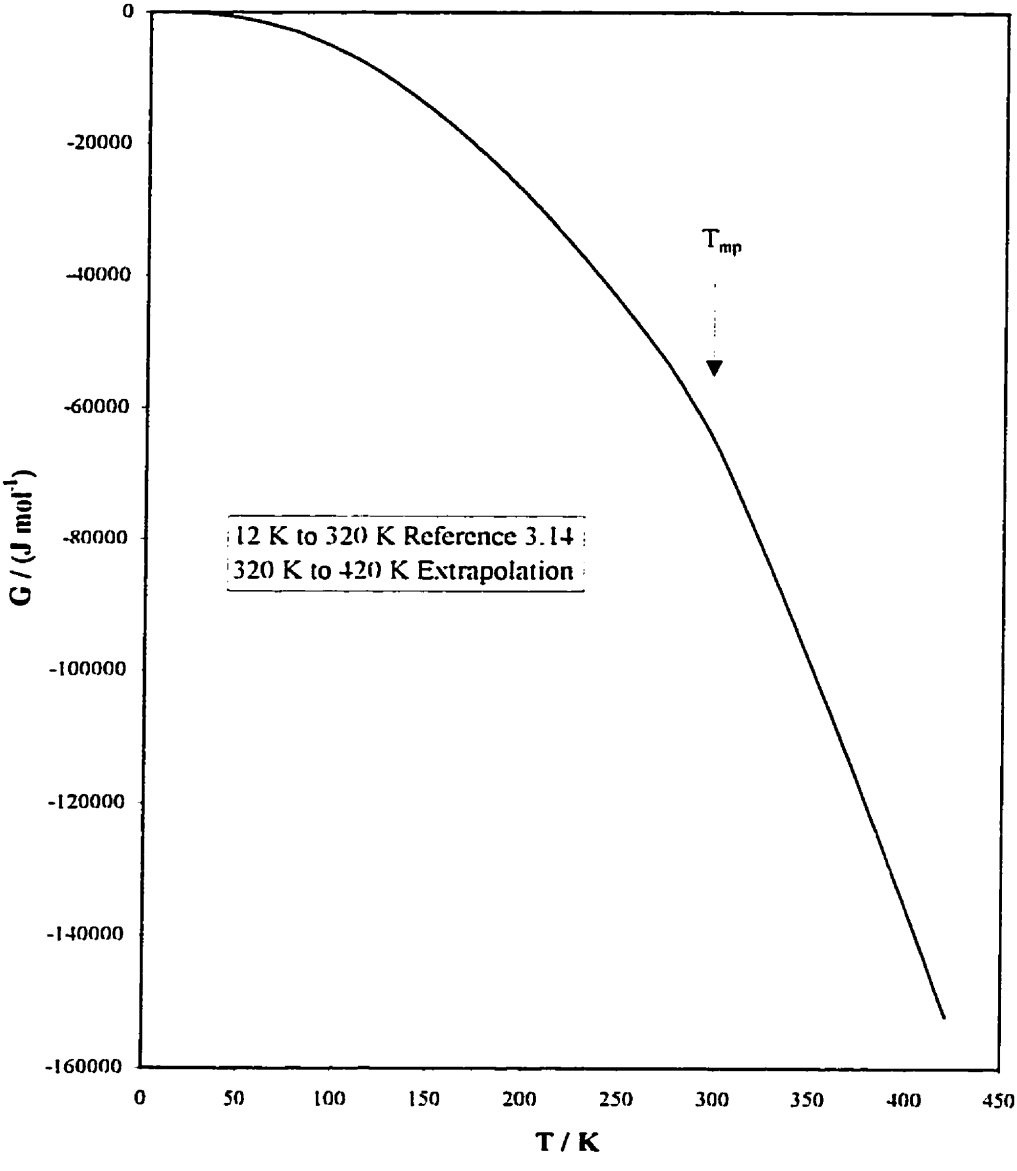

Figure 3.20 Gibbs energy (G) of hexadecane

3.6 Gibbs energy of urea-hexadecane

As explained before, the Gibbs energy is an indication of the stability of a compound. It was proposed, from the d.s.c. thermographs of urea-hexadecane (Section 3.3) that when the inclusion compounds melts, it melts into solid urea and liquid hexadecane. This incongruent melting was confirmed by hot-stage microscopy. From the thermodynamic analysis, the Gibbs energy for the solid urea plus liquid hexadecane is lower than the Gibbs energy for the inclusion compound ($G_{host}+G_{guest} < G_{inclusion\ compound}$) (Table 3.4 and in Figure 3.21). At the melting point of the inclusion compound (384 K) the lower energy system (solid host + liquid guest) is preferred and the compound melts incongruently.

Table 3.4 Gibbs energies of urea, hexadecane and urea-hexadecane (IC)

T	$G_{(IC)}$	$G_{(Urea)}^{3.15}$	$G_{(Hexadecane)}^{3.14}$	$G_{(Urea+\ 1/12.25\ Hexadecane)}$
K	J (mol urea)$^{-1}$	J mol^{-1}	J mol^{-1}	J (mol urea)$^{-1}$
0	0	0	0	0
20	-20	-13	-40	-16
40	-165	-122	-412	-157
60	-522	-406	-1413	-524
80	-1115	-877	-3146	-1139
100	-1941	-1525	-5613	-1993
120	-2986	-2339	-8785	-3071
140	-4240	-3307	-12628	-4359
160	-5706	-4421	-17107	-5847
180	-7366	-5677	-22191	-7526
200	-9208	-7068	-27858	-9390
220	-11229	-8594	-34091	-11435
240	-13425	-10250	-40880	-13657
260	-15794	-12036	-48223	-16054
280	-18334	-13948	-56124	-18625
300	-21047	-15987	-66185	-21502
320	-23932	-18150	-78968	-24730
340	-26988	-20435	-92396	-28135
360	-30216	-22843	-106445	-31713
380	-33616	-25372	-121094	-35463
400	-37186	-28020	-136326	-39381
420	-40929	-30789	-152123	-43466

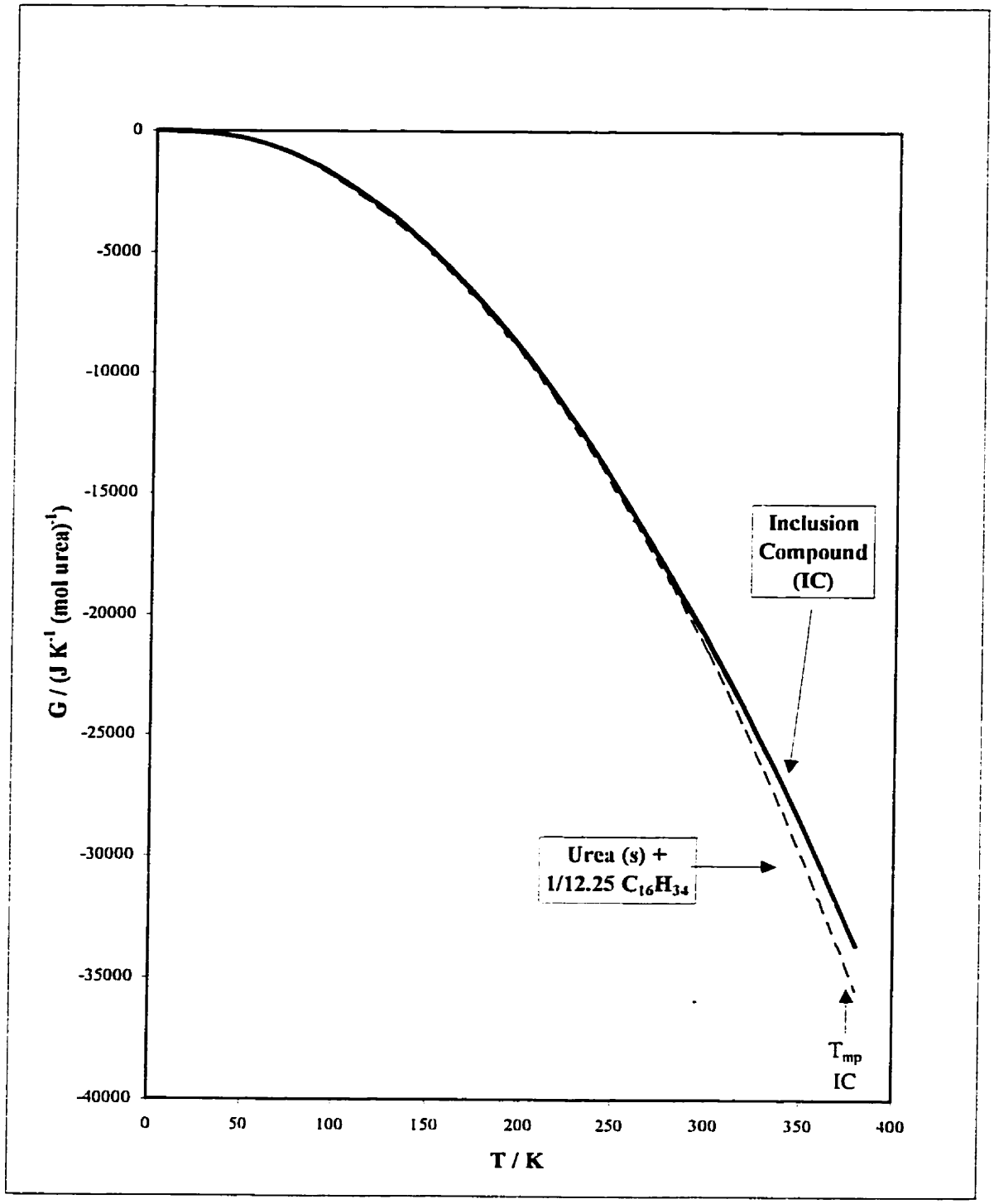

Figure 3.21 Gibbs energy diagram for urea-hexadecane and urea + 1/12.25 hexadecane

3.7 Phase diagram

To calculate the phase diagram for urea-hexadecane, the method derived by M. Farina *et al.*[3.19] was used.

For an AB_n inclusion compound and referring to Figure 3.22, the solid-liquid equilibrium can be expressed by the following [3.3] :

$$\text{Curve A-E}_1: \quad \ln(1 - X_B) = -\frac{L_B}{RT} + \text{A} \tag{3.7}$$

$$\text{Curve E}_1\text{-E}_2: \quad \ln(1 - X_B) + n \ln X_B = -\frac{L_C}{RT} + \text{C} \tag{3.8}$$

$$\text{Curve E}_2\text{-B}: \quad \ln X_B = -\frac{L_B}{RT} + \text{B} \tag{3.9}$$

where X_B is the mole fraction of component B; $A = L_A/RT_A$; $B = L_B/RT_B$; $C = (L_C/RT_C) + n\ln n-(n+1)\ln(n+1)$; L_A, L_B and L_C are the melting enthalpies ($\Delta_{fus}H$) of the corresponding components and T_A, T_B and T_C are the melting temperatures of the corresponding components, where C is the compound AB_n.

This method assumes the following: complete immisibility of the solid phases, absence of solid metastable phases, instability of the adduct in the liquid phase, ideal behavior of the liquid phase and constancy of all the melting enthalpies with temperature.

For urea-hexadecane, the liquid phase is non-ideal (hexadecane and urea are immiscible). This non-ideality is due to the difference in polarity of the two pure components (urea - polar ; hexadecane - non-polar). To account for this non-ideality an interaction term, W, is introduced to Eqs. (3.7)-(3.9) leading to the following new equations[3.3] :

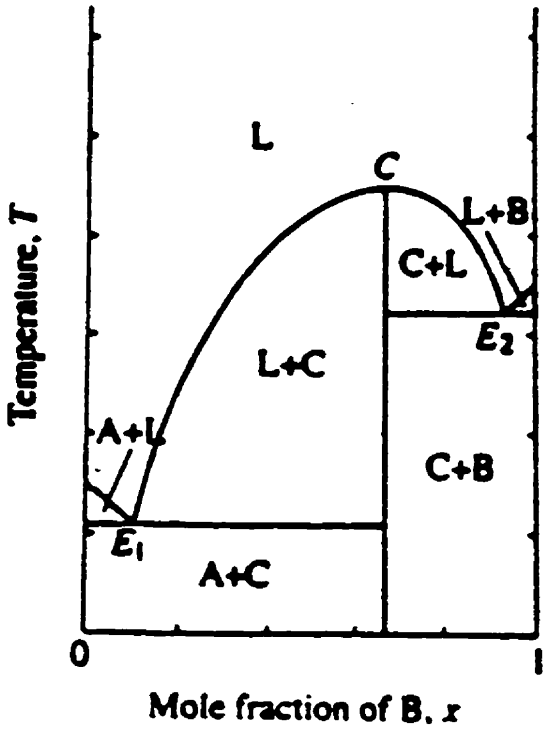

Figure 3.22 T/*x* diagram of a hypothetical AB_2 adduct.[3.19]

Curve A-E_1: $$\ln(1 - X_B) = -\frac{L_B}{RT} + A - (\frac{W}{RT}) X_B^2 \quad \textbf{(3.10)}$$

Curve E_1-E_2: $$\ln(1 - X_B) + n \ln X_B = -\frac{L_C}{RT} + C - (\frac{W}{RT})\{X_B^2 + n(1 - X_B)^2 - [\frac{n}{(n+1)}]\} \quad \textbf{(3.11)}$$

Curve E_2-B: $$\ln X_B = -\frac{L_B}{RT} + B - (\frac{W}{RT})(1 - X_B)^2 \quad \textbf{(3.12)}$$

Note that equations (3.7)-(3.9) follow from (3.10)-(3.12) with W=0 (ideal case).

The best fit value for W for urea-hexadecane that agrees with the observed melting behavior, was found to be 18 kJ / mol. This large interaction term is consistent with the finding that liquid-liquid phase separation is favored for $W > 2RT$,[3.20] and W is comparable to the value found for the $C_{24}F_{50}$-PHTP phase diagram.[3.3] Table 3.5 contains the melting temperatures and melting enthalpies used to calculate the phase diagram shown in Figure 3.23. The value *n* denotes the mole ratio of urea to hexadecane, which in this case is equal to 12.25 ± 0.45. The phase diagram is consistent with the experimental results in that it shows incongruent melting of urea-hexadecane at its melting temperature.

Table 3.5 The melting temperatures and enthalpies of urea, urea-hexadecane and hexadecane

	Melting temperature (T)	
Hexadecane	291.34 K	Ref. #3.14
Urea	406 ± 1 K	Present work
Urea-hexadecane	384 ● 1 K	Present work

	Melting enthalpies (L)	
Hexadecane	53.36 kJ mol^{-1}	Ref. #3.14
Urea	14.4 ± 0.9 kJ mol^{-1}	Present work
Urea-hexadecane	6.4 ± 0.3 kJ mol^{-1}	Present work

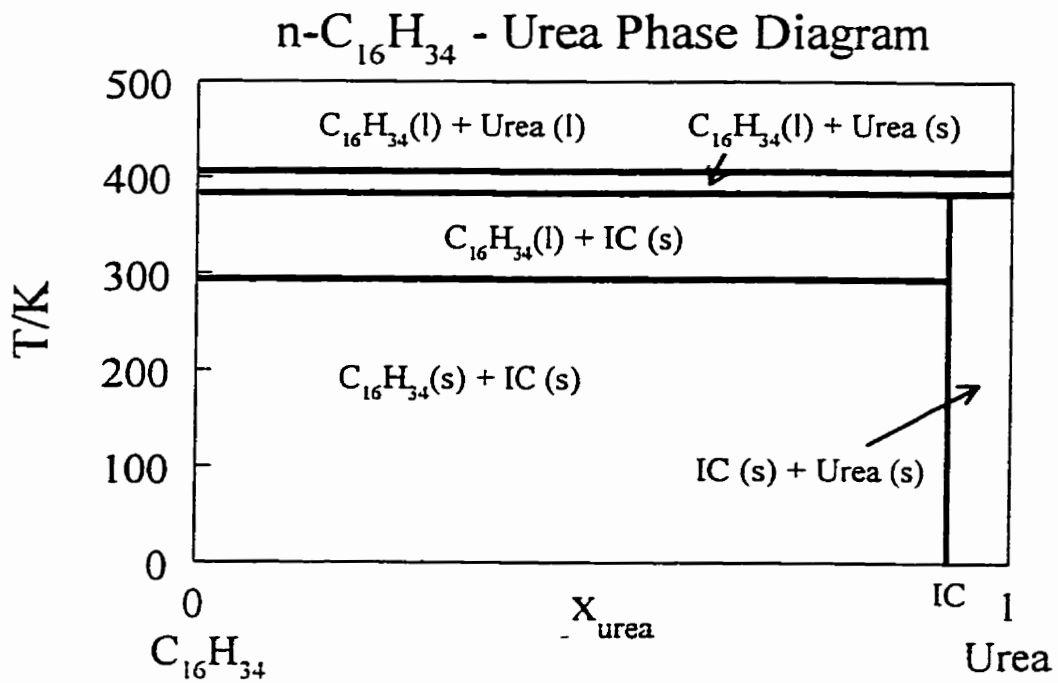

Figure 3.23 **Calculated phase diagram of urea-hexadecane (based on the method of Farina *et al.*[3.16]). IC = inclusion compound.**

CHAPTER 4

PHTP INCLUSION COMPOUNDS

4.1 Introduction

The molecule perhydrotriphenylene (PHTP ; see Figure 4.1 for structure) has only been known for a short period of time. It was first synthesized in 1963[4.1] as a model to study optically active polymers. PHTP can exist in ten stereoisomeric forms. Of the ten, six are enantiometric pairs (either right handed or left handed) and four are meso-forms (containing at least one mirror plane)[4.2] (Figure 4.1). Naming of these stereoisomers is based on the central carbon ring in which the carbon-carbon bonds are divided evenly into two classes, *endo*-cyclic and *exo*-cyclic. The *endo*-cyclic bonds are named either *cis* or *trans* (C or T) and the *exo*-cyclic bonds are named *syn* or *anti* (S or A). Of these isomers, only the ATATAT isomer (racemic mixture) was studied within this thesis. From this point on "PHTP" will be used to describe this particular stereoisomer.

PHTP is a special organic molecule which not only forms inclusion compounds but also belongs to the D_3 symmetry group. In the solid state, PHTP possesses one three-fold axis (c-axis) and three two-fold axes, but no plane of symmetry (and thereby has the enantiometric forms) (Figure 4.2). The molecular packing of pure PHTP has two modifications, one being metastable. The metastable modification (which melts at 117°C)[4.3] can be obtained by the rapid cooling of the melt, but changes completely to the stable modification (which melts at 125.2 °C)[4.3] within a few hours. Figure 4.3 shows both modifications.

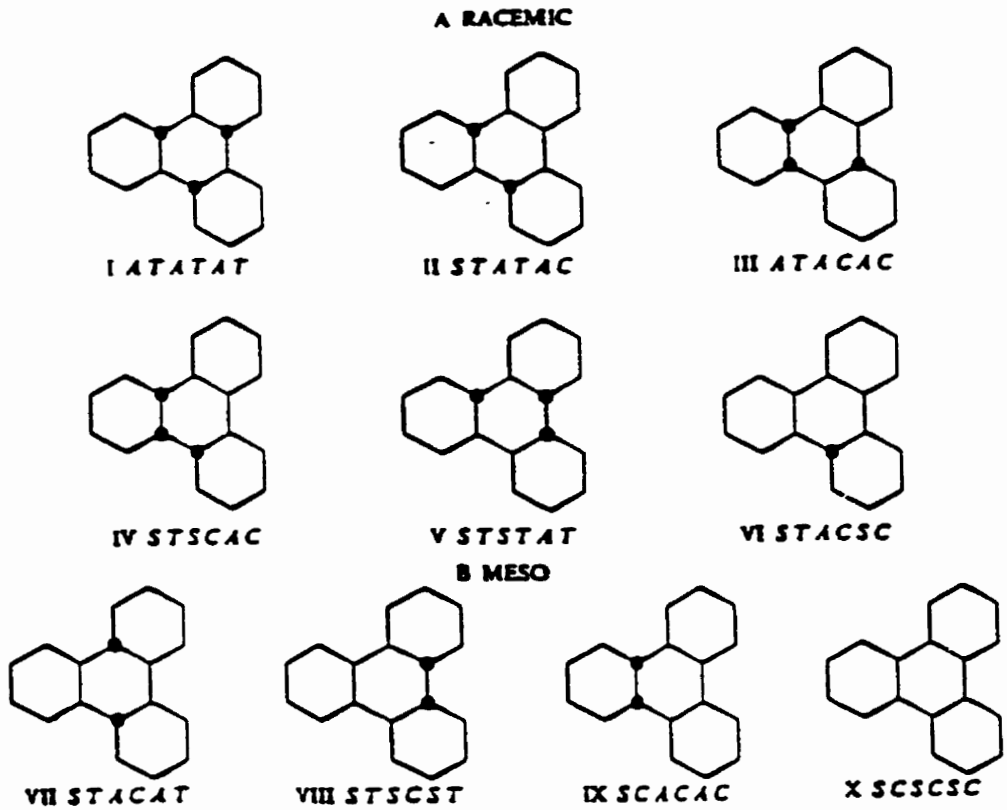

Figure 4.1 Stereoisomeric forms of PHTP. (Racemic - consisting of both the right- and left-handed enantiomers; Meso - each contains a mirror plane, thus no enantiomer pairs. Dot represents a hydrogen atom coming perpendicular out of the plane of the paper).[4.2]

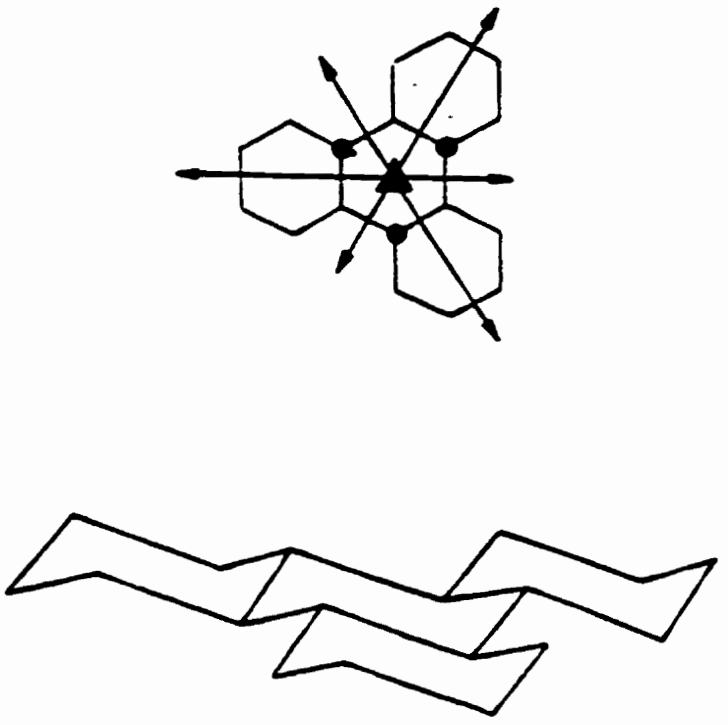

Figure 4.2 Symmetry of PHTP. [4.4]

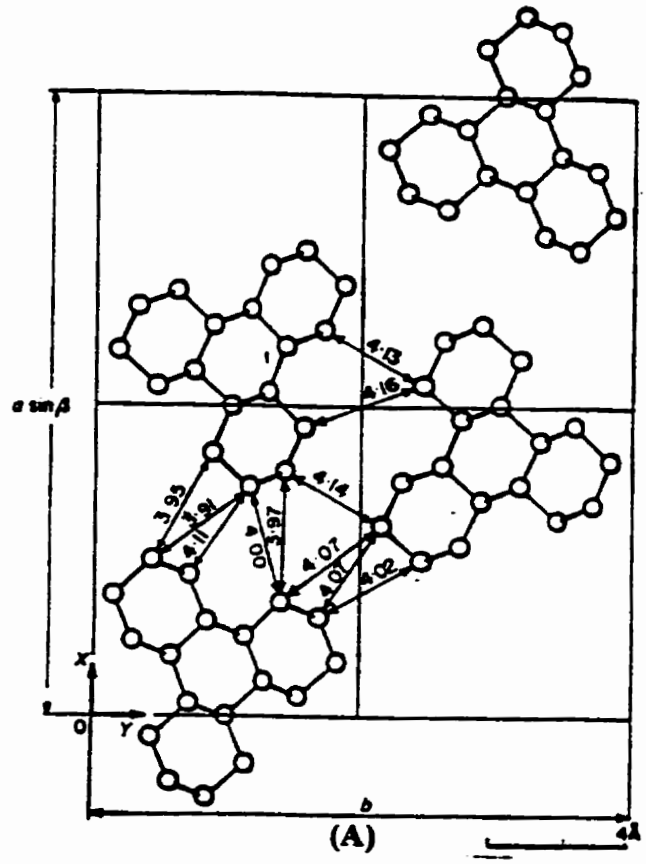

(A)

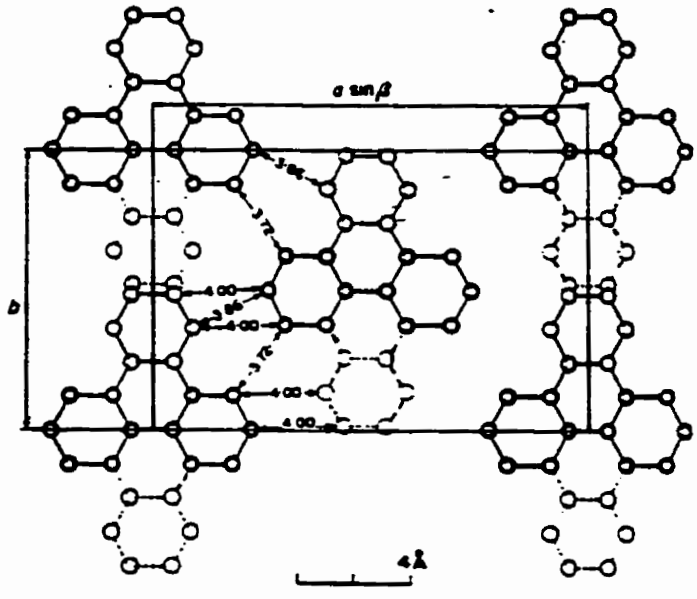

(B)

Figure 4.3 Stable (A) and metastable (B) forms of PHTP. [4,5]

PHTP can form channel inclusion compounds with a wide variety of guest molecules. There is no hydrogen bonding of the host lattice (like that found in urea). The inclusion compound is held together rather loosely (mainly van der Waals forces) so there is greater flexibility of the host lattice towards guest molecules than in more strongly bonded systems such as urea. As a result, molecules such as linear hydrocarbons, branched hydrocarbons and planar molecules can all be included. Table 4.1 lists some guest molecules of PHTP inclusion compounds and the mole ratio of host to guest molecules.

In general, PHTP forms hexagonal rings around the guest molecule(s) and these rings are superimposed. This gives rise to long channels in which the guest molecules reside. These channels run parallel to the c-axis of the structure and can range from 5.7-6.7 Å in width[4.6], with a distance of about 14.3 Å between centers of adjacent channels[4.7]. Figure 4.4 shows an example of a PHTP inclusion compound structure.

Table 4.1 **Composition and melting point of some selected PHTP-inclusion compounds.**[43]

Guest	PHTP-guest molar ratio		*Melting point* (°C)
	X-ray analysis	*Independent analysis*	
n-Heptane	4.47	4.38[a,b]	120
n-Nonane	5.43	5.46[c]	128
n-Hexadecane	9.03		145
n-Tetracontane	13.38		152
Cyclohexane	2.57	2.58[b]	117
Dioxane	2.40	2.42[b]	119
Chloroform (RT)	2.00	2.00[b]	58[f]
Carbon tetrachloride	2.42	2.54[b]	
Butadiene	2.00	1.95[a]	
Caprylic acid	5.00	5.00[d]	
Lauric acid	7.03	6.95[d]	
Palmitic acid			157
Polyethylene	1.0[g]	1.14[c-g]	178
1,4-*trans*-Polybutadiene	2.00[g]	2.09[c-g]	182
Poly(ethylene glycol)	1.44[g]		144

[a] Gas volumetric analysis. [b] Thermogravimetry. [c] IR analysis. [d] Acidmetric titration. [e] Extraction with boiling solvents. [f] Solid-solid phase transition. [g] Referred to 1 monomeric unit.

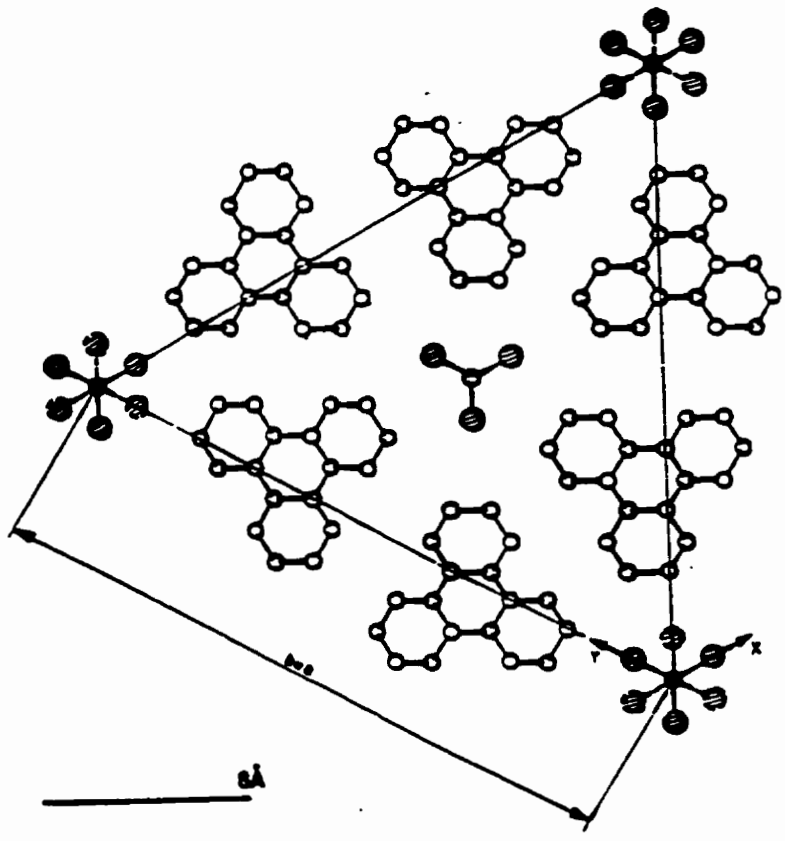

Figure 4.4 Structure of PHTP-chloroform. [4.6]

4.2 Preparation of PHTP and PHTP-hexadecane

Unlike urea, PHTP is not commercially available and must be synthesized. High temperature and pressure equipment was required.

To begin with, dodecahydrotriphenylene (DHTP) was needed as a starting material. The DHTP was prepared by the Friedel-Craft alkylation of benzene[4.9]. In this reaction, 950 g of 1-4 dichlorobutane (Aldrich, 99%) was reacted with 500 mL of benzene (Aldrich, 99%) and 500 g (in small portions) of water free $AlCl_3$ (Aldrich, 98%) over a 48 hour period (without exceeding 20°C) (Figure 4.5). This produced a viscous reddish-brown mixture which was stirred over a 12 hour period. The mixture was then hydrolyzed with ice. The fine yellow crystals of DHTP that were produced were washed with acetone, suction filtered, and allowed to air dry. The melting point of these crystals was 503 K compared to the literature value of 505-506 K.[4.10]

Hydrogenation of DHTP to PHTP[4.1] was carried out by Prof. T. Fyles, University of Victoria. In heptane solution, DHTP was subjected to high temperatures (~ 300°C) and high pressures (~ 200 atm H_2), with Pd/C (Aldrich, 10% Pd) as the catalyst (~25 g of DHTP per run gave ~50% PHTP by mass, ~5 g of pure D_3 PHTP). Hydrogenation can produce a mixture of up to ten stereoisomers. At short reaction times, the main products are of the *cis* configuration which slowly convert to an equilbrium mixture that consists of ~60% of the required D_3 symmetrical PHTP (also the least soluble). Separation consisted of the filtration of the hydrogenation mixture to remove the Pd/C catalyst. The solvent was allowed to evaporate. The resulting crystals were evacuated at 1 Torr for 16 hours. This produced a white crystalline material. This crystalline material is the PHTP-heptane

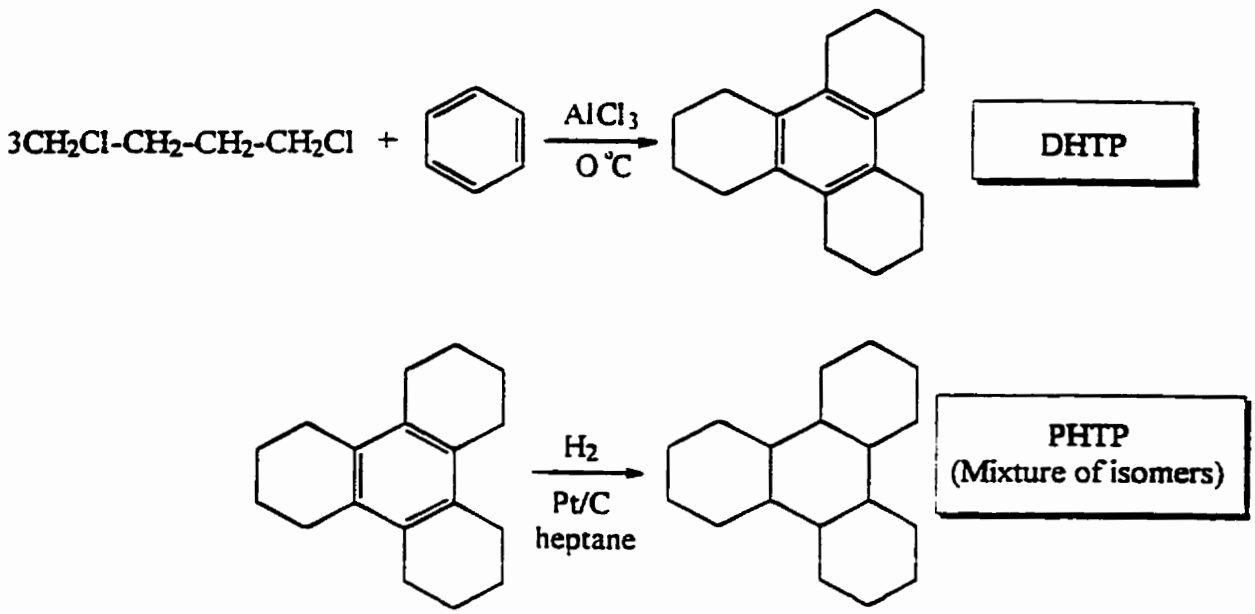

Figure 4.5 Preparation of PHTP.

inclusion compound. To recover pure PHTP, the material was recrystallized from 2-butanone (500 mL for 5 g). The crystals were allowed to air dry and the resulting white needles had a melting point of 125 ± 2 °C compared to the literature value of 125.2 °C [4.3]. These white needle crystals are the pure D_3 PHTP. It is this isomer of PHTP which forms the inclusion compounds that were examined.

There are various methods for preparing the PHTP inclusion compounds[4.8]. Methyl ethyl ketone (MEK) (Aldrich, 99+%) (30 mL) was used as a solvent to dissolve the PHTP (~3 g) in order to prepare the hexadecane adduct. Hexadecane (Aldrich, 99%) (~5 mL) was added directly to this solution and over a period of time (7-10 days) needle-like crystals of PHTP-hexadecane formed. The mole-ratio was known from X-ray diffraction measurements[4.8] to be 9.03 PHTP : hexadecane.

4.3 D.s.c. thermograms of PHTP and PHTP-hexadecane

The conditions and calibration for PHTP and PHTP-hexadecane were the same as for urea (Section 3.3). The d.s.c. instrument used to examine the melting points was the Pyris-1 Perkin Elmer D.S.C.

High grade indium was used to calibrate the instrument. The melting point for PHTP and PHTP-hexadecane falls within the region at which indium melts, making it an excellent choice for the standard.

PHTP and PHTP-hexadecane were heated at a scan rate of 10 K / min. from 343 K to 433 K, then held isothermally for 1 minute at 433 K, cooled at a scan rate of 10 K / min. down to 343 K, held again isothermally for 1 min and re-heated to 433 K. On first heating, both samples gave only one endothermic peak with PHTP-hexadecane melting at a higher temperature (416 ± 2 K; literature value 418.15 K[4.3]) than PHTP (398 ± 1 K ; literature value 398.35 K[4.3]) and hexadecane (literature value 291.34 K[4.11]). On re-heating of the PHTP-hexadecane, the endothermic peak corresponded with the first melting peak and thus confirms that the compound melted congruently and can be prepared from the melt. Plots of the thermographs are given in Figure 4.6 and Figure 4.7 with the onset temperatures (corrected with indium). Table 4.1 lists the melting points for some PHTP inclusion compounds with linear hydrocarbon guest molecules.[4.3]

The enthalpies of fusion ($\Delta_{fus}H$) for PHTP and PHTP-hexadecane were determined to be 26.4 ± 0.5 kJ (mol PHTP)$^{-1}$ and 21.6 ± 1.0 kJ (mol PHTP)$^{-1}$ respectively, with uncertainties determined from duplicate runs.

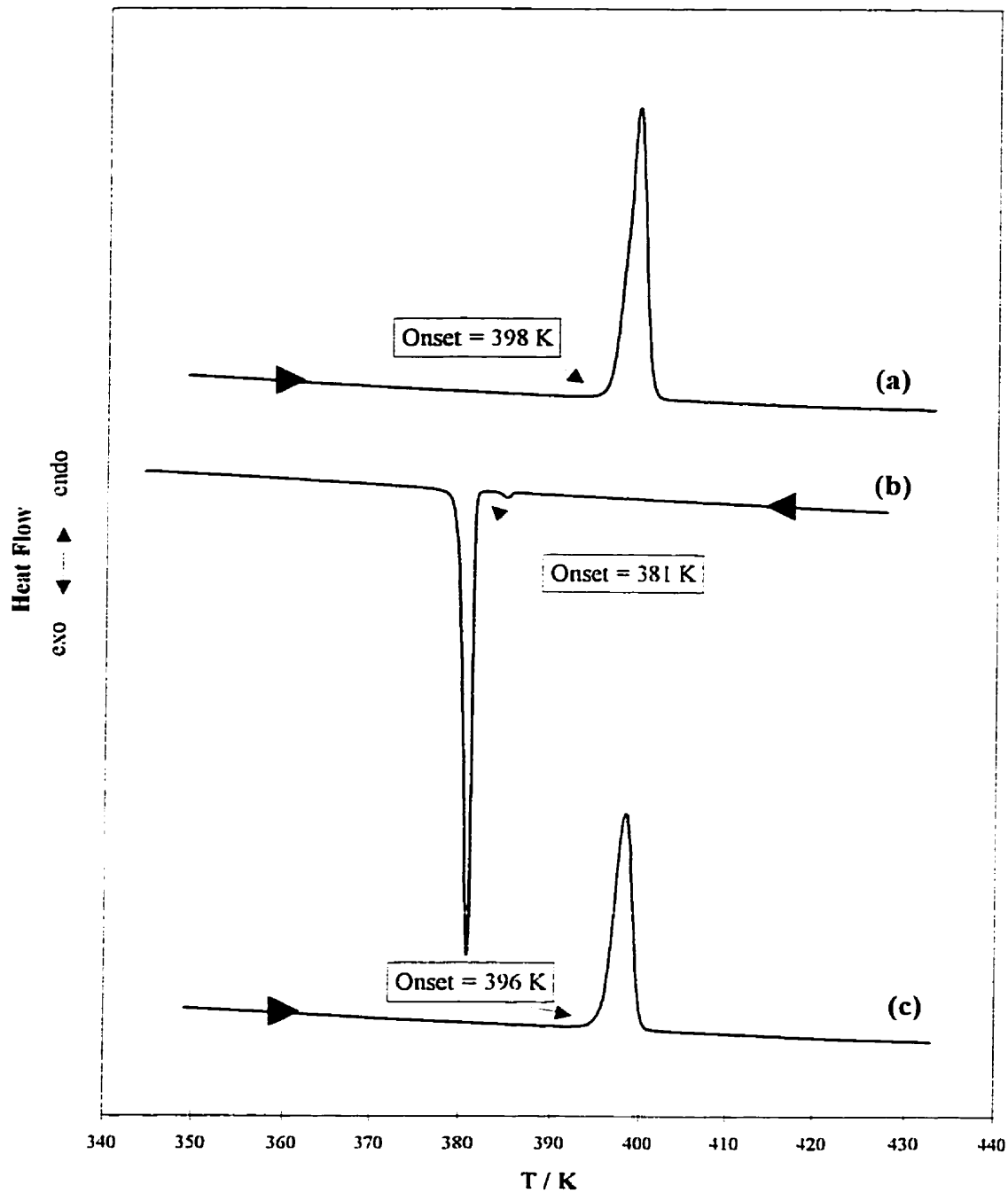

Figure 4.6 **Heating and cooling d.s.c. thermographs of PHTP. (a) Heated from 343 - 433 K at 10 K / min. (b) Held at 433 K for 1 min, then cooled to 343 K at 10 K / min. (c) Held at 343 K for 1 min., then heated to 433 K at 10 K / min.**

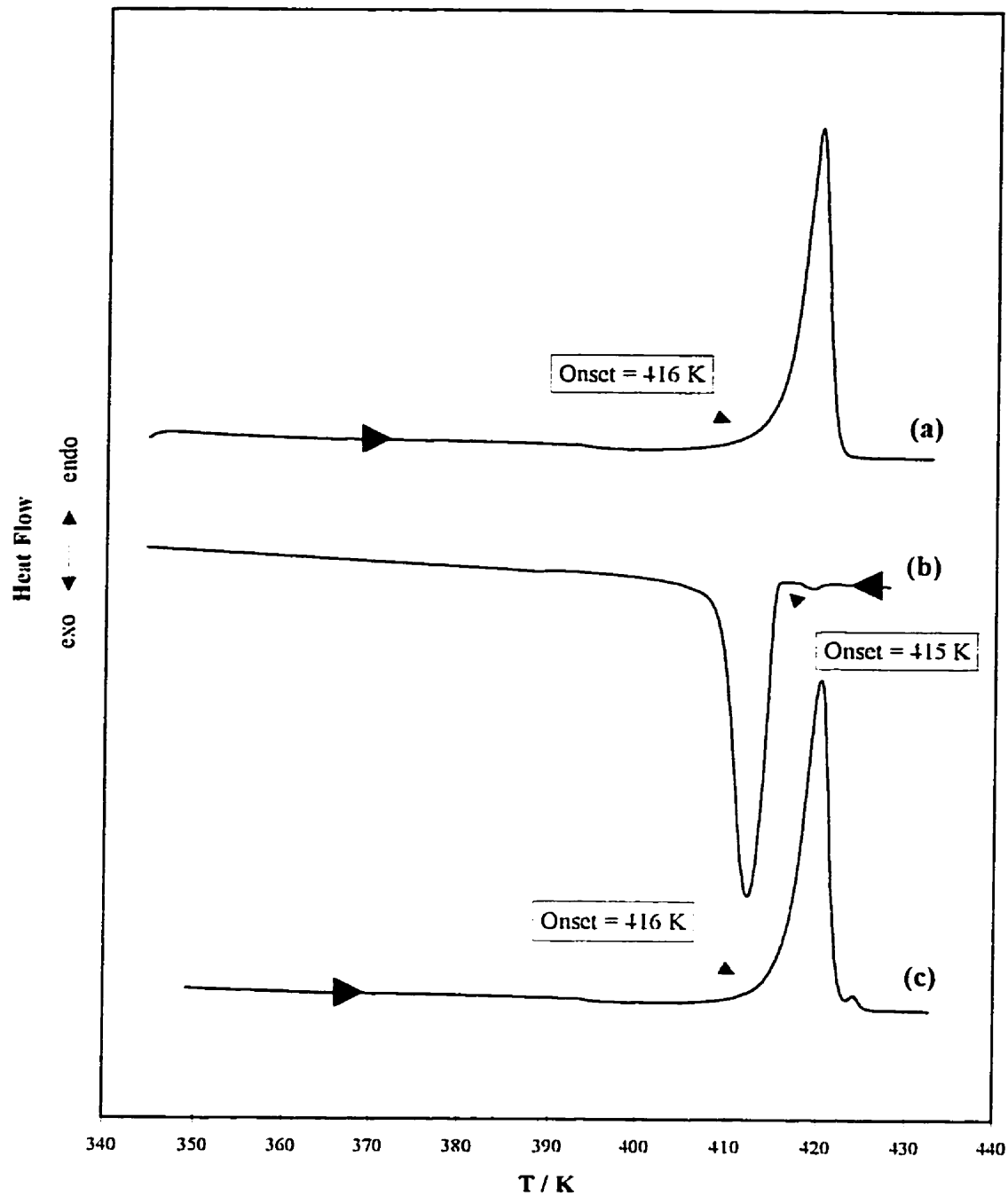

Figure 4.7 Heating and cooling d.s.c. thermographs of PHTP-hexadecane. (a) Heated from 343 - 433 K at 10 K / min. (b) Held at 433 K for 1 min, then cooled to 343 K at 10 K / min. (c) Held at 343 K for 1 min., then heated to 433 K at 10 K / min.

Melting behavior is either incongruent or congruent (Chapter 1). From the d.s.c. thermographs there is only one peak for melting of the inclusion compound. This indicates that the compound melts from a solid inclusion compound directly to a liquid. This is known as congruent melting.

4.4 Hot-stage microscopy

A single crystal of PHTP-hexadecane was melted on a hot-stage microscopy and the melting behavior was observed. The hot-stage microscopy apparatus was supplied by D. Jackson of Biology, Dalhousie University. The apparatus consisted of a black and white video camera, a melting point apparatus and video recording instrument (S-VHS). Once the melting was recorded, still frames were captured on computer and arranged in order of increasing temperature and re-cooling (see Figure 4.8). The melting behavior observed is consistent with the d.s.c. results, *i.e.* congruent melting :

$$\text{PHTP-}C_{16}H_{34} \xrightarrow{T_1 = 416\ K} \text{Liquid}$$

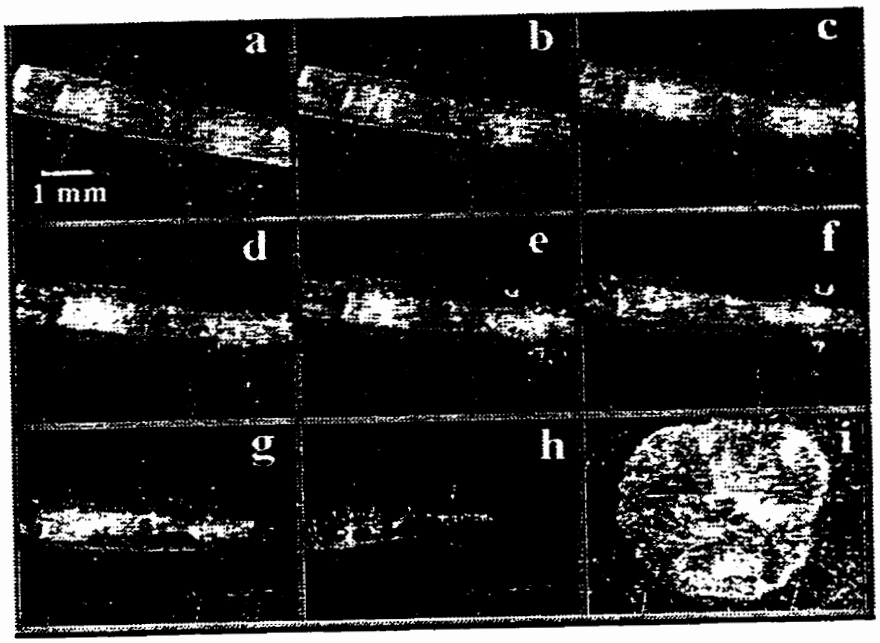

Figure 4.8 A needle of PHTP as it melts congruently. a) Before heat is applied, b),c) the onset of melting, d-h) various stages of the inclusion compound and the liquid phase, i) solidification of PHTP-hexadecane. The sample was heated on a melting point apparatus and filmed using a B&W video camera and recorded on S-VHS.

4.5 Heat capacities of PHTP and PHTP-hexadecane

The melting behaviour of the compounds can be explained through their relative stabilities. These can be determined through the Gibbs energy which in turn can be obtained from the heat capacity (see Section 3.5). This heat capacity data was obtained for PHTP and PHTP-hexadecane (from 30 - 320 K) using an adiabatic calorimeter[4.12,4.13]. The data below 30 K and above 320 K were obtained by extrapolation.

A series of steps was involved in determining the heat capacity of a sample. First, the mass of the sample holder, brass screws and lid were determined. This mass was used in calculating the heat capacity associated with the empty vessel. Then the sample was added to the sample vessel (filled to about ¾ full). The mass of the vessel with the sample, brass screws and lid was determined again to determine the mass of the sample. To ensure a sealed vessel, a thin indium wire (0.1 mm diameter) was used to form an o-ring. The vessel was then reassembled with the brass screws lightly attached. The vessel was then placed in a desiccator and evacuated. The evacuated desiccator with the sample was moved into a glove bag and flushed with helium gas. Once flushed, the helium was allowed into the desiccator. The vessel was then removed from the desiccator inside the glove bag. The screws were now securely tightened and the vessel was sealed with the helium gas inside. The vessel was weighed again in order to determine the mass of the indium wire. The mass was needed to correct the overall heat capacity for contributions from the heat capacity of the indium. The heater and vessel were then weighed together and the mass was recorded. Apiezon T grease was applied between the sample vessel and heater to ensure thermal contact. The mass of the sample and heater with the grease was

determined so that the mass of grease could be obtained. The grease also contributes to the overall heat capacity and must be accounted for. Once the sample vessel and heater were assembled it was suspended inside the shield heater assembly. The wires (38 SWG copper wire) that were connected to the heater were pulled through the bottom of the shield. These wires were attached to the bottom of the shield using thermal-free solder. The wires are the leads for the platinum thermometer, heater resistance, and shield thermocouple (one wire is constantan). The wires were attached to posts on the bottom of the shield which were in turn connected to the top of the shield *via* wires that were wrapped around the shield and held in place by lacquer. The entire shield assembly was suspended from the heat sink with thermal free leads (nylon thread). The top of the shield was wired to the heat sink. Once the entire system was wired it was tested with the voltmeter to ensure all connections were closed. The enclosure can was placed around the shield and screwed shut with stainless steel screws. The seal was ensured by using an indium wire (1.0 mm diameter) o-ring. After being sealed the enclosure can was evacuated with both a roughing pump and a diffusion pump. The roughing pump removes the majority of the gas so that the diffusion pump will not be damaged. A pressure of below $2x10^{-5}$ mbar. was needed to ensure good working adiabatic conditions. When the vacuum had been achieved the enclosure can was lowered into a Dewar of liquid nitrogen to be cooled.

For adiabatic conditions to be ensured, a shield heater was used to maintain the temperature constant ($\pm$ 3 mK min^{-1} drift rate). After an acceptable drift rate was obtained the program AC4AUTO.BAS was used to set up the uninterrupted data

collection of the heat capacity. Table 4.2 lists the various masses for PHTP and PHTP-hexadecane.

A small anomaly in the heat capacity of PHTP-hexadecane was observed at T ~ 291 K (see Figure 4.9). This is similar to the melting point of hexadecane (291.34 K)[4.11], and is attributed to a small amount of excess hexadecane in the sample. This was supported by the additional finding that this anomaly was not observed in all samples examined by d.s.c. Based on the enthalpy of this anomaly (2250 J (mol PHTP)$^{-1}$) and the known enthalpy of fusion of hexadecane (53.36 J mol^{-1})[4.11], it was determined that 3.5 mass % of the adiabatic calorimetry sample was pure hexadecane. The heat capacity data were corrected for this impurity using hexadecane heat capacity data from the literature[4.11].

The heat capacity, H, S and G for PHTP are given in Table 4.3 and graphed in Figures 4.10, 4.11, 4.12 and 4.13 respectively. The heat capacity, H, S and G for PHTP-hexadecane are given in Table 4.4 and graphed in Figures 4.14, 4.15, 4.16 and 4.17 respectively. A greater treatment of the data in regards to stability (Gibbs energy) is given in Section 4.6. Appendices A and B list the measured heat capacity data for PHTP and PHTP-hexadecane (the latter is corrected for hexadecane impurity).

Table 4.2 Various masses used to obtain heat capacity for PHTP and PHTP-hexadecane

PHTP	
Molecular weight :	246.435 g / mol
Mass of empty vessel (vessel + sample + lid) :	9.7499 g
Mass of vessel + indium wire :	9.8517 g
Mass of vessel + indium wire + sample :	10.9674 g
Mass of vessel + indium wire + sample + heater :	20.6552 g
Mass of vessel + indium wire + sample + heater + Apiezon T grease :	20.6732 g
Mass of indium wire :	0.10180 g
Mass of sample :	1.11570 g
Mass of Apiezon T grease :	0.018 g
Number of moles :	0.00453 moles

PHTP-hexadecane	
Molecular weight :	271.510 g / mol
Mass of empty vessel (vessel + sample + lid) :	9.7472 g
Mass of vessel + indium wire :	9.8322 g
Mass of vessel + indium wire + sample :	10.3095 g
Mass of vessel + indium wire + sample + heater :	19.9784 g
Mass of vessel + indium wire + sample + heater + Apiezon T grease :	19.9795 g
Mass of indium wire :	0.085 g
Mass of sample :	0.47730 g
Mass of Apiezon T grease :	0.01110 g
Number of moles :	0.001758 moles

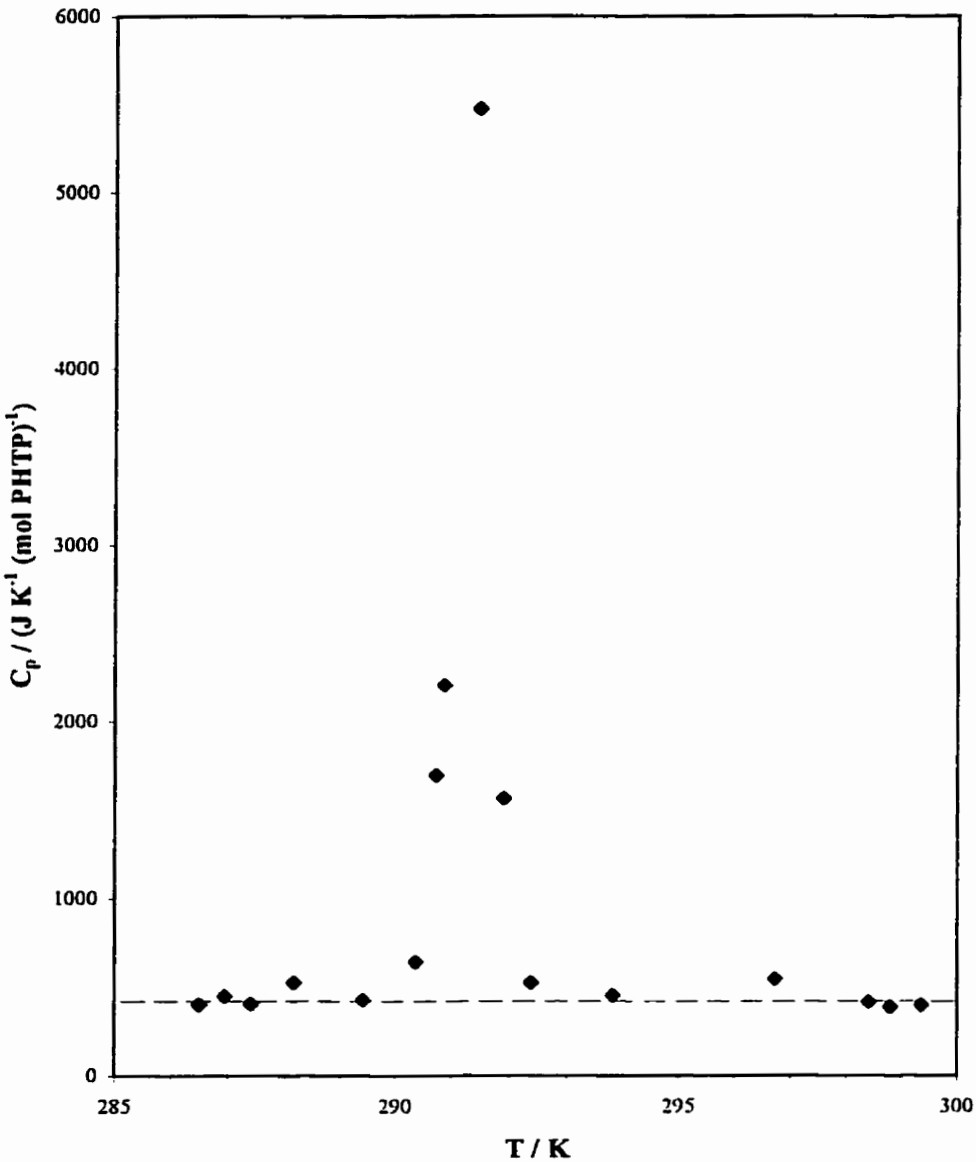

Figure 4.9 **Heat capacity anomaly in PHTP-hexadecane. Dashed line (-----) represents the baseline. This peak corresponds to melting of hexadecane comprising 3.5 mass % of the adiabatic calorimetry sample.**

Table 4.3 Smooth heat capacity, H, S and G data for PHTP

T	C_p	H	S	G
K	J K^{-1} mol^{-1}	J mol^{-1}	J K^{-1} mol^{-1}	J mol^{-1}
(0)	(0)	(0)	(0)	(0)
(20)	(11)	(85)	(6.8)	-(52)
40	36	552	22.0	-327
60	61	1527	41.4	-957
80	87	2995	62.3	-1991
100	110	4974	84.3	-3457
120	134	7420	106.5	-5366
140	158	10348	129.1	-7721
160	182	13728	151.6	-10528
180	205	17621	174.5	-13789
200	229	21971	197.4	-17508
220	255	26797	220.4	-21685
240	283	32165	243.7	-26325
260	312	38110	267.5	-31436
280	337	44605	291.5	-37026
300	361	51597	315.6	-43098
320	392	59130	339.9	-49653
(340)	(417)	(67225)	(364.5)	-(56697)
(360)	(450)	(75892)	(389.2)	-(64234)
(380)	(477)	(85141)	(414.2)	-(72268)

Note : Data below 30 K and above 320 K are by extrapolation

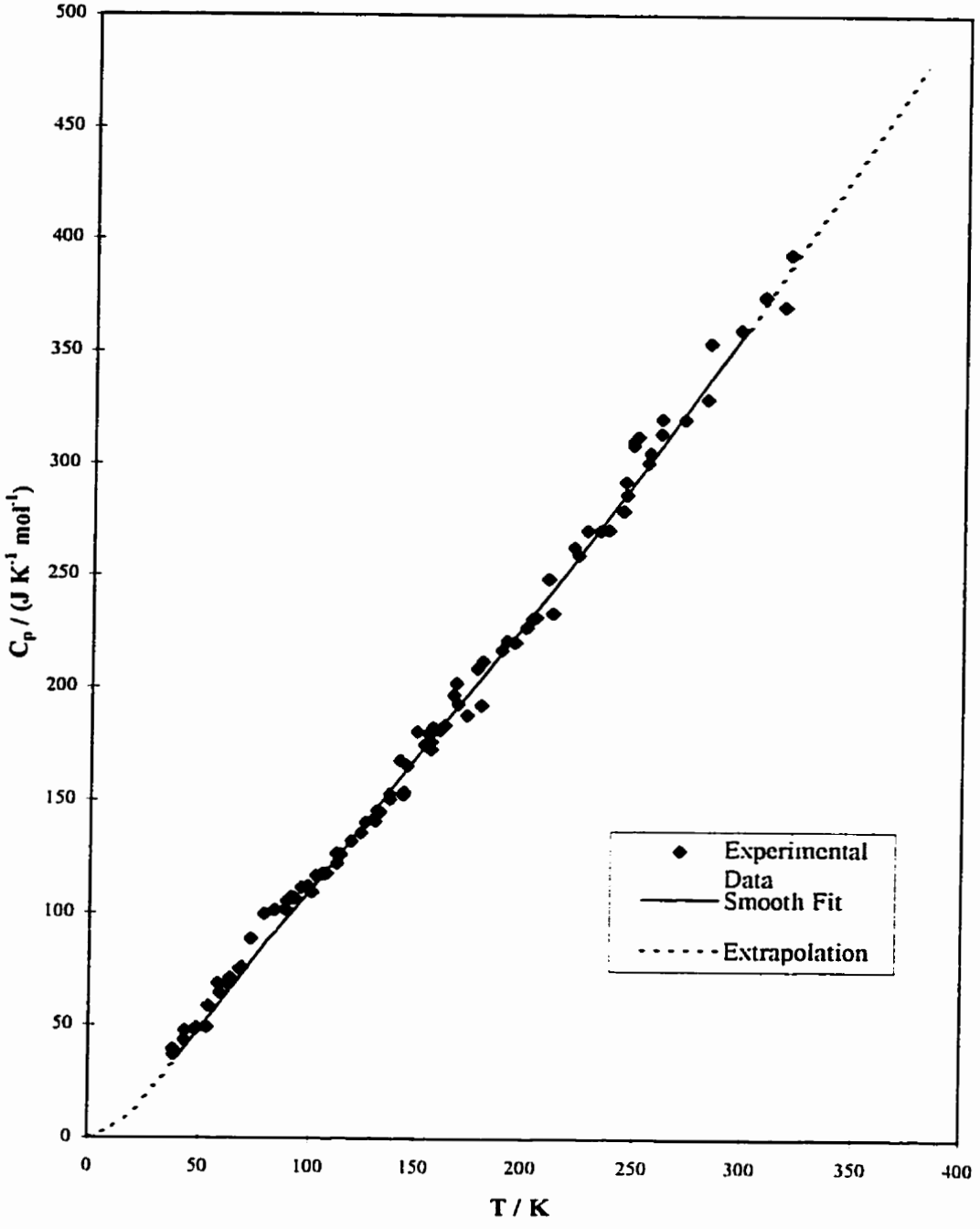

Figure 4.10 **Heat capacity (C_p) of PHTP.**

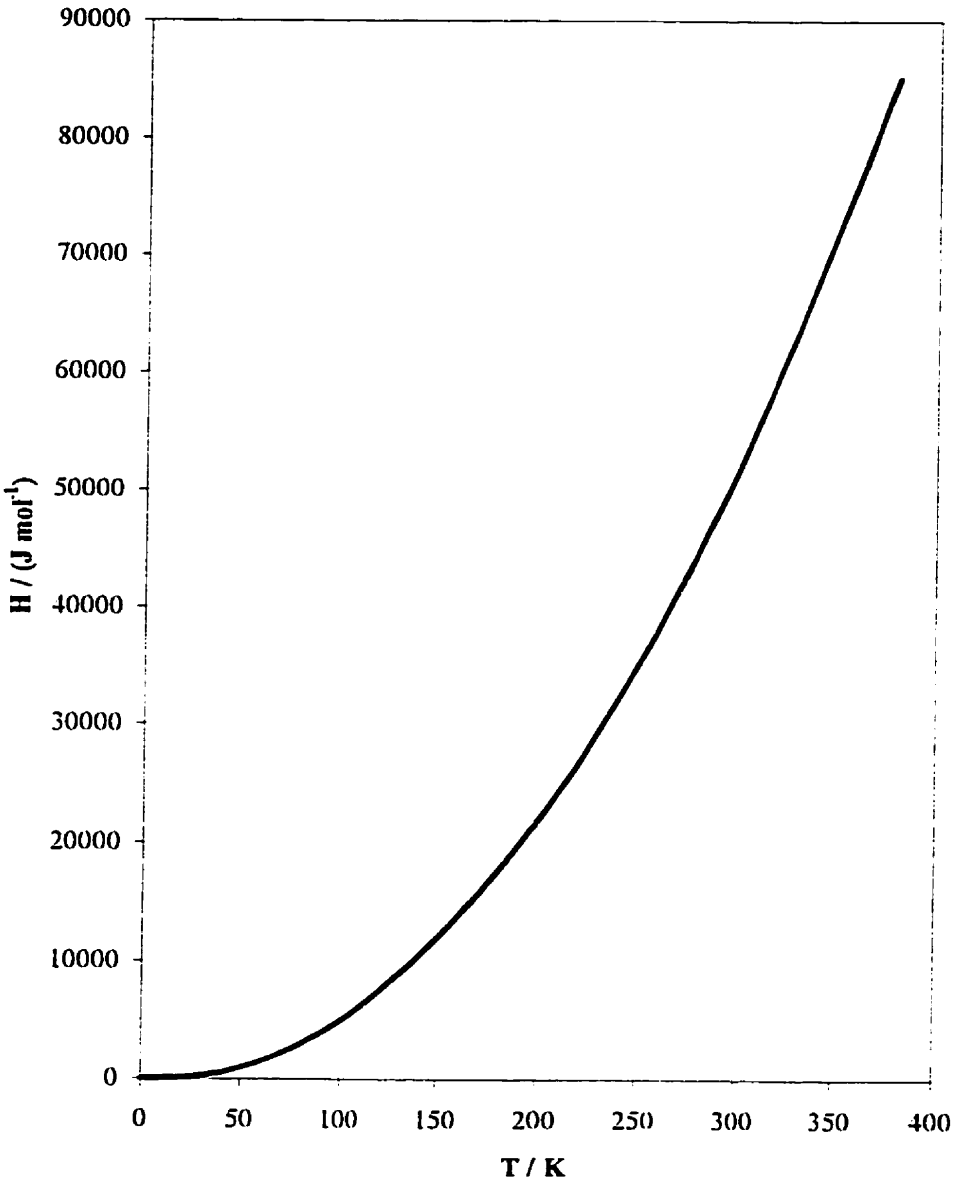

Figure 4.11 **Enthalpy (H) of PHTP.**

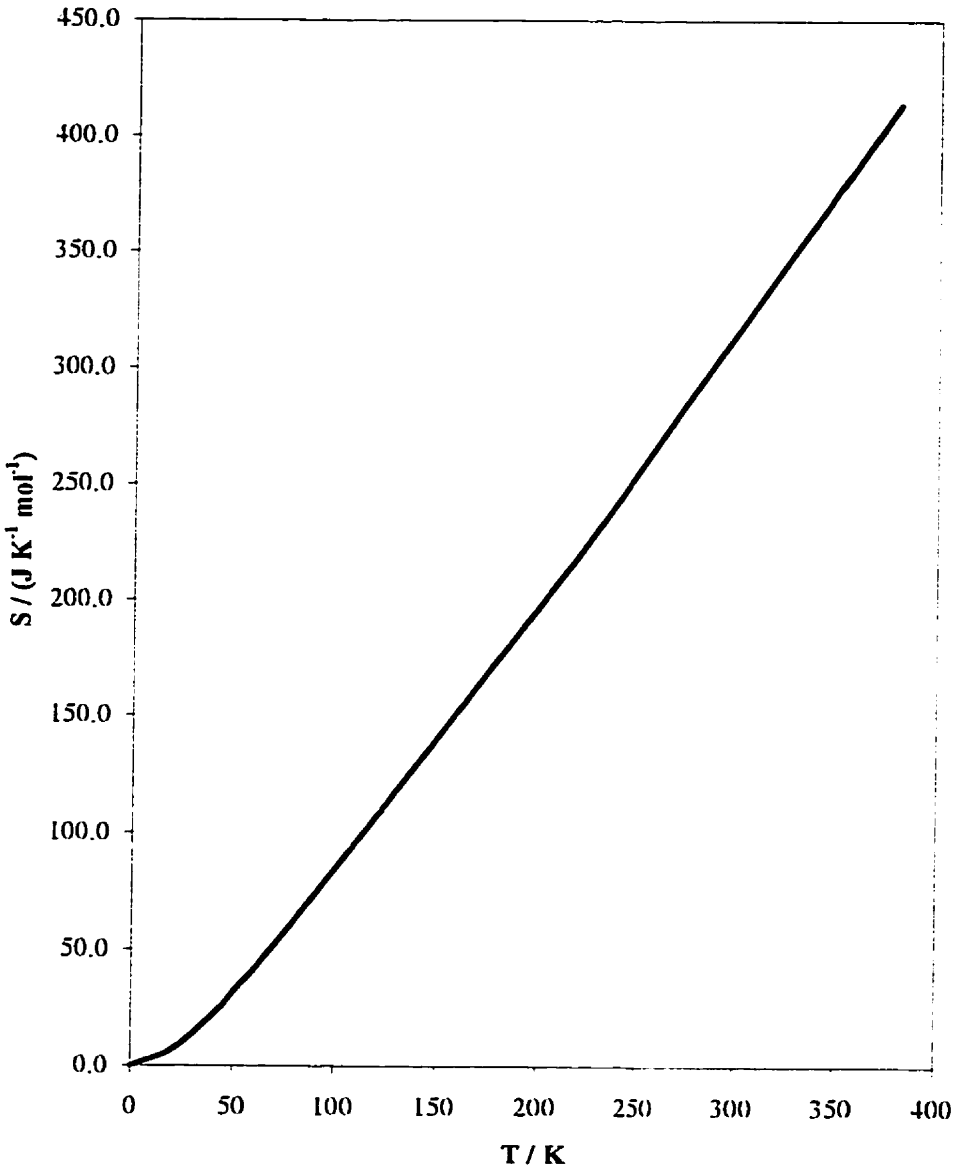

Figure 4.12 **Entropy (S) of PHTP.**

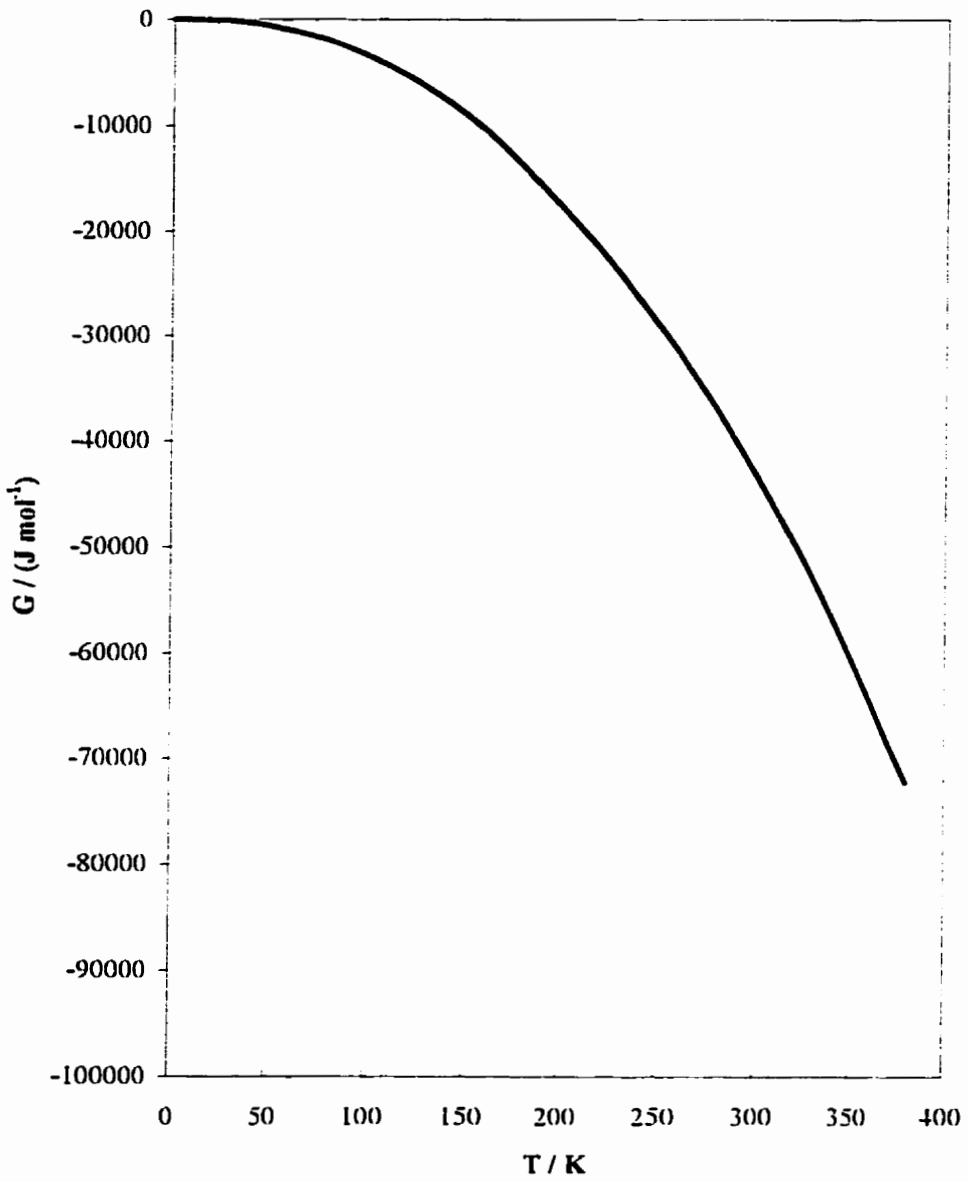

Figure 4.13 **Gibbs energy (G) of PHTP.**

Table 4.4 Smooth heat capacity, H, S and G data for PHTP-hexadecane, corrected for eutectic

T	C_p	H	S	G
K	J K^{-1} (mol PHTP)$^{-1}$	J (mol PHTP)$^{-1}$	J K^{-1} (mol PHTP)$^{-1}$	J (mol PHTP)$^{-1}$
(0)	(0)	(0)	(0)	(0)
(20)	(17)	(170)	(8.5)	(0)
40	42	760	27.5	-340
60	72	1900	50.0	-1100
80	101	3630	74.6	-2340
100	132	5960	100.5	-4085
120	166	8940	127.5	-6358
140	197	12570	155.4	-9184
160	232	16860	184.0	-12574
180	262	21800	213.0	-16543
200	296	27380	242.3	-21094
220	332	33660	272.3	-26238
240	364	40620	302.5	-31985
260	394	48200	332.8	-38338
280	427	56410	363.2	-45298
300	457	65250	393.7	-52868
320	487	74690	424.2	-61047
(340)	(514)	(84700)	(454.5)	-(69835)
(360)	(542)	(95260)	(484.7)	-(79228)
(380)	(569)	(106370)	(514.7)	-(89223)
(400)	(598)	(118040)	(544.6)	-(99817)

Note : Data below 30 K and above 320 K are by extrapolation

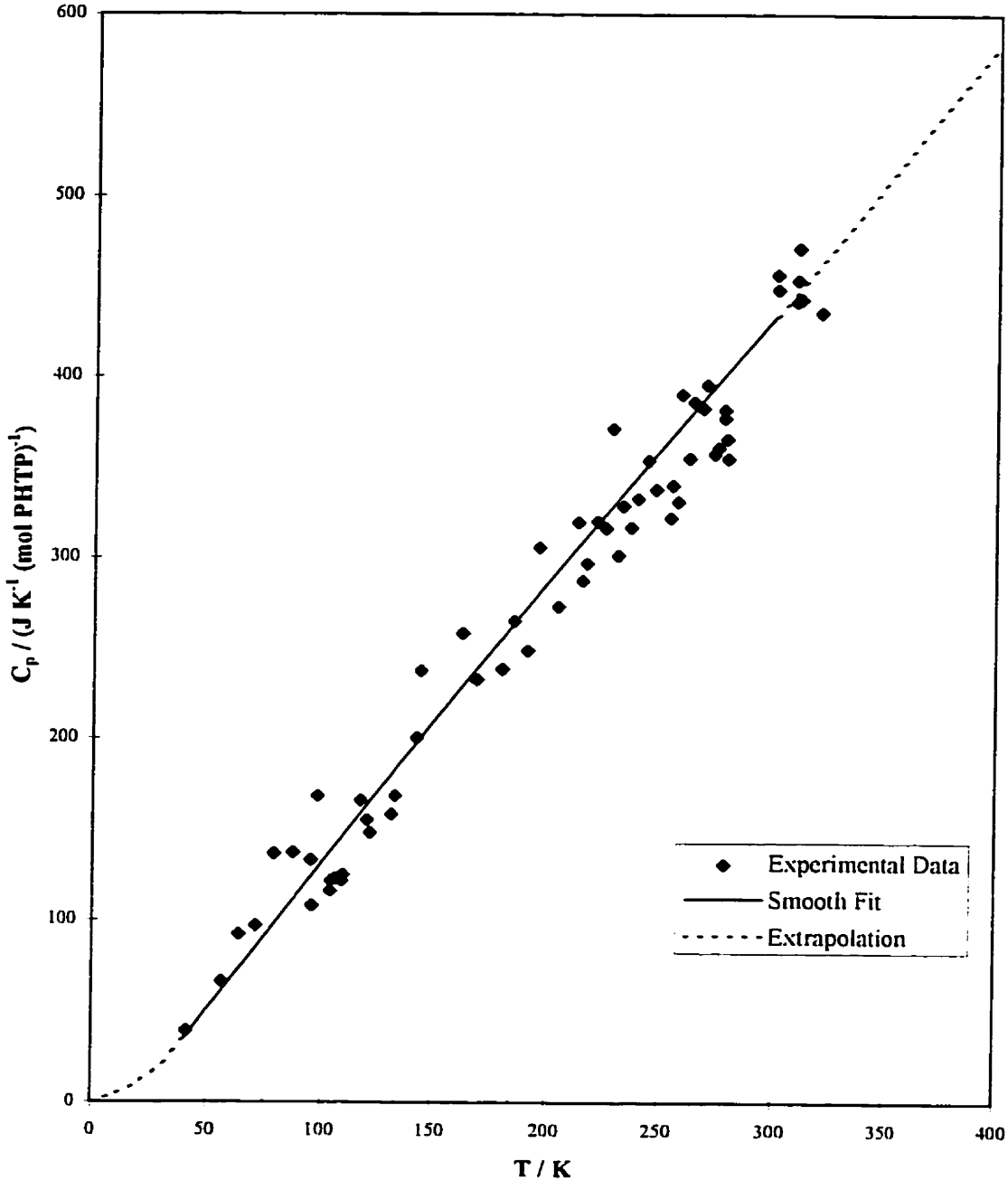

Figure 4.14 **Heat capacity (C_p) of PHTP-hexadecane, corrected for hexadecane eutectic.**

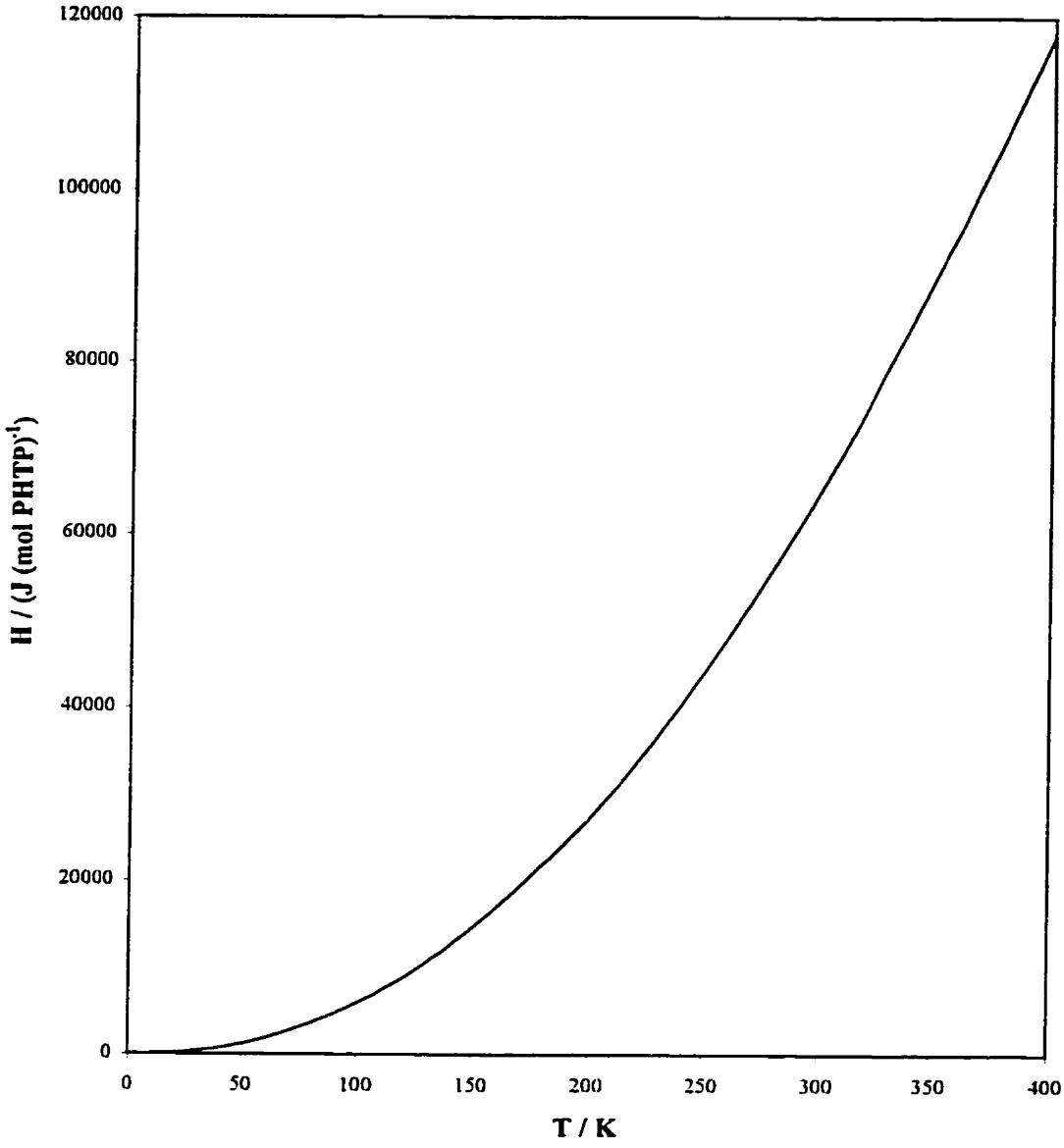

Figure 4.15 **Enthalpy (H) of PHTP-hexadecane**

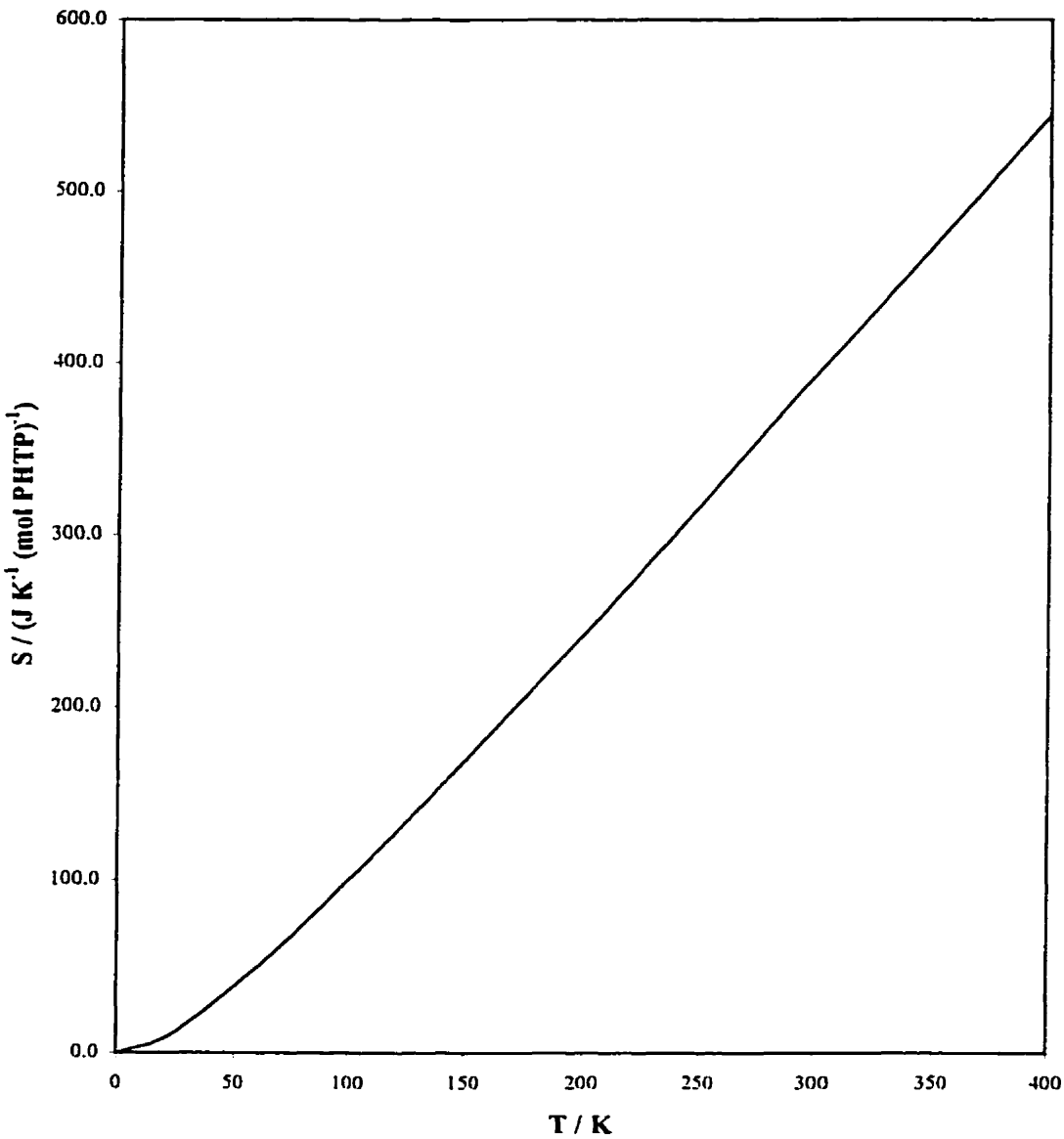

Figure 4.16 Entropy (S) of PHTP-hexadecane

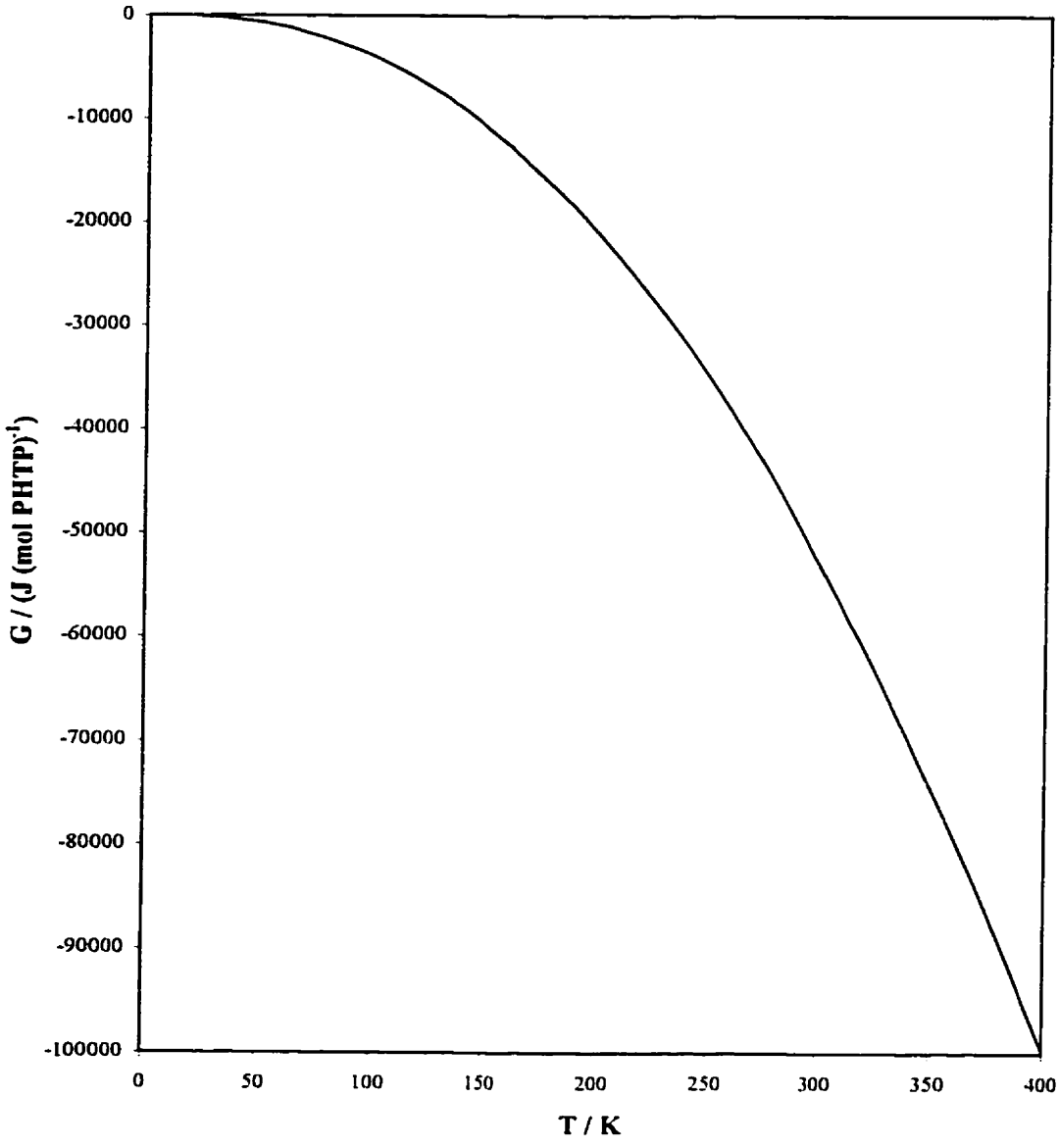

Figure 4.17 Gibbs energy (G) of PHTP-hexadecane

4.6 Gibbs energy of PHTP and PHTP-hexadecane

As mentioned previously, the Gibbs energy can be an indication of the stability of a compound. From the hot-stage microscopy and the d.s.c. thermographs of PHTP-hexadecane (Section 4.3), it can be seen that the inclusion compound melts from a solid directly to a liquid (congruent melting). From the Gibbs energy determinations for PHTP, PHTP-hexadecane and hexadecane[4.11] (Table 4.5 and Figure 4.18) one can see that the Gibbs energy of the PHTP-hexadecane inclusion compound is slightly lower than the Gibbs energy of PHTP plus the appropriate portion of hexadecane. Note that the difference in Gibbs energy of PHTP-hexadecane compared with its components is only about 4 % at the melting point. Heat capacities for a 3.882 g sample of standard benzoic acid contributing 70 % to the total heat capacity with this calorimeter were found to be accurate within ± 0.5 %[4.13]. The small sample masses lead to a scatter in heat capacity results of ~5% for PHTP (Figure 4.10) and ~10% for PHTP-hexadecane (Figure 4.14), with estimated heat capacity accuracies within 2% and 4%, respectively, making the observed difference in Gibbs energy of PHTP-hexadecane and its constituents at the limit of detection for this calorimeter.

Table 4.5 Gibbs energies of PHTP, hexadecane and PHTP-hexadecane

T	$G_{(IC)}$	$G_{(PHTP)}$	$G_{(Hexadecane)}$ [4.11]	$G_{(PHTP+\ 1/9.03\ Hexadecane)}$
K	J (mol PHTP)$^{-1}$	J mol^{-1}	J mol^{-1}	J (mol PHTP)$^{-1}$
0	0	0	0	0
20	0	-52	-40	-56
40	-340	-327	-412	-372
60	-1100	-957	-1413	-1113
80	-2340	-1991	-3146	-2340
100	-4085	-3457	-5613	-4080
120	-6358	-5366	-8785	-6341
140	-9184	-7721	-12628	-9123
160	-12574	-10528	-17107	-12426
180	-16543	-13789	-22191	-16252
200	-21094	-17508	-27858	-20600
220	-26238	-21685	-34091	-25469
240	-31985	-26325	-40880	-30862
260	-38338	-31436	-48223	-36789
280	-45398	-37026	-56124	-43256
300	-52868	-43098	-66185	-50444
320	-61047	-49653	-78968	-58418
340	-69835	-56697	-92396	-66953
360	-79228	-64234	-106445	-76049
380	-89223	-72268	-121094	-85710

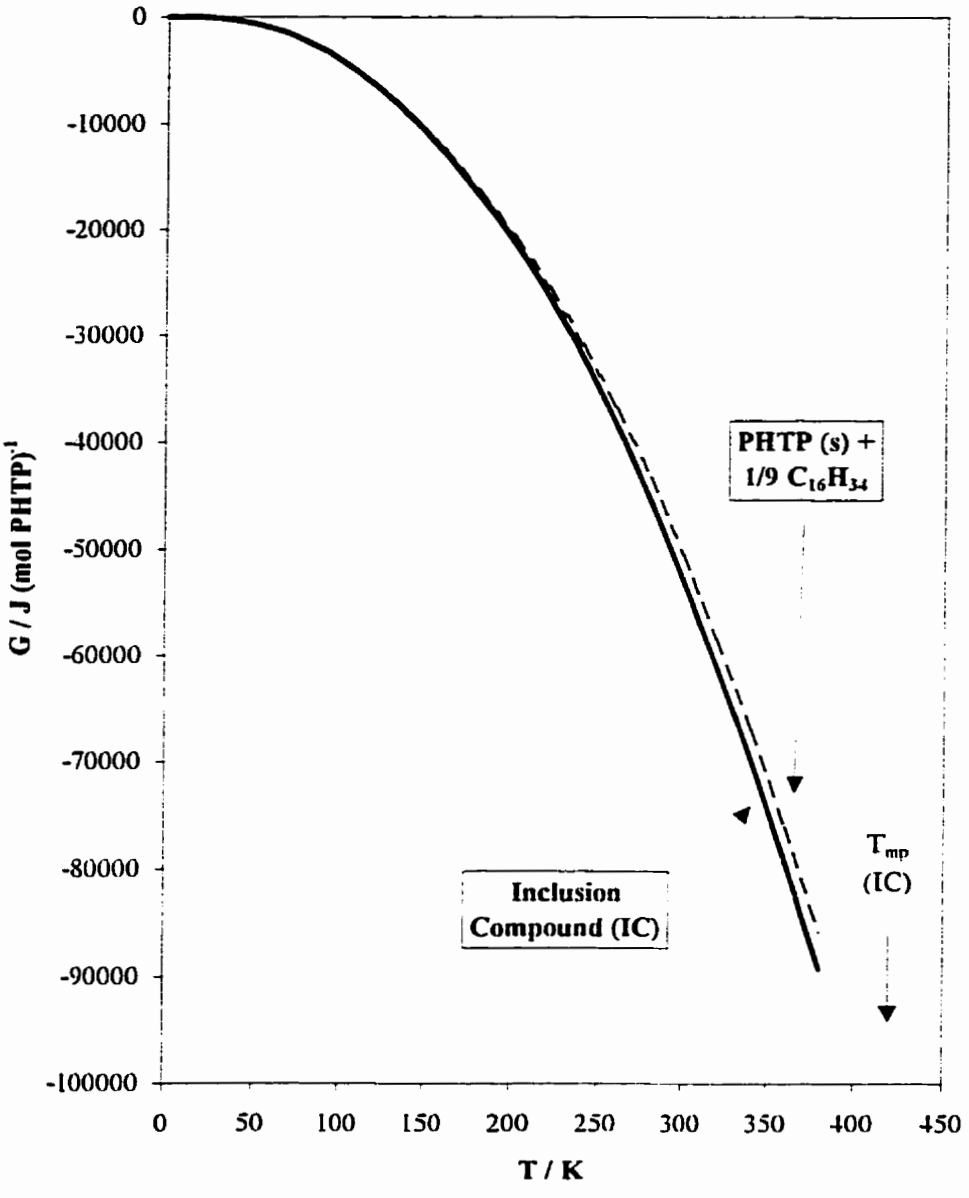

Figure 4.18 **Gibbs energy diagram for PHTP-hexadecane and PHTP + 1 / 9.03 hexadecane.**

4.7 Phase diagram

To calculate the phase diagram for PHTP-hexadecane, the method derived by M. Farina *et al.*[4.14] was used (refer to Section 3.7 with W = 0).

This method assumes the following for a PHTP-*n*-alkane system: complete immiscibility of the solid phases, absence of solid metastable phases, instability of the adduct in the liquid phase, ideal behavior of the liquid phase and constancy of all the melting enthalpies with temperature.

For the PHTP-hexadecane, Table 4.6 contains the melting temperatures and melting enthalpies used to calculate the phase diagram shown in Figure 4.19. The value n denotes the mole ratio of PHTP to hexadecane, which in this case is equal to 9.03[4.3]. The phase diagram is consistent with the present results in that it shows congruent melting of PHTP-hexadecane.

Table 4.6 The melting temperatures and enthalpies of PHTP, PHTP-hexadecane and hexadecane

	Melting temperature (T)	
Hexadecane	291.34 K	Ref. #4.11
PHTP	398 ± 1 K	Present work
PHTP-hexadecane	416 ± 2 K	Present work

	Melting enthalpies (L)	
Hexadecane	53.36 kJ mol^{-1}	Ref. #4.11
PHTP	26.4 ● 0.5 kJ mol^{-1}	Present work
PHTP-hexadecane	21.6 ± 1.0 kJ mol^{-1}	Present work

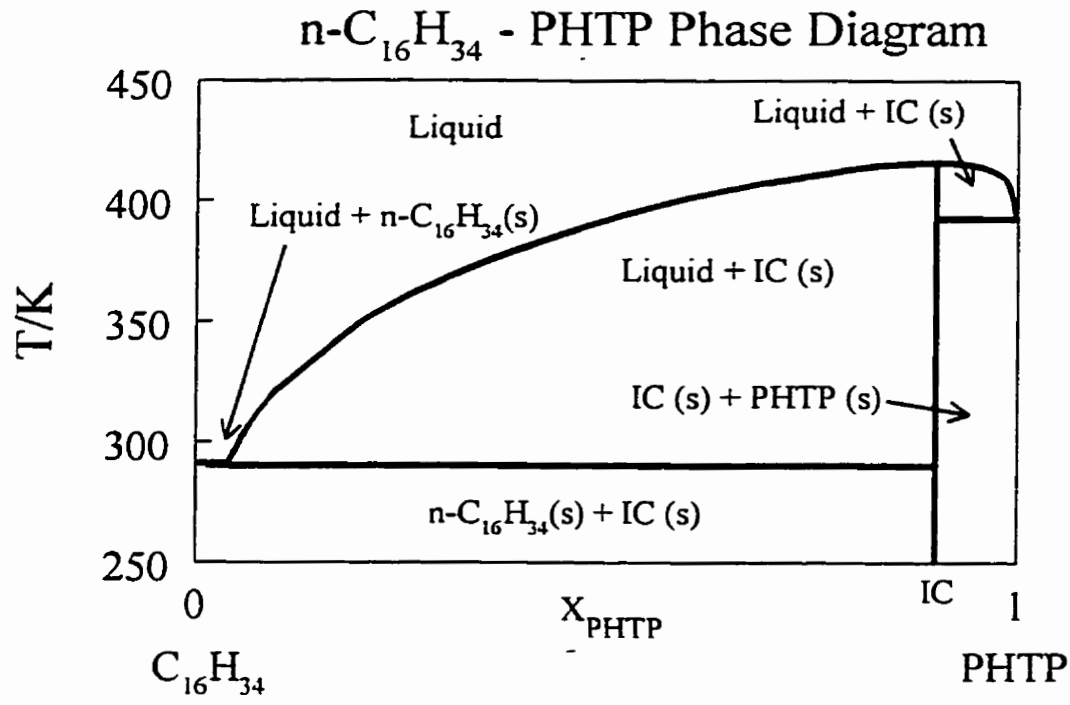

Figure 4.19 **Calculated phase diagram of hexadecane-PHTP (based on the method of Farina and co-worker[4.14]). IC = inclusion compound**

CHAPTER 5

CONCLUSIONS

5.1 Conclusions

As stated in Chapter 1, the melting behavior of binary compounds is an important property. For a binary compound, the melting is either congruent, *i.e.*, the solid compound melts directly to a liquid at its melting point or incongruent, *i.e.*, the binary compound melts, giving a solid (one of the components) and a liquid, and then at a higher temperature the solid melts giving only a liquid.

For the urea-hexadecane compound, the phase diagram (based on the method of Farina *et al.*[5.1]) shows that the melting of urea-hexadecane would be incongruent. This is also confirmed in d.s.c. and hot-stage microscopy. This would produce a mixture of solid urea and liquid hexadecane and eventually melt giving two immiscible liquids. Figure 5.1 shows that at the melting point, the Gibbs energy of liquid hexadecane, urea-hexadecane and solid urea form a line in the G(x) diagram, thus heating the urea-hexadecane inclusion compound leads to the production of solid urea and liquid hexadecane, *i.e.* incongruent melting.

For PHTP-hexadecane, the phase diagram (also based on the method of Farina *et al.*[5.1]) shows that the melting of PHTP-hexadecane would be congruent. This is also confirmed in d.s.c. and hot-stage microscopy. This would produce liquid (PHTP mixed with hexadecane) at the melting point. Figure 5.2 show that at the melting point, the Gibbs energy of the PHTP lies above the hexadecane-inclusion compound line, *i.e.* congruent melting results.

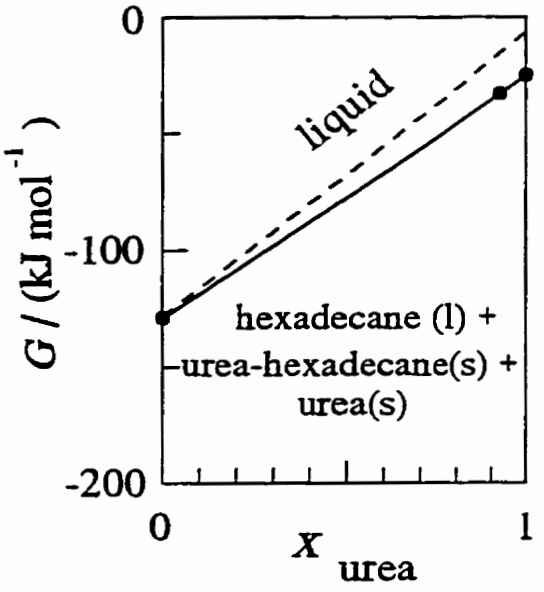

Figure 5.1 Gibbs energy, G as a function of mole fraction of urea, x_{urea}, at T=390 K, the (incongruent) melting point of urea-hexadecane. Solid circles represent Gibbs energies calculated from present data.

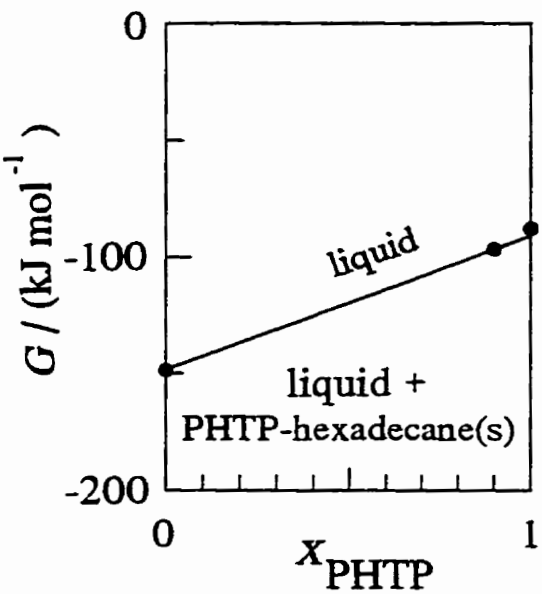

Figure 5.2 **Gibbs energy, G as a function of mole fraction of PHTP, x_{PHTP}, at T=416 K, the (congruent) melting point of PHTP-hexadecane. Solid circles represent Gibbs energies calculated from present data.**

In previous studies of the factors influencing congruency and incongruency of melting in ideal binary systems, it was concluded that the important factor is the relative Gibbs energy of the binary compound and it components[5.2]. For the case of urea-hexadecane, there is no longer an ideal binary system since urea and hexadecane are immiscible in the liquid state.

To understand the melting behavior in the non-ideal case, as it applies to the Gibbs energy, the same treatment of the liquid-solid coexistence regions as in the case of the ideal binary phase diagram is used[5.2]. Consider the generalized phase diagram (Figure 5.3) of a binary compound, AB, which melts incongruently to give liquid A and solid B and then at a higher temperature, two immiscible liquids (A and B). The Gibbs energy curve for the liquid as a function of X_B (mole fraction of B) shows a maximum (Figure 5.4) in order to have the complete phase separation of liquid A and B. In Figure 5.2, the relative Gibbs energies of A, AB, B and liquid are shown at different temperatures and G(AB) > G(B). It can be concluded for the case where the Gibbs energy of a constituent component is lower than that of the binary compound, incongruent melting results.

Farina and co-workers have suggested[5.1] that immiscibility of the constituent components inevitably leads to incongruent melting. If the case where G(AB) < G(B) is considered, the Gibbs energy curves of Figure 5.5 would be observed. This would lead to the melting of the binary compound directly to the liquid, $AB(s) \rightarrow A(l) + B(l)$, as seen in the phase diagram shown in Figure 5.6. This is congruent melting and, although unusual, it would be still possible to prepare crystals of AB by solidification as they would form at the interface of the immiscible liquids, A and B.

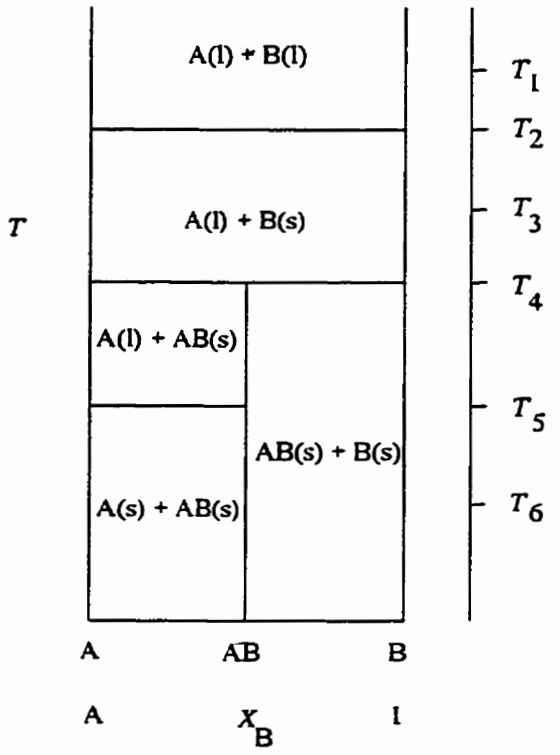

Figure 5.3 **Generalized phase diagram of a binary system in which compound AB melts incongruently, and the compounds A and B are immiscible in the liquid state.**

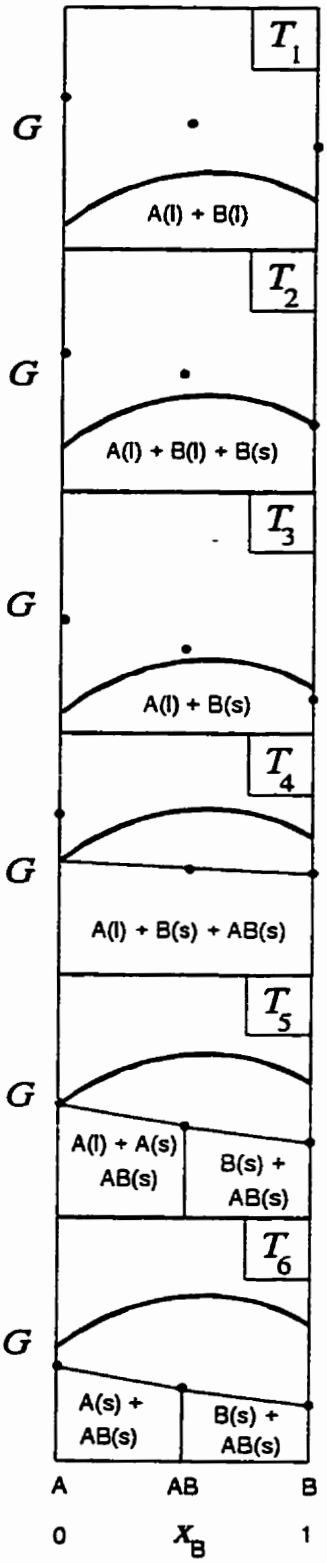

Figure 5.4 **Gibbs energy diagram at different temperatures for the binary diagram shown in Figure 5.3.**

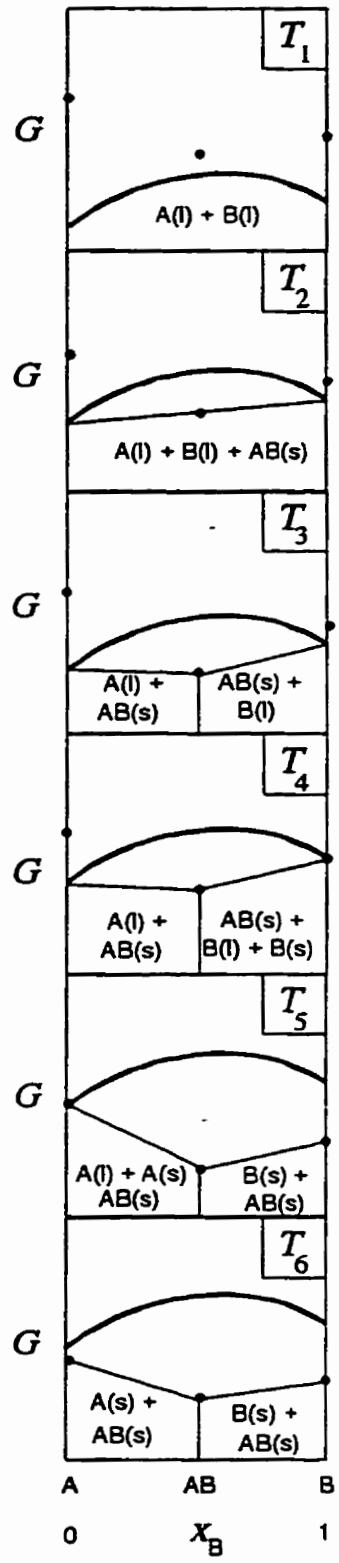

Figure 5.5 **Gibbs energy diagram at different temperatures for the binary phase diagram shown in Figure 5.6.**

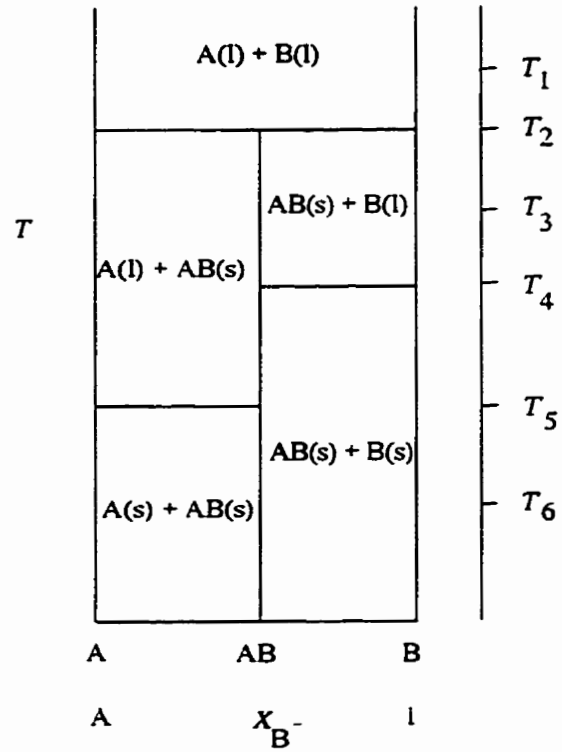

Figure 5.6 **Generalized phase diagram of a binary system in which G(AB) < G(B), as shown in Figure 5.5, with A and B forming immiscible liquids, but AB melts congruently.**

Figure 5.7 shows the results of the relative Gibbs energies of A, AB, B and liquid at the melting point of AB for the four cases : G (AB) < or > G(B), ideal/non-ideal liquids. Therefore, although immisciblity of the liquids plays a role in melting points and melting products, the driving force that determines the congruency of melting in these extreme (ideal or very non-ideal) systems is the relative values of G(AB) and G(B). It is important to note that this model omits intermediate miscibility cases (minima in G_{liquid}) that could further influence melting behavior.

For the comparative study of inclusion compounds composed of different host materials with the same guest species, the general conclusions of the factors which influence the melting behavior of a binary compound have been summarized in Table 5.1. The most important factor is the relative stability of the binary compound with respect to it constituent components.

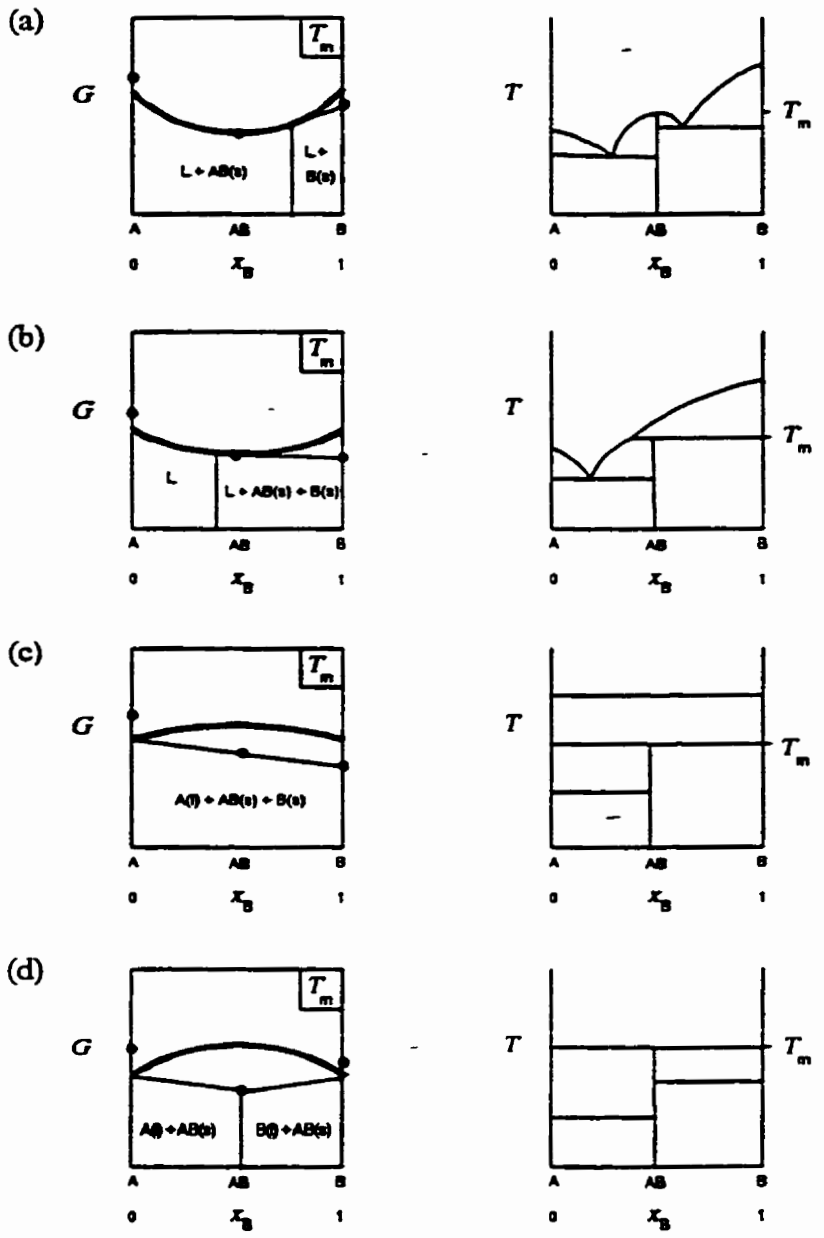

Figure 5.7 Gibbs energy diagrams at the melting point of binary compounds and the corresponding binary phase diagrams for : (a) congruent melting with an ideal liquid phase; (b) incongruent melting with an ideal liquid phase; (c) incongruent melting with a very non-ideal liquid; (d) congruent melting with a very non-ideal liquid.

Table 5.1 **Factors concerning melting behavior in binary compounds, generalized as A_xB_y where the components are A and B.**

Factor	Congruent Melting Favored	Incongruent Melting Favored	Comment
A_xB_y → liq + A(s) or B(s)	$\Delta G > 0$	$\Delta G = 0$	necessary
$S(A_xB_y)$	large $S(A_xB_y)$	small $S(A_xB_y)$	influential
S(A), S(B)	small S(A) or S(B)	large S(A) or S(B)	influential
A-B interaction	like-like (e.g. polar-polar)	like-unlike (e.g. polar-nonpolar)	influential
relative melting temperatures	$T_{fus}(A_xB_y) > T_{fus}$(A or B)	$T_{fus}(A_xB_y) < T_{fus}$(A or B)	influential
A-B enthalpy considerations	ideal solution	immiscible constituents	influential

Experimental heat capacity data for PHTP

T	C_p	T	C_p	T	C_p
K	J K^{-1} mol^{-1}	K	J K^{-1} mol^{-1}	K	J K^{-1} mol^{-1}
37.87	39.4	143.51	152.6	260.22	320.5
38.10	37.2	143.85	153.9	270.92	320.4
43.06	43.6	145.21	165.7	281.69	329.4
43.49	47.7	149.86	180.8	282.60	354.1
48.22	48.3	153.15	174.9	296.61	360.2
48.77	49.0	155.09	179.9	307.52	374.8
53.27	49.4	156.22	176.4	316.78	370.5
53.95	58.6	156.39	173.0	319.17	393.7
58.20	69.0	157.20	182.7		
59.04	64.7	160.32	181.6		
63.09	68.6	162.57	183.7		
64.04	71.2	166.65	196.9		
68.01	75.3	167.67	202.1		
69.03	76.0	168.69	193.1		
73.01	88.7	173.01	187.9		
78.92	99.6	177.54	208.7		
83.82	101.5	179.39	192.6		
88.73	101.8	180.02	211.9		
89.40	105.5	188.79	217.1		
91.22	107.2	191.26	221.3		
92.62	106.7	194.74	220.3		
95.76	111.3	200.02	227.2		
98.94	111.8	202.51	231.0		
100.65	109.3	204.12	231.6		
102.47	116.6	209.36	248.8		
105.60	117.6	211.29	233.4		
107.18	117.7	220.59	262.9		
111.95	126.4	222.58	259.5		
111.98	126.2	226.49	270.4		
112.12	122.2	232.47	270.6		
113.84	126.0	236.10	270.7		
118.60	132.1	242.88	279.4		
123.23	135.7	243.69	292.5		
125.35	140.3	244.35	286.8		
130.14	140.8	247.15	310.8		
130.75	145.5	247.19	308.7		
132.52	144.9	249.08	312.7		
136.83	153.1	254.05	301.1		
137.15	150.7	254.70	305.4		
141.72	168.0	259.83	313.9		

Experimental heat capacity data for PHTP-hexadecane

T	C_p^{Corr}	T	C_p^{Corr}	T	C_p^{Corr}
K	J K^{-1} mol^{-1}	K	J K^{-1} mol^{-1}	K	J K^{-1} mol^{-1}
41.07	39	195.76	306	278.86	366
56.47	67	204.29	273	279.34	355
63.90	93	212.95	320	300.44	457
71.27	97	215.25	287	300.67	449
79.11	137	217.06	297	309.18	442
87.42	137	221.65	320	309.47	454
95.34	133	225.40	317	309.88	471
95.73	108	228.22	372	311.09	443
98.03	168	230.93	301	319.77	436
103.92	116	232.89	329		
104.25	122	236.62	317		
106.45	123	239.41	333		
109.19	122	244.03	354		
109.49	125	247.67	338		
117.54	166	254.02	322		
120.36	155	254.99	340		
121.84	148	257.48	331		
131.53	158	258.71	390		
133.11	168	262.25	355		
142.66	201	264.02	386		
144.26	238	268.24	383		
162.55	258	269.85	396		
168.77	233	273.43	357		
179.74	239	274.96	361		
184.71	265	277.62	382		
190.77	249	277.65	377		

Note: C_p^{Corr} are corrected heat capacities which take in account the 3.5 mass % of hexadecane in the adiabatic calorimeter sample

REFERENCES

1.1 White, M.A. *J. de Phys. (Paris)*, **1987**, *C1*, 565.

1.2 Tse, J.S.; White, M.A. *J. Phys. Chem.* **1988**, *92*, 5006.

1.3 Zakrzewski, M.; White, M.A. *Phys. Rev. B* **1992**, *45*, 2809.

1.4 Michalski, D.M.; White, M.A. *J. Phys. Chem.* **1995**, *99*, 3774.

1.5 Michalski, D.M.; White, M.A. *J. Phys. Chem.* **1997**, *106*, 6202.

1.6 White, M.A.; MacLean, M.T. *J. Phys. Chem.* **1985**, *89*, 1380.

1.7 White, M.A.; Zakrzewski, M. *J. Incl. Phenom. Molec. Recog. Chem.* **1990**, *8*, 215.

1.8 Zakrzewski, M.; White, M.A.; Abriel, W. *J. Phys. Chem.* **1990**, *94*, 2203.

1.9 Abriel, W.; du Bois, A.; Zakrzewski, M.; White, M.A. *Can. J. Chem.* **1990**, *68*, 1352.

1.10 Zakrzewski, M.; Mróz, B.; Kiefte, H.; White, M.A.; Clouter, M.J. *J. Phys. Chem.* **1991**, *95*, 1783.

1.11 Zakrzewski, M. and White, M.A. *J. Phys.: Cond. Matt.* **1991**, *3*, 6703.

1.12 White, M.A.; Powell, B.M.; Sears, V.F. *Molec. Cryst. Liq. Crystal.* **1992**, *211*, 177.

1.13 Zakrzewski, M.; Mróz, B.; Kiefte, H.; White, M.A.; Clouter, M.J. *J. Phys. Chem.* **1993**, *97*, 12949.

1.14 Michalski, D.; White, M.A.; Bakshi, P.; Cameron, T.S.; Swainson, I. *Can. J. Chem.* **1995**, *73*, 513.

1.15 Michalski, D.; Perry, R.T.; White, M.A. *J. Phys.: Cond Matt.* **1996**, *8*, 1647.

1.16 White, M.A.; Perry, R.T. *Chem. Mater.* **1994**, *6*, 603.

1.17 Farina, M.; Di Silvestro, G.; Colombo, A. *Mol. Cryst. Liq. Cryst.* **1986**, *137*, 265.

2.1 Watson, E.S.; O'Neill J.; Justin J.; Brenner, N. *Anal. Chem.* **1964**, *36*, 1233.

2.3 Mraw, S.C. in Chapter 11 of *Specific Heat of Solids*, Ed. Ho, C.Y. Hemisphere: New York, **1988**.

2.4 Skoog, D.A.; Leary, J.J in Chapter 23 of *Principles of Instrumental Analysis*, Saunders College Publishing: New York, **1992**.

2.5 Wendlandt, W.W. in *Thermal Analysis 3rd ed.*, Wiley: New York, **1986**.

2.6 Perrenot, B.; Widmann, G. *Thermochimica Acta*, **1994**, *234*, 31.

2.7 Cammenga, H.K.; Eysel, W.; Gmelin, E.; Hemminger, W.; Höhme, G.W.H.; Sarge, S.H. *Thermochimica Acta*, **1993**, *219*, 333.

2.8 White, M.A. in Chapter 4 of *Comprehensive Supramolecule Chemistry, Vol 8: Solid-state Supramolecular Chemistry: Crystal Engineering*, Ed. By Davis, J.E.D.; Ripmeester, J.A. Elsevier: Oxford, **1996**.

2.9 Goldberg, R.N.; Weir, R.D. *Pure Appl. Chem.*, **1992**, *64(10)*, 1545.

2.10 Van Oort, M.J.M *Ph.D. Thesis: Studies of Polymorphic Substituted Ammonium Salts*, Dalhousie University, **1987**.

2.11 Van Oort, M.J.M; White, M.A. *Rev. Sci Instrum.*, **1987**, *27*, 1239.

2.12 Hultgren, R.; Orr, R.L.; Anderson, P.D.; Kelly, K.K. in *Selected Values of Thermodynamic Properties of Metals and Alloys*, Wiley: New York, **1963.**

2.13 Gronvold, F. *J. Thermal Anal.*, **1978**, *13*, 419.

2.14 Westrum, E.F. *Jr.*; Chou, C.; Osborne, D.W.; Flotow, H.E. *Cryogenics*, **1967**, *7*, 43.

2.15 White, M.A.; Perry, R.T. *Chem. Matter.*, **1994**, *6*, 603.

3.1 Bengen, M.F. (I.G. Farbenindustrie) *Ger. Pat. Appl.*, **1940**, OZ 123438.

3.2 Smith, A.E. *Acta Crystallogr.*, **1952**, *5*, 224.

3.3 Hollingsworth, M.D.; Harris, K.D.M. in Chapter 7 of *Comprehensive Supramolecule Chemistry, Vol 6: Solid-state Supramolecular Chemistry: Crystal Engineering*, Ed. By MacNicol, D.D.; Toda, F.; Bishop, R. Elsevier: Oxford, **1996**.

3.4 Harris, K.D.M.; Thomas, J.M. *J. Chem. Soc. Faraday Trans.*, **1990**, *86(17)*, 2985.

3.5 Monobe, K.; Murakami, Y.; Yokoyama, F. *Mem. Sch. Eng., Okayama Univ.*, **1971**, *6(1)*, 57.

3.6 George, A.R.; Harris, K.D.M. *J. Mol. Graphics* **1995**, *13*, 138.

3.7 Zimmerschied, W.J.; Dinerstein, R.A.; Weitkamp, A.W.; Marschner, R.F. *Ind. Eng. Chem.*, **1950**, *40*, 1300.

3.8 Harris D.M; Jonsen P. *Chem. Phys. Lett.*, **1989**, *154*, 593.

3.9 Vold, R.L.; Vold, R.R.; Heaton N.J. in *Advances in Magnetic Resonance : The Waugh Symposium, Vol 13*, Ed. Warren W.S., Academic Press: New York, **1989**.

3.10 Heaton N.J.; Vold, R.L.; Vold, R.R. *J. Am. Chem. Soc.*, **1989**, *111*, 3211.

3.11 Takemoto, K.; Sonoda, N. in Chapter 2 of *Inclusion Compounds, Vol 2*, Ed. Atwood, J.L.; Davies, J.E.D.; MacNicol, D.D. Academic Press: New York, **1984**.

3.12 McAdie, H.G. *Can. J. Chem.*, **1962**, *40(12)*, 2195.

3.13 Pemberton, R.C.; Parsonage, N.G. *Trans. Far. Soc.*, **1965**, *61*, 2112

3.14 Finke, H.L.; Gross, M.E.; Waddington, G.; Huffman, H.M. *J. Amer. Chem. Soc.*, **1954**, *76*, 333.

3.15 Andersson, O.; Matsuo, T.; Suga, H.; Ferloni, P. *Int. J. Thermophys.*, **1993**, *14*, 149.

3.16 *The Merck Index, Tenth Edition* Ed. Windholz, M. Merck & Co: New Jersey, **1983**.

3.17 Van Oort, M.J.M *Ph.D. Thesis: Studies of Polymorphic Substituted Ammonium Salts*, Dalhousie University, **1987**.

3.18 Van Oort, M.J.M.; White, M.A. *Rev. Sci. Instrum.*, **1987**, *27*, 1239.

3.19 Farina, M.; Di Sivesto, G.; Colombo, A. *Mol. Cryst. Liq.*, **1986**, *137*, 265.

3.20 Guggenheim, E.A. *Mixtures*, Oxford Press, **1952**.

4.1 Farina, M. *Tetrahedron Lett.*, **1963**, 2097.

4.2 Farina, M.; Audisio, G. *Tetrahedron*, **1970**, *26*, 1827.

4.3 Farina, M.; Di Silvestro, G.; Sozzani, P. in Chapter 12 of *Comprehensive Supramolecule Chemistry, Vol 8: Solid-state Supramolecular Chemistry: Crystal Engineering*, Ed. By MacNicol, D.D.; Toda, F.; Bishop, R. Elsevier: Oxford, **1996**.

4.4 Farina, M.; Audisio, G. *Tetrahedron Lett.*, **1967**, 1285.

4.5 Allegra G.; Farina M.; Immizzi A.; Colombo, A.; Rossi, U.; Broggi, R.; Natta G. *J. Chem. Soc. (B)*, **1967**, 1020.

4.6 Gavezotti, A. *J. Am. Chem. Soc.*, **1983**, *105*, 5220.

4.7 Colombo, A.; Allegra, G. *Atti. Accad. Naz. Lincei, Cl. Sci. Fis., Mat. Nat., Rend.*, **1967**, *43*, 41.

4.8 Farina, M. in Chapter 3 of *Inclusion Compounds, Vol 2*, Ed. Atwood, J.L.; Davies, J.E.D.; MacNicol, D.D. Academic Press: New York, **1984**.

4.9 Reppe, W. *Justus Liebigs Ann. Chem.*, **1955**, *596*, 134.

4.10 Buess, C.M.; Lawson, D.D. *Chem. Rev.*, **1960**, *60*, 313.

4.11 Finke, H.L.; Gross, M.E.; Waddington, G.; Huffman, H.M. *J. Amer. Chem. Soc.*, **1954**, *76*, 333.

4.12 Van Oort, M.J.M *Ph.D. Thesis: Studies of Polymorphic Substituted Ammonium Salts*, Dalhousie University, **1987**.

4.13 Van Oort, M.J.M.; White, M.A. *Rev. Sci. Instrum.*, **1987**, *27*, 1239.

4.14 Farina, M.; Di Sivesto, G.; Colombo, A. *Mol. Cryst. Liq.*, **1986**, *137*, 265.

5.1 Farina, M.; Di Sivesto, G.; Colombo, A. *Mol. Cryst. Liq.*, **1986**, *137*, 265.

5.2 White, M.A.; Perry, R.T. *Chem. Mater.* **1994**, *6*, 603.

TEST TARGET (QA-3)

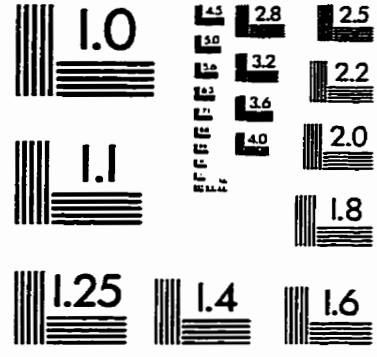

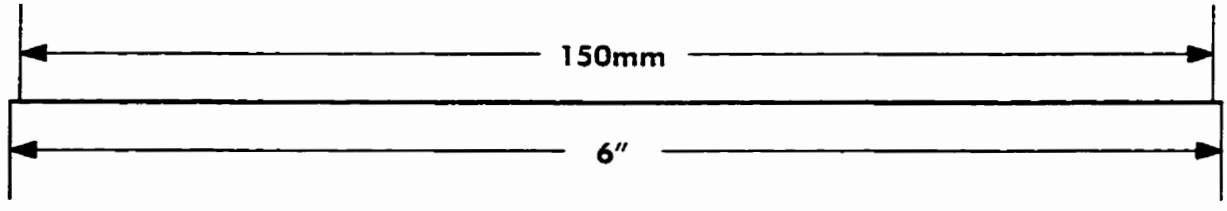

APPLIED IMAGE, Inc
1653 East Main Street
Rochester, NY 14609 USA
Phone: 716/482-0300
Fax: 716/288-5989